Aus der Medizinischen Klinik mit Schwerpunkt Kardiologie (CVK)
der Medizinischen Fakultät Charité – Universitätsmedizin Berlin

DISSERTATION

"Cellular mechanisms of left atrial contractile dysfunction in heart failure with preserved ejection fraction and hypertensive heart disease"

„Zelluläre Mechanismen der linksatrialen kontraktilen Dysfunktion bei Herzinsuffuzienz mit erhaltener Auswurfleistung und hypertensiver Herzerkrankung"

zur Erlangung des akademischen Grades
Medical Doctor - Doctor of Philosophy (MD/PhD)

vorgelegt der Medizinischen Fakultät
Charité – Universitätsmedizin Berlin

von

David Bode

aus Berlin-Steglitz

Datum der Promotion: 17. September 2021

Table of Contents

1. Abbreviations

AT2	angiotensin II
Ca^{2+}	calcium
CANTOS	Canakinumab Antiinflammatory Thrombosis Outcome Study
CaT	calcium transient
CM	conditioned medium
CRISPR	clustered regularly interspaced short palindromic repeats
ECC	excitation-contraction-coupling
EF	ejection fraction
EHRA	European Heart Rhythm Association
ESC	European Society of Cardiology
ET-1	endothelin-1
HF	heart failure
HFA	Heart Failure Association
HFpEF	heart failure with preserved ejection fraction
HHD	hypertensive heart disease
IL	interleukin 1 beta
iPSC-CM	induced pluripotent stem cells - cardiomyocytes
LA	left atrium / left atrial
NCX	sodium calcium exchanger
RyR	ryanodine receptor
SERCA	sarcoplasmic / endoplasmic reticulum calcium ATPase
SHHF	spontaneously hypertensive heart failure rats
SR	sarcoplasmic reticulum
T-tubules	transverse tubules
TNF	tumor necrosis factor
VUS	variant of uncertain significance
WKY	Wistar Kyoto
WT	wild type

2. Abstract

2.1 Introduction

Heart failure with preserved ejection fraction (HFpEF) is present in ~50% of all heart failure (HF) patients. Left atrial (LA) dysfunction is common in HFpEF patients and associated with increased mortality. We hypothesized, that atrial dysfunction *in-vivo* is related to alterations of Ca^{2+} signaling in cardiomyocytes *in-vitro*. We investigated the role of neuro-humoral activation via angiotensin II (AT2) and paracrine activity of the fibroblast secretome as potential contributors to dysregulated Ca^{2+} signaling.

2.2 Methods

21- and 27 weeks- old ZSF-1 rats with a leptin receptor mutation and fed with a high caloric diet served as an HF model. Diseased rats showed a lean (heterozygous; hypertensive heart disease (HHD)) or obese (homozygous; HFpEF) phenotype. LA were imaged by echocardiography. LA myocytes were isolated using a novel Langendorff-based approach. Excitation-contraction-coupling (ECC) was assessed using Ca^{2+}-sensitive fluorescent indicators, confocal imaging (cytosol, nucleus) and video edge detection. Myocardial fibrosis was quantified in histologic sections. Conditioned medium (CM) of primary cardiac fibroblasts was acquired after stretch. CM and LA tissue were screened for various cytokines with enzyme-linked immunosorbent assays.

2.3 Results

HHD showed preserved LA size and ejection fraction (EF) *vs.* wild type (WT). In LA myocytes from HHD, amplitude of cytosolic calcium transients (CaT) was increased. Sarcoplasmic reticulum (SR) Ca^{2+} content was preserved while Ca^{2+} spark frequency and tetracaine-dependent SR Ca^{2+} leak were increased. In HFpEF, LA area was significantly increased and LA EF was impaired. However, atrial myocytes from HFpEF showed increased CaT amplitude and enhanced contractile performance *in vitro*. CaT kinetics and SR Ca^{2+} in HFpEF were not significantly different *vs.* WT, but SR Ca^{2+} leak remained increased. AT2 reduced cytosolic CaT amplitudes and enhanced nuclear Ca^{2+} release in HFpEF. No structural alterations of fibrosis could be detected in HHD or HFpEF. Upon treatment with their respective CM, cardiomyocytes

of WT showed increased CaT. Concentration of ET-1 was increased in CM and LA tissue from WT as compared to HHD and HFpEF. In HHD, CM showed no relevant effect on CaT. However, in HFpEF, CM increased diastolic Ca^{2+} and slowed Ca^{2+} removal, potentially contributing to *in-vivo* decompensation. During disease progression (*e.g.* at 27 weeks), HFpEF displayed dysfunctional ECC due to lower SR Ca^{2+} content and enhanced nuclear Ca^{2+}. In human patients, tissue ET-1 was unrelated to the presence of arterial hypertension or obesity.

2.4 Conclusion

Atrial remodeling is a complex entity that is disease and stage dependent. At early stages, neurohumoral activation (*e.g.* AT-2) and the activity of fibrosis related to the paracrine interaction (*e.g.* ET-1) might contribute to atrial contractile dysfunction *in-vivo*. However, at later stages ECC of LA cardiomyocytes is impaired unrelated to external triggers.

3. Zusammenfassung

3.1 Einleitung

Bei ~50% der Patienten mit Herzinsuffizienz (HF) lässt sich eine erhaltene Ejektionsfraktion (EF) feststellen (HFpEF). HFpEF geht häufig mit einer links-atrialen (LA) Dysfunktion einher, welche mit einer erhöhten Mortalität assoziiert ist. Wir prüften die Hypothese, dass diese LA Dysfunktion *in-vivo* mit Veränderungen im Ca^{2+}-Stoffwechsel von Kardiomyozyten *in vitro* in Beziehung steht. Wir untersuchten den Einfluss der neurohumoralen Aktivierung durch Angiotensin II (AT2) sowie der parakrinen Aktivität des Sekretoms der Fibroblasten auf den Ca^{2+}-Stoffwechsel.

3.2 Methoden

21 und 27 Wochen alte ZSF-1 Ratten mit einer Leptinrezeptormutation (Wildtyp (WT): Wistar Kyoto) dienen als HF Modell. Erkrankte Ratten zeigen einen normal- (heterozygot; Hypertensive Herzerkrankung (HHD)) oder übergewichtigen (homozygot; HFpEF) Phänotyp. LA wurden *in-vivo* mittels Echokardiographie untersucht. LA-Kardiomyozyten wurden nach einer adaptierten Langendorff-Prozedur isoliert. Die elektromechanische Kopplung (excitation-contraction coupling, ECC) wurde mittels Ca^{2+}-sensitiver Farbstoffe, konfokaler Mikroskopie (Zytosol, Nukleus) und Kantendetektion untersucht. Zudem wurde die LA Fibrose in histologischen Schnitten begutachtet. Das konditionierte Medium (CM) primärer, kardialer Fibroblasten wurde nach Dehnung gesammelt. Die Quantifizierung der Zytokine im CM und LA Gewebe erfolgte mittels Enzyme-Linked Immunosorbent Assay.

3.3 Ergebnisse

Ratten mit HHD zeigten keine Veränderungen in LA Größe und EF *vs.* WT. In atrialen Kardiomyozyten von HHD war die Amplitude der zytosolischen Ca^{2+}-Transienten (CaT) erhöht. Der Ca^{2+}-Gehalt des sarkoplasmatischen Retikulums (SR) war unverändert, das Tetracain-abhängige SR-Leck und die Inzidenz von Ca^{2+}-Sparks waren größer. Bei HFpEF zeigte sich eine Zunahme der LA Größe und eine Abnahme der LA EF. Bei HFpEF zeigten sich gesteigerte CaT-Amplituden und eine erhöhte Kontraktilität. Die Kinetik der CaT und SR Ca^{2+}-Gehalt waren unverändert. AT2 reduzierte die zytosolische CaT-Amplitude und induzierte eine gesteigerte

nukleäre Ca^{2+}-Ausschüttung bei HFpEF-Zellen. Strukturelle Unterschiede der Fibrose konnten nicht festgestellt werden. Nach Behandlung mit ihrem jeweiligen CM zeigten Kardiomyozyten vom WT eine erhöhte CaT-Amplitude. Die Konzentration von ET-1 im CM und LA Gewebe war bei WT höher als bei HHD und HFpEF. Bei HHD zeigte das CM keinen relevanten Effekt auf die CaT. Bei HFpEF erhöhte das CM das diastolische Ca^{2+} und verlangsamte die Ca^{2+}-Wiederaufnahme, wodurch möglicherweise zur Dekompensation *in-vivo* beigetragen wurde. Bei fortgeschrittener Erkrankung zeigte HFpEF ein dysfunktionales ECC, bedingt durch einen erniedrigten Ca^{2+}-Gehalt im SR. Bei Patienten war die kardiale ET-1 Konzentration nicht mit dem Auftreten eines arteriellen Bluthochdruckes oder Übergewicht assoziiert.

3.4 Schlussfolgerung

LA Remodeling ist eine komplexe Entität, dessen Pathologie abhängig vom Stadium und von der Grunderkrankung ist. Im frühen Stadium tragen neurohumorale Aktivierung (z.B. AT2) und parakrine Interaktion fibrotischer Aktivität (z.B. ET-1) potenziell zur LA Dysfunktion *in-vivo* bei. Im späten Stadium zeigen LA Kardiomyozyten ein gestörtes ECC unabhängig von äußeren Faktoren.

4. Synopsis

4.1 Current State of Scientific Research

4.1.1 Heart Failure with Preserved Ejection Fraction (HFpEF)

Heart failure with preserved ejection fraction (HFpEF) is highly prevalent. A study from 2016 identified 4.9% of the general population >60 years to suffer from HFpEF[1]. Approximately 50% (range: 40 – 71%) of all heart failure (HF) patients show preserved EF[2]. HFpEF is periodically referred to as 'diastolic heart failure' and 'heart failure with normal ejection fraction' (HFnEF), but 'HFpEF' is currently the most established term in scientific literature.

Generally, HFpEF patients suffer from dyspnea and diastolic dysfunction of the heart. However, since the first consensus statement of the European Society of Cardiology (ESC) on HFpEF in 2007, the definition of HFpEF and the diagnostic criteria are evolving rapidly and are continuously debated in the scientific community. The recently proposed algorithm published by the Heart Failure Association (HFA) of the ESC in 2019 (Fig. 1) incorporates a structured diagnostic approach following an initial evaluation of clinical symptoms, patient demographics, laboratory tests, electrocardiogram and echocardiography.

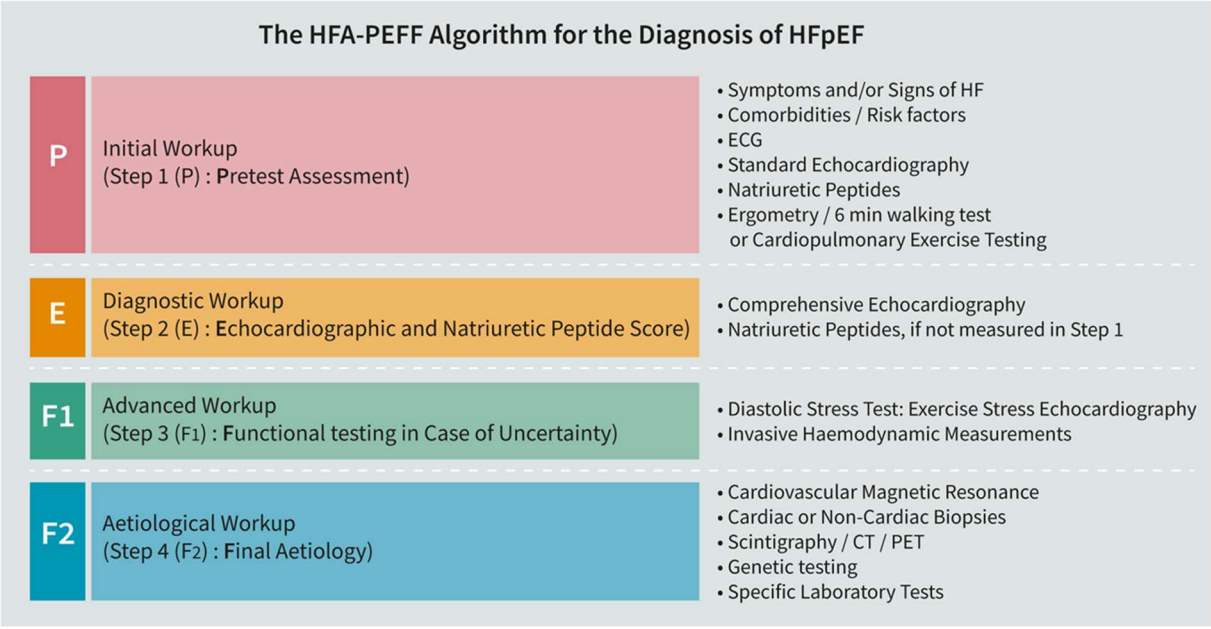

Fig. 1: The HFA-PEFF algorithm for the diagnosis of HFpEF as published by the ESC in 2019 (with permission)[3].

The etiology of HFpEF is complex and heterogeneous. It is thought to evolve from a multitude of risk factors and co-morbidities including age, female sex, obesity, diabetes, arterial hypertension and renal dysfunction. Various systemic triggers have been identified in HFpEF, such as a pro-inflammatory state, arterial and microvascular dysfunction, increased systemic vascular resistance, arterial stiffness, fluid retention and an expanded plasma volume. The LV may suffer from impaired systolic function, slowed diastolic relaxation and reduced compliance with increase end-diastolic stiffness. A reduced reserve of stroke volume, heart rate, cardiac output and LV filling pressures at rest or during exercise, as well as chronotropic incompetence can occur. Changes during LV cardiac remodeling include myocyte hypertrophy, energetic abnormalities and interstitial fibrosis[3]. In addition, LA remodeling and dysfunction is an active contributor to HFpEF in many patients (see *4.1.2).* Any of these pathologies pose potential targets for intervention and a thorough diagnostic workup is required to provide adequate clinical management of the patient. So far, HFpEF patients have not responded to existing medication for HF with reduced ejection (HFrEF) in clinical studies, including AT2 receptor - neprilysin inhibitor sacubitril-valsartan (Entresto®)[4].

4.1.2 Atrial Remodeling

Atria are integral to heart function and their structural, electrical and mechanical properties differ vastly from the ventricles (Fig. 2). They have a unique role in the electrical cardiac system by regulating rhythm and rate (chronotropy). They contribute to mechanical output passively, by serving as a reservoir and conduit, as well as actively, by boost pumping fluid to the ventricular compartment (“atrial kick”). Additionally, the atria operate as mechanical sensors and secrete hormones (*e.g.* natriuretic peptides).

Atrial remodeling is often used synonymously with LA enlargement. While LA enlargement is a typical feature of atrial remodeling and therefore serves as a diagnostic parameter of diastolic function, distinct features of atrial remodeling (hypertrophy, fibrosis and atrial fibrillation) may also occur in the absence of enlargement. For diagnostic purposes, atrial volumes can be estimated from echocardiographic images and normalized to body size to produce the LA volume index. Atrial volumes measured at different phases of the cardiac cycle

can also be utilized to derive information about contractile function (LA emptying fraction, LA expansion index) and allow for differentiation of passive and active contractile properties.

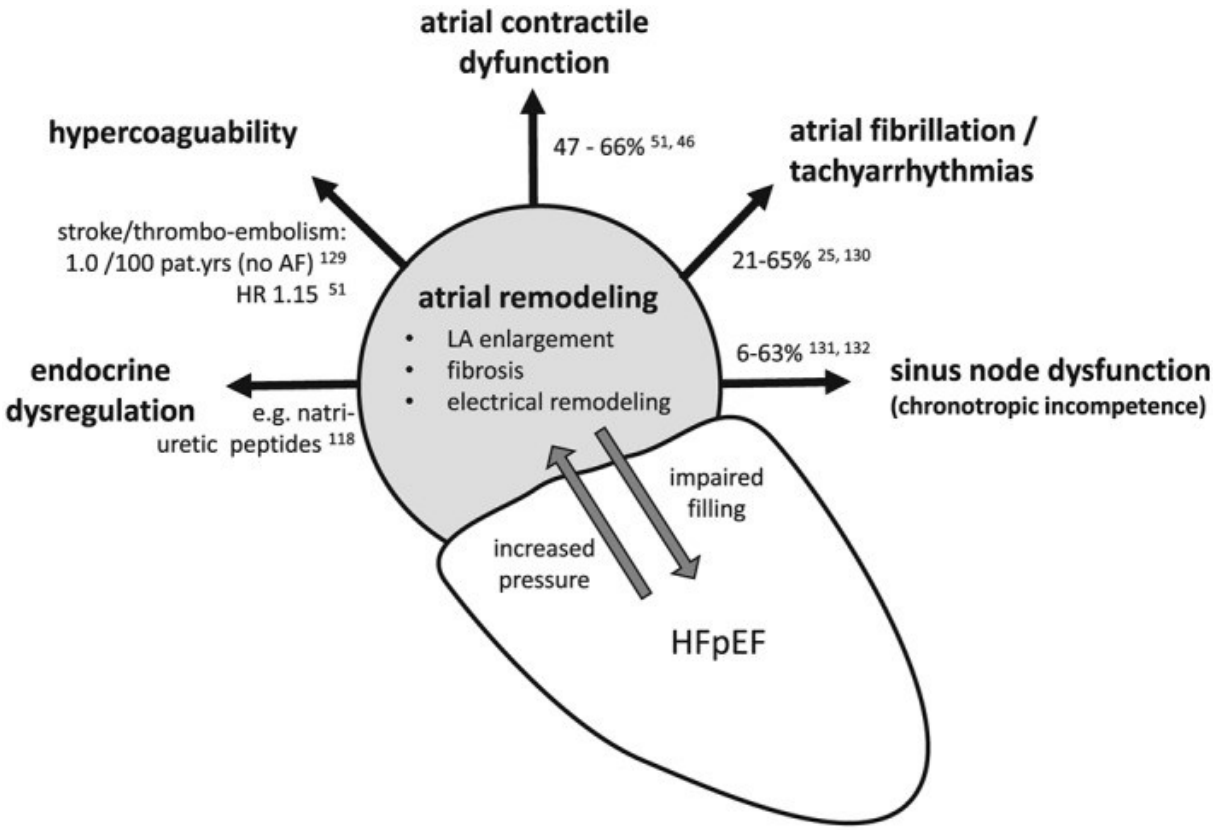

Fig. 2: Clinically relevant effects of atrial remodeling in HFpEF (with permission)[5].

LA enlargement can be found in roughly half of all HFpEF patients[6]. Atrial remodeling is a widely accepted hallmark of HFpEF and its absence has been associated with lower mortality. Additionally, active contractile dysfunction has been shown to be an independent predictor of mortality in HFpEF and impaired conduit function has been associated with exercise intolerance[7, 8].

Cardiomyopathies of the ventricular myocardium have been studied and classified intensively in the past. The growing awareness of atria as unique, specialized compartments with individual structural and functional impairment in disease is giving rise to the concept of atrial cardiomyopathies. In 2018, the European Heart Rhythm Association (EHRA) of the ESC, the Heart Rhythm Society, Sociedad Latino Americana de Estimulacion Cardiaca y Electrofisiologia and the Asia Pacific Heart Rhythm Society released a joint expert consensus defining atrial cardiomyopathies as ‘any complex of structural, architectural, contractile or

electrophysiological changes affecting the atria with the potential to produce clinically-relevant manifestations'[9]. The authors proposed a novel classification scheme based on structural changes as observed in histology (Fig. 3).

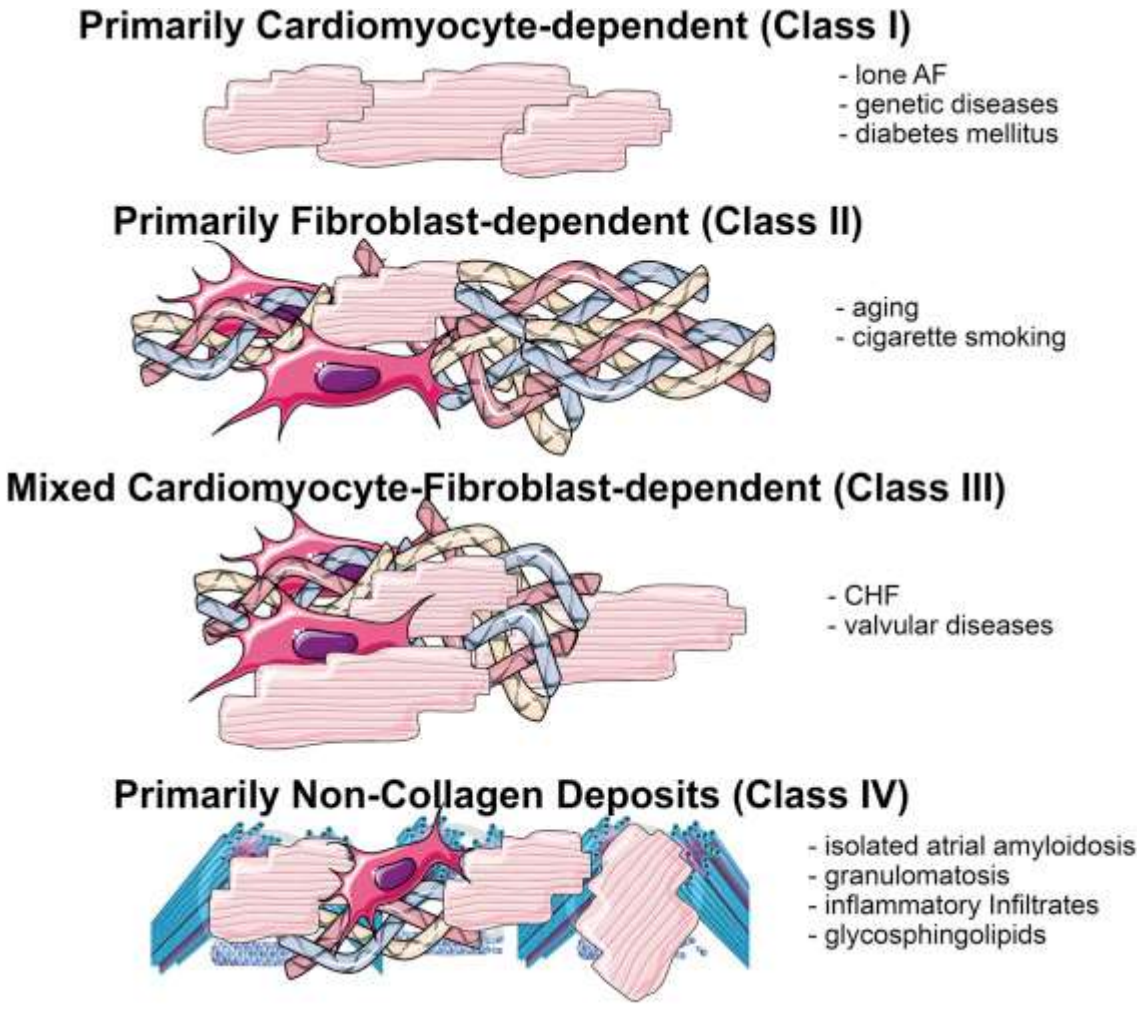

Fig.3: 'EHRAS' Classification Scheme of Atrial Cardiomyopathies (with permission)[9].

While the existence and relevance of atrial cardiomyopathies is widely acknowledged in the scientific community, the EHRA classification scheme has sparked criticism[10]. The classification is based solely on histologic observations. Procedures to obtain biopsies of the atrial myocardium are not part of the clinical routine and pose a certain risk to the patient. The classification does also not adequately account for etiology, co-morbidities and risk factors.

Our knowledge on LA cardiomyocyte function in HF is still sparse. Pluteanu *et al.* were able to demonstrate the pivotal role of dysfunctional LA cardiomyocyte contractility and sarcoplasmic reticulum (SR) Ca^{2+} handling in the transition of compensated LV hypertrophy to HF in

spontaneously hypertensive rats[11]. The role of LA cardiomyocyte function in metabolic syndrome-related HFpEF and its preceding stages (*i.e.* HHD) still remains elusive.

4.1.3 Hypertensive Heart Disease

Hypertensive heart disease describes a constellation of structural and functional changes including LV hypertrophy, diastolic and systolic dysfunction, arrhythmias and an increased risk of myocardial infarction and transition to HF. LV hypertrophy, as a hallmark of hypertensive heart disease, is thought to occur in response to elevated blood pressure in order to minimize wall stress[12]. LV hypertrophy can develop either an eccentric (to the outside) or concentric (to the inside) phenotype and is generally accompanied by an increase in LV mass and LV filling pressures. HHD is a common predecessor of HFpEF, however triggers for the transition to HF and LA dysfunction (*e.g.* RAAS activation, intercellular paracrine communication) are still poorly understood.

4.1.4 Metabolic Syndrome

Metabolic syndrome has been described in different ways, though it is generally referred to as a cluster of risk factors including an increased arterial blood pressure, central obesity, increased fasting glucose and dyslipidemia (high triglycerides and low high-density lipoprotein cholesterol). Prevalence of the metabolic syndrome increases with age and body weight and has been reported between 16-37% depending on the study population[13]. Metabolic syndrome is associated with an increased prevalence of LV diastolic dysfunction (35% *vs.* 9%) and LA enlargement, as well as LA contractile dysfunction[14]. ECC of LA cardiomyocytes in metabolic syndrome-related HFpEF has not previously been studied and might shed insight into the pivotal role of the metabolic risk cluster for LA dysfunction.

4.1.5 Excitation-Contraction-Coupling in Atrial Cardiomyocytes

Excitation-Contraction-Coupling (ECC) describes a series of events in cardiomyocytes from electrical activation to contraction. In brief, membrane depolarization by an electrical stimulus (or neighboring cells) leads to Ca^{2+}-induced Ca^{2+} release (CICR) and subsequent Ca^{2+}-induced contraction of myofilaments. It has been shown numerous times that disrupted Ca^{2+} signaling is closely interrelated with cardiac arrhythmogenesis and cardiac contractile dysfunction[15].

Membrane depolarization (excitation) opens voltage-dependent Ca^{2+} channels (L-type Ca2+ channels) and enables Ca^{2+} to enter the cytosol via its electrochemical gradient. Ventricular cardiomyocytes contain a highly organized network of transverse tubules (T-tubules), which can be described as invaginations of the cellular membrane running perpendicular to the long axis of the cell towards its center (Fig. 4).

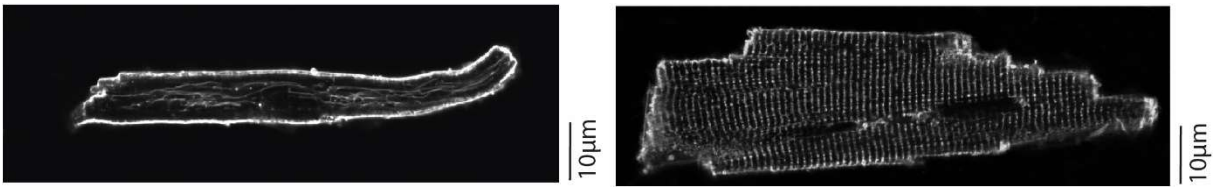

Fig. 4: Example visualization of the tubule system using the fluorescent dye Di8-ANNEPS, LA (left) and LV (right) cardiac myocytes from rodents.

The action potential synchronizes Ca^{2+} influx via LTCC, the T-tubules form junctions (dyads) with the SR to synchronize CICR. Atrial cardiomyocytes have a less evolved tubular system and propagation of Ca^{2+} release towards the center of the cardiomyocyte (facilitated by a chain of RyR clusters) is generally slower (Fig. 5)[16].

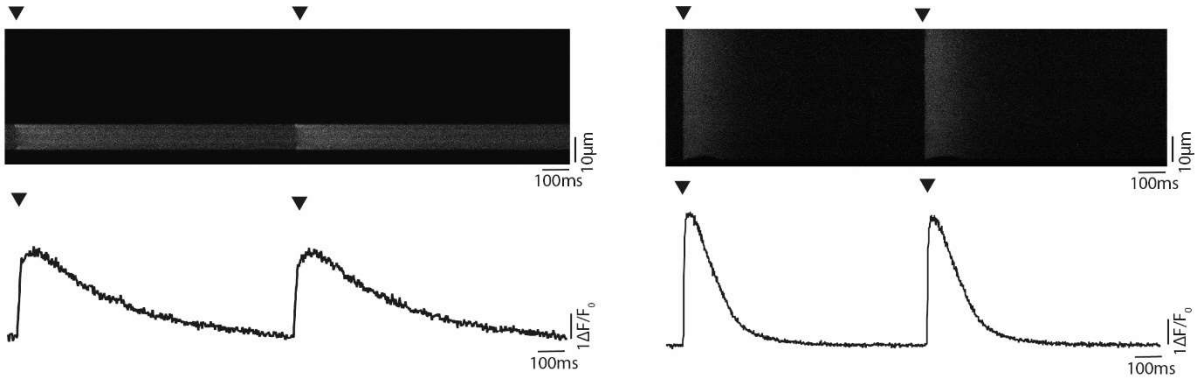

Fig. 5: Example visualization of the tubule system using the fluorescent dye Di8-ANNEPS, LA (left) and LV (right) cardiac myocytes from rodents.

Ca^{2+} binds to troponin C on the thin filaments, allowing the myosin heads of the thick filament to bind to actin on the thin filaments and therefore causing contraction. A synchronous release of Ca^{2+} throughout cardiomyocytes is essential for the contraction of ventricular cardiomyocytes. The mechanism behind atrial cardiomyocytes' ability to maintain contractile function despite their less synchronous Ca^{2+} release is not yet completely understood. One possible explanation may be the colocalization of highly phosphorylated RyR clusters at junctions of axial tubules and the SR, which have been shown to lead to a more rapid shortening of central sarcomeres[17].

A decline of the cytosolic Ca^{2+} concentration, leading to a dissociation of Ca^{2+} from troponin C, is critical for myocardial relaxation and filling. Ca^{2+} reuptake into the SR is driven by the SR Ca^{2+} ATPase (SERCA). Extrusion of Ca^{2+} ions from the cell is mainly driven by the sarcolemmal Na^{+} / Ca^{2+} exchanger (NCX).

4.1.6 Inflammatory Mediators as Pharmacological Targets in Heart Failure

Inflammatory cytokine levels are increased in patients suffering from HF. Cytokines and their receptors have been shown to be independent predictors of mortality in patients with advanced HF[18]. Cytokines have the potential to induce detrimental effects on the heart. Tumor necrosis factor (TNF) α and interleukin (IL) 1β induce a downregulation of SERCA and RyR and act as direct negative ionotropic effectors of cardiomyocyte contractile function[19]. Both cytokines promote cardiomyocyte hypertrophy and apoptosis[20]. IL-6 has been shown to reduce phosphorylation of titin and consecutively increase cardiomyocyte stiffness[21].

As TNFα is a detrimental factor for myocardial impairment in HF, the cytokine or its soluble receptor may be targets for pharmaceutical intervention. Two antagonists where developed in the early 2000s and tested in clinical trials. Etanercept is a recombinant human TNF receptor, binding circulating TNF-α and thus functionally inactivating the cytokine by preventing it from binding to its target receptors. The second compound, infliximab, is a chimeric IgG monoclonal antibody, binding the soluble and transmembrane TNF-α. The Randomized Etanercept North American Strategy of Study Antagonism of Cytokines (RENAISSANCE) trial evaluated the efficacy of etanercept in HF in North America, while the Research into Etanercept Cytokine Antagonism in Ventricular Dysfunction (RECOVER) trial was conducted in Europe. Both trials were combined in the Randomized Etanercept Worldwide Evaluation (RENEWAL) study and included a total of 1500 patients. However, no effect of the therapy could be observed in primary and secondary outcomes and both trials were terminated prematurely[22]. The efficacy of infliximab was evaluated in the anti-TNF Therapy Against Congestive Heart Failure (ATTACH) trial. The TNF α antagonist did not improve, and high doses even adversely affected the clinical condition of patients with moderate-to-severe chronic HF. Thus, doses of infliximab > 5 mg/kg are now contraindicated in patients with moderate-to-severe congestive HF (New York Heart Association functional class III/IV)[23].

The more recent Canakinumab Antiinflammatory Thrombosis Outcome Study (CANTOS) trial tested the efficacy of the IL-1β antibody canakinumab in patients with prior myocardial infarction within the last 30 days and a high sensitive C-reactive protein > 2 mg/L. 10,061 patients were included in the study. The anti-inflammatory therapy led to a significantly lower rate of recurrent cardiovascular events (primary outcomes: nonfatal myocardial infarction, nonfatal stroke, cardiovascular death) independent of lipid-level lowering[24]. Even though the effect size has been criticized as being too minor, likely preventing widespread clinical adoption of the treatment, the CANTOS trial provided the first proof that anti-inflammatory therapy can be of benefit to patients with cardiovascular disease[25]. In addition, post-hoc analysis revealed a dose-dependent reduction in HF hospitalizations and HF-related mortality[26]. Cytokines remain a potential pharmacological target in HFpEF and HHD. Thus, their respective role for fibroblast – cardiomyocyte communication and effects on cardiomyocyte Ca^{2+} handling was studied as part of this thesis (Fig. 6).

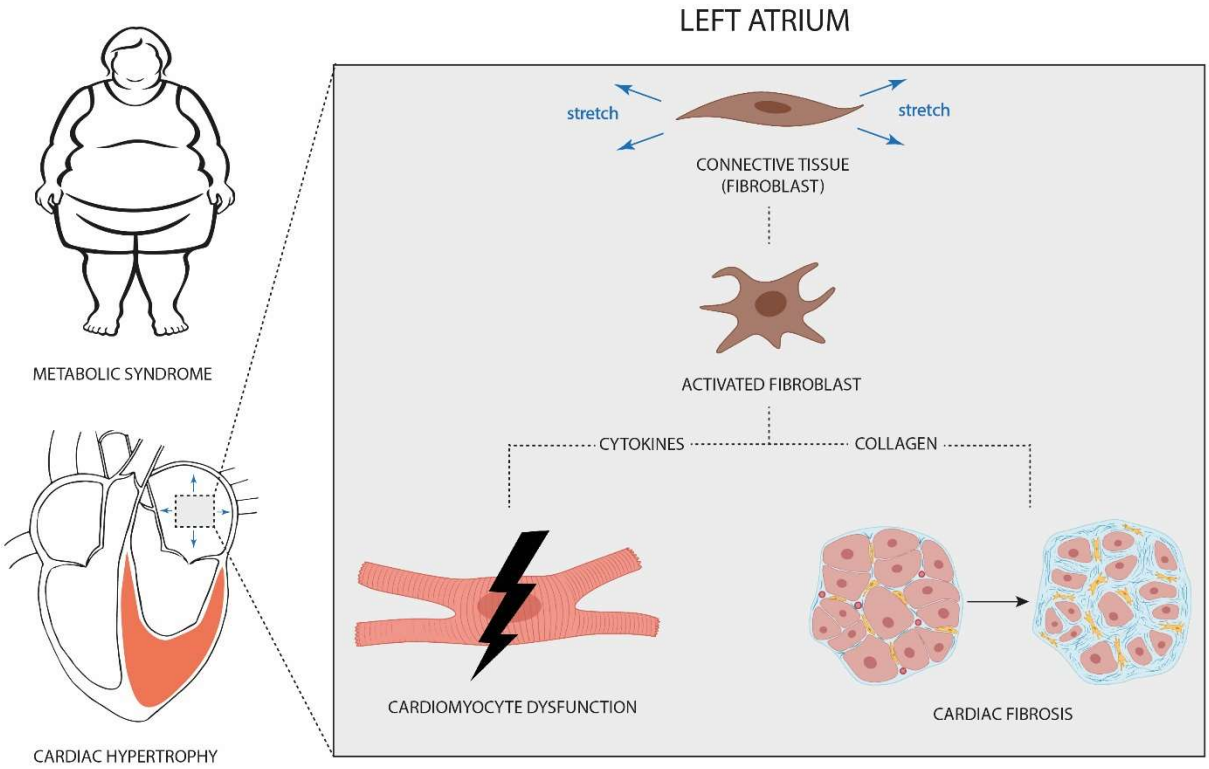

Fig. 6: Schematic outline of fibroblast-mediated cardiomyocyte dysfunction by paracrine secretion of cytokines and induction of cardiac fibrosis through collagen deposition.

4.2 Extended Methods

4.2.1 ZSF-1 Rat Model of Heart Failure

ZFS-1 rats are a hybrid cross of the Zucker Diabetic Fatty and Spontaneously Hypertensive Heart Failure (SHHF) rats, which were developed by Genetic Models and Charles River in 2001 (Fig. 7). The pathogenic background is based on a leptin receptor mutation resulting in either a lean (heterozygous mutation) or obese (homozygous mutation) phenotype. ZSF-1 lean rats offer an arterial hypertension-based model of hypertensive heart disease. As compared to other HDD models, ZSF-1 lean rats show a moderate arterial hypertension with increased activity of the renin-angiotensin-aldosterone-system (as compared to low-renin models with arterial hypertension due to volume expansion (e.g. following partial nephrectomy)[27, 28]. The ZSF-1 obese phenotype combines a metabolic risk model (metabolic syndrome) with a predisposition for arterial hypertension.

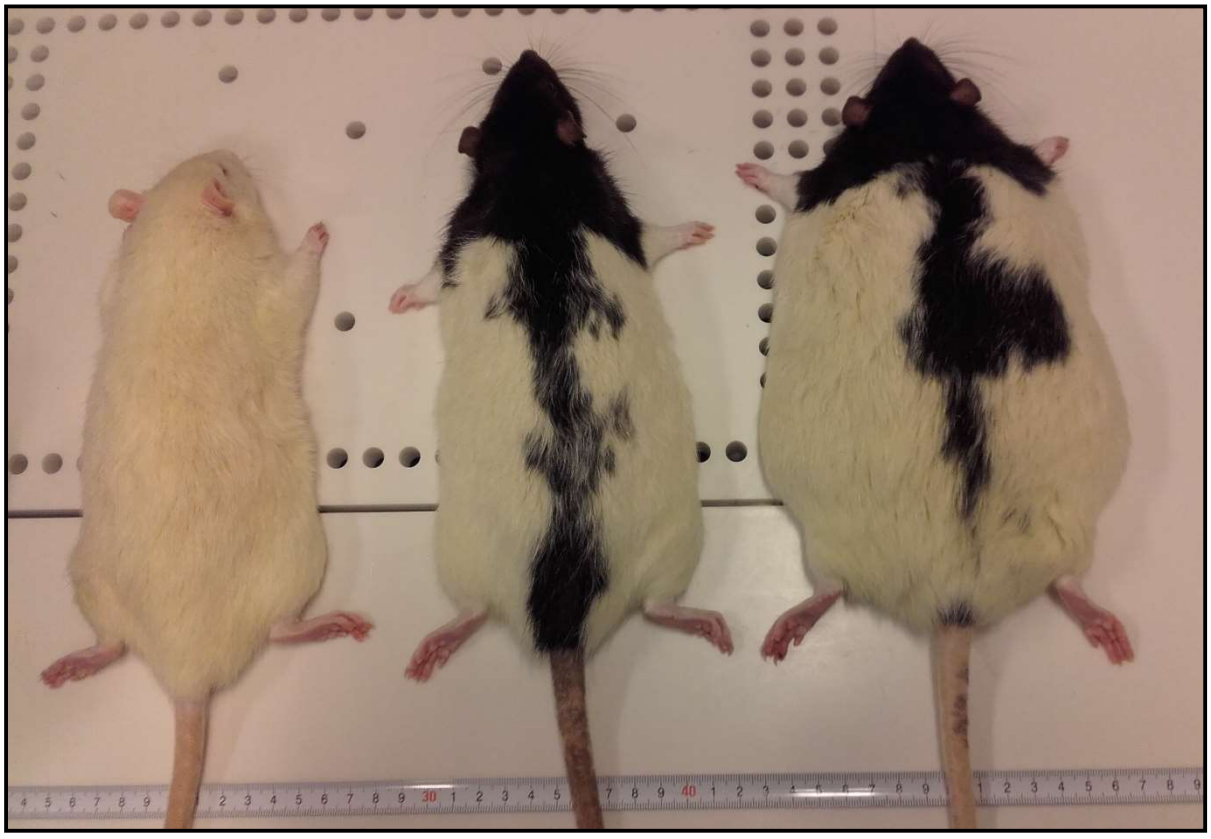

Fig. 7: ZSF-1 rat HF model. From left to right: Wistar Kyoto (WT), ZSF-1 lean (HHD), ZSF-1 obese (HFpEF).

The first in-depth characterization of the cardiac phenotype was published by Hamdani *et al.* in 2013[29]. The authors obtained 9-weeks old WKY, ZSF-1 lean and ZSF-1 obese rats from

Charles River. After a one-week adaptation period, the animals were evaluated with metabolic cages, blood samples and echocardiography studies. No differences in metabolism and renal function could be observed in hypertensive ZSF-1 lean vs. WKY at 10, 14 and 18 weeks. ZSF-1 obese rats however showed increased plasma proteins, proteinuria, oral glucose tolerance, insulin resistance, glycosuria, urine output and water intake. At the age of 18 weeks, ZSF-1 obese rats also developed increased glycaemia and creatine levels.

While there were no initial differences in echocardiographic parameters of ZSF-1 lean animals at baseline, mild differences could be observed in cardiac index at 14 and heart rate at 18 weeks. The authors did not detect a significant difference in LA area at 18 weeks. Experiments conducted as part of this thesis however, detected a significant difference at 21[30] and 28 weeks[31]. At baseline, ZFS-1 obese rats presented with increased heart rate and diastolic LV posterior wall thickness. The animals developed characteristic features of LV diastolic dysfunction at the age of 14 weeks: a lower E/A ratio, a higher E/E' ratio, an increase in LV mass and LA area. Hemodynamic evaluation was performed after 20 weeks. ZSF-1 lean and obese rats showed an increase in body surface area, systolic, diastolic and mean arterial pressure, slower LV relaxation (dP/dt_{min}). ZSF-1 obese rats additionally showed increased end-diastolic pressure and LV contractility (dP/dt_{max}). Notably, EF was preserved in ZSF-1 lean, as well as ZSF-1 obese rats.

ZSF-1 obese rats show distinct features of cardiac diastolic dysfunction and metabolic conditions of the metabolic syndrome. In patients, criteria for the diagnosis of HFpEF would also entail the presence of clinical symptoms, predominantly dyspnea. Naturally, this parameter is difficult to obtain, as the animals cannot be verbally asked. One way to address this issue has been the quantification of lung edema. The parameter is generally obtained by determination of the wet-to-dry lung weight ratio *post mortem*. In their article, Hamdani *et al.* assume mere lung weight (normalized to tibia length) to be a parameter of lung congestion. A more appropriate evaluation was supplied by Miranda-Silva *et al.*, who observed an increased wet-to-dry lung ratio in ZSF-1 obese *vs.* lean rats at the age of 28 weeks[32]. As such, ZSF-1 obese rats were considered to be a metabolic syndrome-related model of HFpEF for the work of this thesis.

4.2.2 Isolation of Single-Cell Cardiac Myocytes

4.2.2.1 Introduction

Since the first description of a successful isolation of viable, primary cardiac myocytes in 1955, a vast amount of protocols has been developed and applied to different species, such as mice, rats, guinea pigs, rabbits, pigs and humans. Isolated single-cell cardiomyocytes can be used for a variety of different experiments including structural, biochemical, genetic and pharmacological studies. Single cells have allowed for a detailed study of ion channel properties *e.g.* through the patch clamp technique and the visualization of ion handling by fluorescent dyes and have therefore made an important contribution to our knowledge of cardiac electrophysiology (Fig. 8).

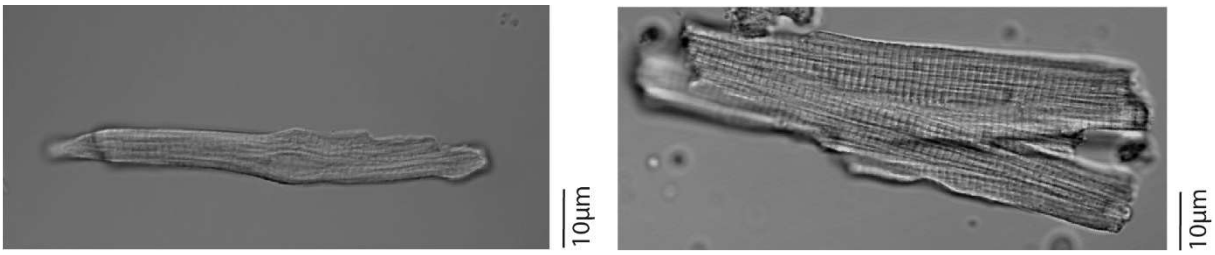

Fig. 8: Example of light-microscopic images of primary, LA (left) and LV (right) cardiac myocytes from rodents.

A major limitation to working with primary cells lies in their inability to proliferate and stay viable in a cell culture without undergoing continuous degradation. An alternative to primary myocytes is offered by commercially available, immortalized cell lines, such as the AT-2 and HL-1 line. HL-1 cells can be serially passaged and contract spontaneously. However, they show structural and functional differences compared to primary cardiac myocytes, *e.g.* a less organized ultrastructure, a high occurrence of developing myofibrils and a hyperpolarization-activated inward current[33].

Another viable option that is receiving an increasing amount of interest from the scientific community are patient derived induced pluripotent stem cells-derived cardiomyocytes (iPSC-CM). The human origin of iPSC-CM has made them an attractive platform for drug safety and development. Another elegant feature of iPSC-CM lies in their containment of the patients' genetic fingerprint. iPSC-CM have been shown to exhibit features of disease phenotypes *in-vitro* and are therefore anticipated to play a key role in precision medicine. The relevance of genetic variants of uncertain significance (VUS) can be assessed by comparing experimental

data to an isogenic control group (iPSC-CM of the same origin, where the VUS has been corrected utilizing the Clustered Regularly Interspaced Short Palindromic Repeats (CRISPR) / Cas9 gene editing technology).

The following protocol describes a procedure for the isolation of adult LA cardiomyocytes from rats, as used for the work of this thesis.

4.2.2.2 Buffers

The composition of buffers used in this protocol is largely based on physiological Tyrode's buffers. These have been developed by systematic adaptation of compound concentrations until a good survival rate of the specific tissue had been established. The exact composition of buffers is given in Table 1.

Reagent (mM)	Perfusion Buffer	Cannulation Buffer	Digestion Buffer	Stop Buffer	Step 1	Step 2	Step 3	Normal Tyrode
NaCl	135	135	135	135	135	135	135	135
KCl	4.7	4.7	4.7	4.7	4.7	4.7	4.7	4
KH_2PO_4	0.6	0.6	0.6	0.6	0.6	0.6	0.6	
Na_2HPO_4	0.6	0.6	0.6	0.6	0.6	0.6	0.6	
$MgSO_4$	1.2	1.2	1.2	1.2	1.2	1.2	1.2	
MgCl								1
HEPES	10	10	10	10	10	10	10	10
Taurine	30	30	30	30	30	30	30	
Glucose	10	10	10	10	10	10	10	
BDM	10	10	10	10	10	10	10	
$CaCl_2$		1	0.01		0.125	0.25	0.5	1
BSA				150	70	70	70	
Purified enzyme blend (medium Thermolysin)			0.195 Wünsch units/mL					
pH adjusted to	7.4	7.4	7.4	7.4	7.4	7.4	7.4	7.4
pH adjusted at	37 °C	4 °C	37 °C	37 °C	37 °C	37 °C	37 °C	37 °C
pH adjusted with	NaOH	NaOH	NaOH	NaOH	NaOH	NaOH	NaOH	NaOH

Table 1: Buffers used for isolation of single-cell cardiac myocytes and sub-sequent experiments.

4.2.2.3 Excision

In order to minimize micro-infarctions during the isolation procedure, the animal is heparinized with 500 I.U. / 100 g body weight. After 30 minutes, the animal is euthanized by decapitation using a guillotine suitable for rodents. The skin covering the xiphoid process is removed with surgical scissors. The peritoneum is opened below the rib cages on both sides and the diaphragm exposed. An incision is made along the anterior arc. The ribs are opened on both sides along the *linea mediaclavicularis* ascending to the clavicular bone and the mediastinum is exposed *in-situ.* The lungs are removed at the distal ends of the hila. The thymus is removed and the aortic arch exposed. The base of the heart is pinched using forceps and gently pulled downwards. The aorta is then cut across while maintaining pull on the heart, leaving a small segment of the aorta attached to the heart for subsequent cannulation. The heart is then quickly transferred into ice-cold cannulation buffer.

4.2.2.4 Cannulation

The heart is then transferred to a petri-dish containing ice-cold cannulation buffer. A custom-made cannula, which is attached to a 10mL syringe filled with ice-cold cannulation buffer, is then inserted into the aorta and fixated with 3/0 silk suture using two knots. The aorta is gently flushed with 5 mL of cannulation buffer, anterogradely perfusing the coronary arteries and thus removing the blood.

4.2.2.5 Digestion

The heart is transferred to a Langendorff apparatus and perfused with perfusion buffer at 3 mL/min and 37 °C. Key feature of the perfusion buffer is the nominally free Ca^{2+} content, which is detrimental to destabilize the intercalated disks connecting adjacent cardiomyocytes. It is thought to disrupt Ca^{2+}-dependent cadherins, which mediate cell adherence and desmosomal junctions between myocytes[34]. After an initial period of approximately 3 min, perfusion is changed to digestion buffer. Digestion buffer additionally contains highly purified collagenase 1 and 2 (Liberase®), which facilitates digestion of extracellular tissue, as well as cell dissociation. Liberase® has been shown to be superior to less targeted and less pure enzymes like collagenases. This enzyme does not only allow for higher yield of morphologically sound and functionally intact cardiomyocytes, but also minimizes cell clumping[35]. Purified enzyme

blends of collagenases with additional high dispase or medium thermolysin content are most commonly used for rat cardiomyocyte isolations.

4.2.2.6 Pressure Manipulation

A double overhand knot is tied around the base of the heart, excluding the aorta (*i.e. venae cavae, truncus pulmonalis, venae pulmonales*). This step is repeated until an inflation of the right and LA, as well as the coronary sinus, can be observed. The LA is punctured with a butterfly needle and the atrium is allowed to deflate. Intraluminal pressure of the atrium is now adjusted by altering the elevation of the butterfly hose. The atrium is being kept slightly inflated throughout the rest of the procedure.

The above-mentioned procedure leads to an increase of right atrial cavity pressure, while maintaining a lower LA pressure. This leads to an attenuated coronary perfusion of the LA, which likely facilitates improved isolation results of this approach[36].

4.2.2.7 Tissue Dispersion

Upon finished digestion of the LA, the tissue is removed from the heart with scissors and transferred into stop buffer at room temperature. Stop buffer contains a high concentration of bovine serum albumin, which inhibits activity of the digestive enzyme on atrial tissue by competitive binding. The atrial tissue is minced into small pieces. Consecutively, the tissue is dispersed by gentle suction and ejection of tissue chunks using a transfer pipette. This procedure is continued for approximately 5 min until a macroscopic dissociation of the tissue can be observed. Air bubbles should be avoided during this step, since exposure to air will result in cardiomyocyte death. The minced atrial tissue is transferred to a 15 ml conical tube and the tissue allowed to settle for 30 s. The supernatant (containing single cell cardiomyocytes) is filtered through a 300 nm pore mesh into another 15 mL conical tube and the cells allowed to settle for another 15 min.

4.2.2.8 Ca^{2+} Re-adaptation

While perfusion of the heart with Ca^{2+} free solution is necessary for single-cell isolation (as described previously), it has a major disadvantage. Reintroduction of Ca^{2+} causes tissue disruption, hypercontraction and release of intracellular enzymes. This phenomenon is known

as the 'Ca^{2+} paradox'. It is thought to be mediated by an excessive, sudden increase of intracellular Ca^{2+} resulting in an exhaustion of high-energy phosphates, enzyme release and ultrastructural damage (*e.g.* mitochondrial swelling and contracture of myofilaments)[37]. The damage of the Ca^{2+} paradox can be minimized by a step-wise adjustment of intracellular Ca^{2+} concentration to physiological levels using step 1, 2 and 3 buffers.

4.2.2.9 Cell plating

A glass-bottom dish is coated with 25% laminin and allowed to dry prior to the isolation procedure. Laminin is a protein complex which can naturally be found in the basal lamina and facilitates cell adhesion. The cardiomyocytes are transferred onto the glass-bottom dish and allowed to settle and attach for 10 min. The dish is filled with Normal Tyrode containing 2mM Ca^{2+} and transferred to the microscope for sub-sequent experiments.

4.2.3 Histology

4.2.3.1 Fixation

The rat hearts are excised, cannulated (as described above) and flushed with phosphate buffered saline. The LA is removed with small scissors and transferred into a petri dish containing 4% paraformaldehyde and is allowed to incubate for 48 hours. This procedure (also known as 'fixation') is well established through the life sciences and ensures preservation of biological tissue from decay due to autolysis or putrefaction.

4.2.3.2 Dehydration and Paraffinization

Subsequentially the water of the specimen must be removed in order to be infiltrated with paraffin wax. This is commonly achieved through a series of ethanol buffers with increasing concentration until pure, water-free alcohol is reached. Since water is miscible with ethanol, it is progressively removed from the specimen. As ethanol and paraffin are not miscible, the ethanol has to be replaced by a clearing agent (*e.g.* xylene). Consecutively, the tissue is infused with paraffin wax at 60°C.

The paraffin wax solidifies upon cooling to 20°C to a consistency, which allows coherent cutting of the sections. The specimen is now embedded into paraffin blocks using an appropriate embedding center. The specimen is placed in a metal mold, filled with paraffin

wax and a cassette placed on top of the mold. After cooling, the block is stored at room temperature until microtomy is being carried out. The paraffin block is transferred to a microtome, cut into sections of 2 µm thickness and placed in a water bath of 60 °C temperature, ensuring removal of unwanted wax ribbons. The sections are then transferred onto a glass cover slip and allowed to dry overnight at 60°C.

4.2.3.3 Deparaffinization and Rehydration

Prior to staining, the sections must be deparaffinized and rehydrated. To achieve this, the previously described procedure is performed in a reverse manner at shorter durations.

4.2.3.4 Staining

The staining procedure to visualize cardiac fibrosis is performed with the commercially available dye Picrosirius Red. Picrosirius Red is an azo dye primarily used for the visualization of collagen and amyloid. For the staining, tissue slides are incubated for 60 min in Picrosirius Red Solution. The slides are then quickly rinsed in 2 changes of acetic acid solution, 3 changes of 100% ethanol, cleared with tap water and mounted in synthetic resin.

4.2.3.5 Imaging

The dye stains collagen (red), muscle fibers (yellow) and cytoplasm (yellow; Fig. 9).

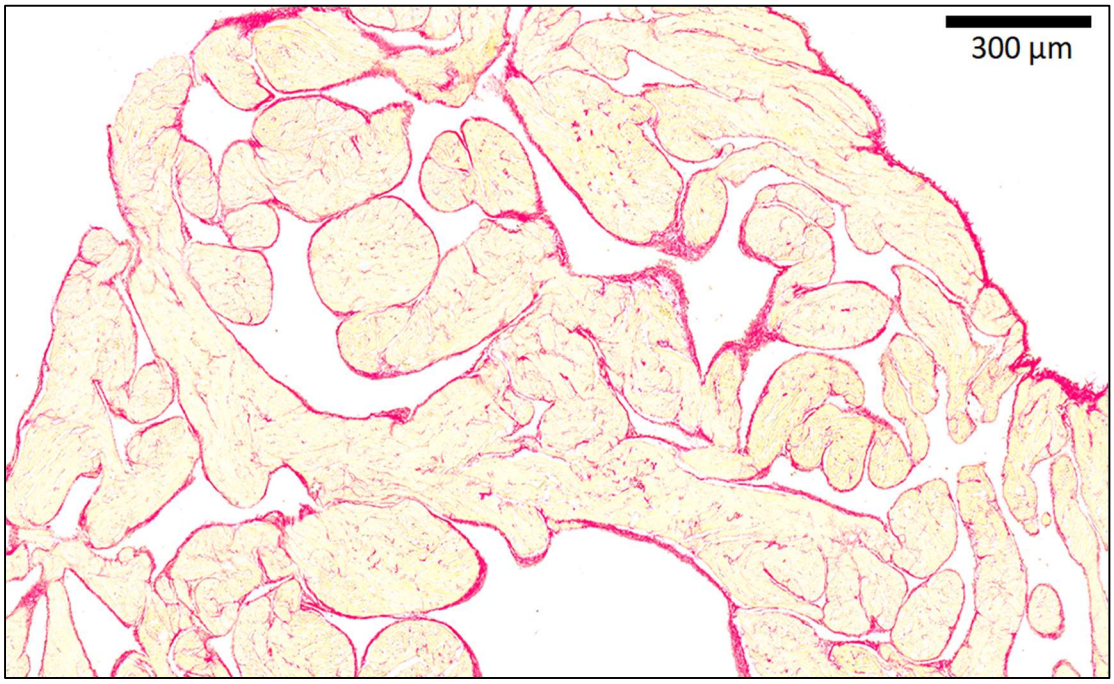

Fig. 9: Example of light-microscopic image of Picrosirius Red-stained LA myocardial tissues from rodents.

4.2.3.6 Analysis

The images are analyzed by digital image analysis and expert scoring. Each method has distinct advantages and drawbacks. For digital image analysis, the image is segmented by a fixed threshold to identify the fraction of red pixels in the total image area defined as the total collagen content. The analysis can be performed with automated analysis software (Table 2). This procedure results in a quantitative, largely unbiased parameter. However, this analysis is unable to discriminate between different types of fibrosis, which have been defined as replacement/scarring fibrosis, reactive interstitial fibrosis and perivascular fibrosis[38].

```
min=newArray(3);
max=newArray(3);
filter=newArray(3);
a=getTitle();
run("HSB Stack");
run("Convert Stack to Images");
selectWindow("Hue");
rename("0");
selectWindow("Saturation");
rename("1");
selectWindow("Brightness");
rename("2");
min[0]=179;
max[0]=255;
filter[0]="pass";
min[1]=40;
max[1]=247;
filter[1]="pass";
min[2]=0;
max[2]=231;
filter[2]="pass";
for (i=0;i<3;i++){
  selectWindow(""+i);
  setThreshold(min[i], max[i]);
  run("Convert to Mask");
  if (filter[i]=="stop")  run("Invert");
}
imageCalculator("AND create", "0","1");
imageCalculator("AND create", "Result of 0","2");
for (i=0;i<3;i++){
  selectWindow(""+i);
  close();
}
selectWindow("Result of 0");
close();
selectWindow("Result of Result of 0");
rename(a);
   run("Set Measurements...", "area area_fraction limit display
redirect=None decimal=3");
   run("Measure");
   selectWindow("Results");
```

Table 2: ImageJ macro used for the quantification of fibrotic tissue in myocardial sections.

In addition, expert visual scoring may take into account patterns of distribution (endocardial, epicardial) and composition (fibrocyte content as measure of activity). For the work of this thesis, endocardial, epicardial and interstitial fibrosis was assessed according to the following scoring system:

0 = no abnormality

1 = well-differentiated granulation tissue as a sign of resolved damage (mostly fibrocytes with elongated, spindle-shaped nuclei; mostly well-definable collagen fibers arranged in parallel)

2 = less differentiated granulation tissue as a sign of subacute damage (fibrocytes with both elongated, spindle-shaped and more blastic, round nuclei; some collagen fibers arranged in parallel)

3 = low-differentiated granulation tissue as a sign of acute damage (mostly fibrocytes with plump, blastic, round nuclei; more homogenous extracellular matrix).

The disadvantage of this approach lies in its semi-quantitative nature, negatively impacting statistical resolution in the case of moderate effect sizes and/or a low amount of data points.

4.2.4 Sample Size Calculation

The sample size was calculated prior to the studies with the software G*Power (Heinrich-Heine-Universität Düsseldorf) where applicable.

4.2.4.1 Publication 1: The role of fibroblast - Cardiomyocyte interaction for atrial dysfunction in HFpEF and hypertensive heart disease.

Endpoint 1:	Total fibrosis (histology)
α error probability:	0.05
Power (1 – β error probability):	0.8
Groups:	3
Statistical test:	ANOVA (one-way)
Effect size (estimated):	0.7
Sample size:	24

Endpoint 2:	Cardiomyocyte cell shortening (microscopy)
α error probability:	0.05
Power (1 – β error probability):	0.8

Groups:	3
Statistical test:	ANOVA (one-way)
Effect size (estimated):	0.5
Sample size (cells):	42
Cells per animal (estimated):	10
Risk of failure (cell isolation):	20%
Sample size (animal):	18

Additionally, 12 animals (4 per group) were shipped to the cooperation partner in Hamburg for cardiac fibroblast isolation, culture and stretch experiments.

4.2.4.2 Publication 3: Cellular mechanisms of metabolic syndrome-related atrial decompensation in a rat model of HFpEF.

Endpoint:	Left atrial size (echocardiography)
α error probability:	0.05
Power (1 – β error probability):	0.8
Groups:	3
Statistical test:	ANOVA (one-way)
Effect size (estimated):	0.6
Sample size:	30

4.3 Summary and Outlook

4.3.1 Summary

The work of this thesis establishes a spectrum of stage- (early, 21w *vs.* late, 28w) and etiology-dependent (metabolic syndrome-related HFpEF *vs.* HHD) triggers for LA cardiomyocyte dysfunction in rats. At 21 weeks, HFpEF, but not HHD, showed distinct features of LA remodeling *in-vivo* (increased LA area, reduced LA EF). *In-vitro*, LA cardiomyocytes of both disease entities showed a rather compensated phenotype (improved contractile function, increased CaT amplitude). However, neurohumoral activation with AT-2 revealed an increased SR Ca^{2+} leak in HFpEF and HHD, indicating a pivotal role for RAAS activation in the induction of LA cardiomyocyte dysfunction in either condition at early stages.

We continued to explore the involvement of cardiac fibrosis in mediating LA contractile dysfunction at 21 weeks. The quantitative assessment of myocardial collagen deposition *ex-vivo*, showed differences neither in HHD nor HFpEF. Taking another approach by considering the role of fibroblast activity, we evaluated the effects of the stretch-induced secretions (supernatant) of cardiac fibroblasts on Ca^{2+} handling in LA cardiomyocytes *in-vitro*. In WT we could observe a 2-fold increase of CaT amplitudes, indicating a potentially positive ionotropic effect of stretch-dependent paracrine activity of fibroblasts. This enhancement of systolic Ca^{2+} release could not be observed in HHD and HFpEF. Contrarily, LA cardiomyocytes of HFpEF showed impaired CaT kinetics (time-to-peak, decay) upon exposure to the secretome of their respective stretched fibroblasts. This observation could explain the discrepancy of *in-vivo / in-vitro* contractile function in LA and LA cardiomyocytes in HFpEF. Furthermore, we could identify ET-1 as the primary mediator of enhanced cytosolic CaT amplitudes in WT.

At 27 weeks, HHD and HFpEF continued to show signs of LA remodeling (increased LA diameter), which was more predominant in HFpEF. The compensated phenotype of LA cardiomyocytes gave way to manifestly dysregulated Ca^{2+} signaling (reduced SR Ca^{2+} load, prolonged cytosolic Ca^{2+} decay) in HFpEF. LA cardiomyocytes from HFpEF rats also had a notable alterations of nuclear Ca^{2+} signaling (increase CaT amplitude), which has been shown to be relevant in the context of hypertrophic signaling (*i.e.* 'Excitation-Transcription-Coupling')[39].

4.3.2 Limitations

There are several limitations to our studies. The ZSF-1 HF model mimics certain 'human' features of HHD and metabolic syndrome-related HFpEF (see chapter 4.2.1). Yet, failure to transfer knowledge of disease pathology from animal models to humans ('translation') is common and could potentially apply to (part of) this work. Another limitation is the *in-vitro* single-cell cardiomyocyte model (see chapter 4.2.2.1), which is unlikely to portray all *in-vivo* facets of cardiomyocyte function.

Our investigations are focused on LA dysfunction, allowing us to study its particular pathology. However, LA dysfunction is often only one component of complex disease clusters (arterial hypertension, metabolic disorders, diastolic dysfunction, HHD, HFpEF, *etc.*). While one treatment strategy could seem logical in the context of our experiments on LA dysfunction, it's beneficial effect might not scale to the remaining organ and/or body. For example, our data indicate that patients with LA dysfunction could benefit from positive inotropic therapy with ET-1 agonists / substitution. This is not a viable systemic treatment strategy in HF. ET-1 is a potent vasoconstrictor and ET-1 antagonists are currently used in the treatment of pulmonary arterial hypertension. However, other cytokines (IL-1β, IL-6, IL-10, IL-33, *etc.*) might prove to be appropriate pharmacological targets for futures therapies.

4.3.3 Outlook

Our data suggest that patients with LA dysfunction may benefit from RAAS inhibition (HHD, HFpEF) and anti-inflammatory therapy (HFpEF). While the former is a widely practiced intervention in cardiology, anti-inflammatory therapies are still in their infancy and are likely to improve during this decade. The CANTOS trial provided the first proof of an effective anti-inflammatory treatment in HF, yet with dissatisfactory effect size. Our studies contribute to the quest of identifying appropriate target compounds.

Following a rather compensatory early cellular phenotype, manifest LA cardiomyocyte dysfunction developed during disease progression in HFpEF. This raises the questions whether and to what extent the patient would benefit from stage-dependent adjustment of pharmacotherapy. If so, what diagnostic methods and criteria could be utilized to make an informed decision? The etiologic heterogeneity of the HF population, as well as the

phenotype-specific development during disease progression, could make it a particularly effective entity for personalized and precision medicine approaches[40].

4.4 References

1. van Riet EE, Hoes AW, Wagenaar KP, Limburg A, Landman MA, Rutten FH. Epidemiology of heart failure: the prevalence of heart failure and ventricular dysfunction in older adults over time. A systematic review. *Eur J Heart Fail* 2016;18:242-252.
2. Owan TE, Redfield MM. Epidemiology of diastolic heart failure. *Prog Cardiovasc Dis* 2005;47:320-332.
3. Pieske B, Tschope C, de Boer RA, Fraser AG, Anker SD, Donal E, Edelmann F, Fu M, Guazzi M, Lam CSP, Lancellotti P, Melenovsky V, Morris DA, Nagel E, Pieske-Kraigher E, Ponikowski P, Solomon SD, Vasan RS, Rutten FH, Voors AA, Ruschitzka F, Paulus WJ, Seferovic P, Filippatos G. How to diagnose heart failure with preserved ejection fraction: the HFA-PEFF diagnostic algorithm: a consensus recommendation from the Heart Failure Association (HFA) of the European Society of Cardiology (ESC). *Eur Heart J* 2019;40:3297-3317.
4. Solomon SD, McMurray JJV, Anand IS, Ge J, Lam CSP, Maggioni AP, Martinez F, Packer M, Pfeffer MA, Pieske B, Redfield MM, Rouleau JL, van Veldhuisen DJ, Zannad F, Zile MR, Desai AS, Claggett B, Jhund PS, Boytsov SA, Comin-Colet J, Cleland J, Dungen HD, Goncalvesova E, Katova T, Kerr Saraiva JF, Lelonek M, Merkely B, Senni M, Shah SJ, Zhou J, Rizkala AR, Gong J, Shi VC, Lefkowitz MP, Investigators P-H, Committees. Angiotensin-Neprilysin Inhibition in Heart Failure with Preserved Ejection Fraction. *The New England journal of medicine* 2019;381:1609-1620.
5. Hohendanner F, Messroghli D, Bode D, Blaschke F, Parwani A, Boldt LH, Heinzel FR. Atrial remodelling in heart failure: recent developments and relevance for heart failure with preserved ejection fraction. *ESC Heart Fail* 2018;5:211-221.
6. Shah AM, Shah SJ, Anand IS, Sweitzer NK, O'Meara E, Heitner JF, Sopko G, Li G, Assmann SF, McKinlay SM, Pitt B, Pfeffer MA, Solomon SD, Investigators T. Cardiac structure and function in heart failure with preserved ejection fraction: baseline findings from the echocardiographic study of the Treatment of Preserved Cardiac Function Heart Failure with an Aldosterone Antagonist trial. *Circulation Heart failure* 2014;7:104-115.
7. Melenovsky V, Hwang SJ, Redfield MM, Zakeri R, Lin G, Borlaug BA. Left atrial remodeling and function in advanced heart failure with preserved or reduced ejection fraction. *Circ Heart Fail* 2015;8:295-303.
8. von Roeder M, Rommel KP, Kowallick JT, Blazek S, Besler C, Fengler K, Lotz J, Hasenfuss G, Lucke C, Gutberlet M, Schuler G, Schuster A, Lurz P. Influence of Left Atrial Function on Exercise Capacity and Left Ventricular Function in Patients With Heart Failure and Preserved Ejection Fraction. *Circ Cardiovasc Imaging* 2017;10.
9. Goette A, Kalman JM, Aguinaga L, Akar J, Cabrera JA, Chen SA, Chugh SS, Corradi D, D'Avila A, Dobrev D, Fenelon G, Gonzalez M, Hatem SN, Helm R, Hindricks G, Ho SY, Hoit B, Jalife J, Kim YH, Lip GY, Ma CS, Marcus GM, Murray K, Nogami A, Sanders P, Uribe W, Van Wagoner DR, Nattel S. EHRA/HRS/APHRS/SOLAECE expert consensus on

atrial cardiomyopathies: Definition, characterization, and clinical implication. *Heart Rhythm* 2017;14:e3-e40.

10. Guichard JB, Nattel S. Atrial Cardiomyopathy: A Useful Notion in Cardiac Disease Management or a Passing Fad? *J Am Coll Cardiol* 2017;70:756-765.
11. Pluteanu F, Nikonova Y, Holzapfel A, Herzog B, Scherer A, Preisenberger J, Plackic J, Scheer K, Ivanova T, Bukowska A, Goette A, Kockskamper J. Progressive impairment of atrial myocyte function during left ventricular hypertrophy and heart failure. *Journal of molecular and cellular cardiology* 2018;114:253-263.
12. Drazner MH. The progression of hypertensive heart disease. *Circulation* 2011;123:327-334.
13. Ford ES, Giles WH, Dietz WH. Prevalence of the metabolic syndrome among US adults: findings from the third National Health and Nutrition Examination Survey. *JAMA* 2002;287:356-359.
14. Nyman K, Graner M, Pentikainen MO, Lundbom J, Hakkarainen A, Siren R, Nieminen MS, Taskinen MR, Lundbom N, Lauerma K. Metabolic syndrome associates with left atrial dysfunction. *Nutrition, metabolism, and cardiovascular diseases : NMCD* 2018;28:727-734.
15. Eisner DA, Caldwell JL, Kistamas K, Trafford AW. Calcium and Excitation-Contraction Coupling in the Heart. *Circ Res* 2017;121:181-195.
16. Bootman MD, Smyrnias I, Thul R, Coombes S, Roderick HL. Atrial cardiomyocyte calcium signalling. *Biochimica et biophysica acta* 2011;1813:922-934.
17. Brandenburg S, Kohl T, Williams GS, Gusev K, Wagner E, Rog-Zielinska EA, Hebisch E, Dura M, Didie M, Gotthardt M, Nikolaev VO, Hasenfuss G, Kohl P, Ward CW, Lederer WJ, Lehnart SE. Axial tubule junctions control rapid calcium signaling in atria. *J Clin Invest* 2016;126:3999-4015.
18. Deswal A, Petersen NJ, Feldman AM, Young JB, White BG, Mann DL. Cytokines and cytokine receptors in advanced heart failure: an analysis of the cytokine database from the Vesnarinone trial (VEST). *Circulation* 2001;103:2055-2059.
19. Yokoyama T, Vaca L, Rossen RD, Durante W, Hazarika P, Mann DL. Cellular basis for the negative inotropic effects of tumor necrosis factor-alpha in the adult mammalian heart. *J Clin Invest* 1993;92:2303-2312.
20. Yokoyama T, Nakano M, Bednarczyk JL, McIntyre BW, Entman M, Mann DL. Tumor necrosis factor-alpha provokes a hypertrophic growth response in adult cardiac myocytes. *Circulation* 1997;95:1247-1252.
21. Savvatis K, Muller I, Frohlich M, Pappritz K, Zietsch C, Hamdani N, Grote K, Schieffer B, Klingel K, Van Linthout S, Linke WA, Schultheiss HP, Tschope C. Interleukin-6 receptor inhibition modulates the immune reaction and restores titin phosphorylation in experimental myocarditis. *Basic Res Cardiol* 2014;109:449.
22. Anker SD, Coats AJ. How to RECOVER from RENAISSANCE? The significance of the results of RECOVER, RENAISSANCE, RENEWAL and ATTACH. *Int J Cardiol* 2002;86:123-130.

23. Chung ES, Packer M, Lo KH, Fasanmade AA, Willerson JT, Anti TNFTACHFI. Randomized, double-blind, placebo-controlled, pilot trial of infliximab, a chimeric monoclonal antibody to tumor necrosis factor-alpha, in patients with moderate-to-severe heart failure: results of the anti-TNF Therapy Against Congestive Heart Failure (ATTACH) trial. *Circulation* 2003;107:3133-3140.
24. Ridker PM, Everett BM, Thuren T, MacFadyen JG, Chang WH, Ballantyne C, Fonseca F, Nicolau J, Koenig W, Anker SD, Kastelein JJP, Cornel JH, Pais P, Pella D, Genest J, Cifkova R, Lorenzatti A, Forster T, Kobalava Z, Vida-Simiti L, Flather M, Shimokawa H, Ogawa H, Dellborg M, Rossi PRF, Troquay RPT, Libby P, Glynn RJ, Group CT. Antiinflammatory Therapy with Canakinumab for Atherosclerotic Disease. *N Engl J Med* 2017;377:1119-1131.
25. Gamad N, Shafiq N, Malhotra S. Effect size in CANTOS trial. *BMJ Evid Based Med* 2018;23:44.
26. Everett BM, Cornel JH, Lainscak M, Anker SD, Abbate A, Thuren T, Libby P, Glynn RJ, Ridker PM. Anti-Inflammatory Therapy With Canakinumab for the Prevention of Hospitalization for Heart Failure. *Circulation* 2019;139:1289-1299.
27. Sharkovska Y, Kalk P, Lawrenz B, Godes M, Hoffmann LS, Wellkisch K, Geschka S, Relle K, Hocher B, Stasch JP. Nitric oxide-independent stimulation of soluble guanylate cyclase reduces organ damage in experimental low-renin and high-renin models. *Journal of hypertension* 2010;28:1666-1675.
28. van Dijk CG, Oosterhuis NR, Xu YJ, Brandt M, Paulus WJ, van Heerebeek L, Duncker DJ, Verhaar MC, Fontoura D, Lourenco AP, Leite-Moreira AF, Falcao-Pires I, Joles JA, Cheng C. Distinct Endothelial Cell Responses in the Heart and Kidney Microvasculature Characterize the Progression of Heart Failure With Preserved Ejection Fraction in the Obese ZSF1 Rat With Cardiorenal Metabolic Syndrome. *Circulation Heart failure* 2016;9:e002760.
29. Hamdani N, Franssen C, Lourenco A, Falcao-Pires I, Fontoura D, Leite S, Plettig L, Lopez B, Ottenheijm CA, Becher PM, Gonzalez A, Tschope C, Diez J, Linke WA, Leite-Moreira AF, Paulus WJ. Myocardial titin hypophosphorylation importantly contributes to heart failure with preserved ejection fraction in a rat metabolic risk model. *Circulation Heart failure* 2013;6:1239-1249.
30. Hohendanner F, Bode D, Primessnig U, Guthof T, Doerr R, Jeuthe S, Reimers S, Zhang K, Bach D, Wakula P, Pieske BM, Heinzel FR. Cellular mechanisms of metabolic syndrome-related atrial decompensation in a rat model of HFpEF. *Journal of molecular and cellular cardiology* 2018;115:10-19.
31. Bode D, Lindner D, Schwarzl M, Westermann D, Deissler P, Primessnig U, Hegemann N, Blatter LA, van Linthout S, Tschope C, Schoenrath F, Soltani S, Stamm C, Duesterhoeft V, Rolim N, Wisloff U, Knosalla C, Falk V, Pieske BM, Heinzel FR, Hohendanner F. The role of fibroblast - Cardiomyocyte interaction for atrial dysfunction in HFpEF and hypertensive heart disease. *J Mol Cell Cardiol* 2019;131:53-65.

32. Miranda-Silva D, Wust RCI, Conceicao G, Goncalves-Rodrigues P, Goncalves N, Goncalves A, Kuster DWD, Leite-Moreira AF, van der Velden J, de Sousa Beleza JM, Magalhaes J, Stienen GJM, Falcao-Pires I. Disturbed cardiac mitochondrial and cytosolic calcium handling in a metabolic risk-related rat model of heart failure with preserved ejection fraction. *Acta physiologica* 2019:e13378.
33. Sartiani L, Bochet P, Cerbai E, Mugelli A, Fischmeister R. Functional expression of the hyperpolarization-activated, non-selective cation current I(f) in immortalized HL-1 cardiomyocytes. *J Physiol* 2002;545:81-92.
34. Leckband D, Sivasankar S. Cadherin recognition and adhesion. *Current opinion in cell biology* 2012;24:620-627.
35. van Deel ED, Najafi A, Fontoura D, Valent E, Goebel M, Kardux K, Falcao-Pires I, van der Velden J. In vitro model to study the effects of matrix stiffening on Ca(2+) handling and myofilament function in isolated adult rat cardiomyocytes. *J Physiol* 2017;595:4597-4610.
36. Bode D, Guthof T, Pieske BM, Heinzel FR, Hohendanner F. Isolation of Atrial Cardiomyocytes from a Rat Model of Metabolic Syndrome-related Heart Failure with Preserved Ejection Fraction. *Journal of visualized experiments : JoVE* 2018.
37. Piper HM. The calcium paradox revisited: an artefact of great heuristic value. *Cardiovasc Res* 2000;45:123-127.
38. de Boer RA, De Keulenaer G, Bauersachs J, Brutsaert D, Cleland JG, Diez J, Du XJ, Ford P, Heinzel FR, Lipson KE, McDonagh T, Lopez-Andres N, Lunde IG, Lyon AR, Pollesello P, Prasad SK, Tocchetti CG, Mayr M, Sluijter JPG, Thum T, Tschope C, Zannad F, Zimmermann WH, Ruschitzka F, Filippatos G, Lindsey ML, Maack C, Heymans S. Towards better definition, quantification and treatment of fibrosis in heart failure. A scientific roadmap by the Committee of Translational Research of the Heart Failure Association (HFA) of the European Society of Cardiology. *European journal of heart failure* 2019;21:272-285.
39. Wu X, Zhang T, Bossuyt J, Li X, McKinsey TA, Dedman JR, Olson EN, Chen J, Brown JH, Bers DM. Local InsP3-dependent perinuclear Ca2+ signaling in cardiac myocyte excitation-transcription coupling. *The Journal of clinical investigation* 2006;116:675-682.
40. Ahmad FA, Petrie MC, McMurray JJV, Lang NN. Personalized medicine and hospitalization for heart failure: if we understand it, we may be successful in treating it. *Eur J Heart Fail* 2019;21:699-702.

5. Eidesstattliche Versicherung

„Ich, David Bode, versichere an Eides statt durch meine eigenhändige Unterschrift, dass ich die vorgelegte Dissertation mit dem Thema: “Cellular mechanisms of left atrial contractile dysfunction in heart failure with preserved ejection fraction and hypertensive heart disease” bzw. „Zelluläre Mechanismen der linksatrialen kontraktilen Dysfunktion bei Herzinsuffuzienz mit erhaltener Auswurfleistung und Hypertensiver Herzerkrankung“ selbstständig und ohne nicht offengelegte Hilfe Dritter verfasst und keine anderen als die angegebenen Quellen und Hilfsmittel genutzt habe.

Alle Stellen, die wörtlich oder dem Sinne nach auf Publikationen oder Vorträgen anderer Autoren/innen beruhen, sind als solche in korrekter Zitierung kenntlich gemacht. Die Abschnitte zu Methodik (insbesondere praktische Arbeiten, Laborbestimmungen, statistische Aufarbeitung) und Resultaten (insbesondere Abbildungen, Graphiken und Tabellen) werden von mir verantwortet.

Ich versichere ferner, dass ich die in Zusammenarbeit mit anderen Personen generierten Daten, Datenauswertungen und Schlussfolgerungen korrekt gekennzeichnet und meinen eigenen Beitrag sowie die Beiträge anderer Personen korrekt kenntlich gemacht habe (siehe Anteilserklärung). Texte oder Textteile, die gemeinsam mit anderen erstellt oder verwendet wurden, habe ich korrekt kenntlich gemacht.

Meine Anteile an etwaigen Publikationen zu dieser Dissertation entsprechen denen, die in der untenstehenden gemeinsamen Erklärung mit dem/der Erstbetreuer/in, angegeben sind. Für sämtliche im Rahmen der Dissertation entstandenen Publikationen wurden die Richtlinien des ICMJE (International Committee of Medical Journal Editors; www.icmje.og) zur Autorenschaft eingehalten. Ich erkläre ferner, dass ich mich zur Einhaltung der Satzung der Charité – Universitätsmedizin Berlin zur Sicherung Guter Wissenschaftlicher Praxis verpflichte.

Weiterhin versichere ich, dass ich diese Dissertation weder in gleicher noch in ähnlicher Form bereits an einer anderen Fakultät eingereicht habe.

Die Bedeutung dieser eidesstattlichen Versicherung und die strafrechtlichen Folgen einer unwahren eidesstattlichen Versicherung (§§156, 161 des Strafgesetzbuches) sind mir bekannt und bewusst.“

_____ _____

Datum Unterschrift

6. Anteilserklärung

David Bode hatte folgenden Anteil an den folgenden Publikationen:

Publikation 1: Bode D, Lindner D, Schwarzl M, Westermann D, Deissler P, Primessnig U, Hegemann N, Blatter LA, van Linthout S, Tschöpe C, Schoenrath F, Soltani S, Stamm C, Duesterhoeft V, Rolim N, Wisløff U, Knosalla C, Falk V, Pieske BM, Heinzel FR, Hohendanner F, "The role of fibroblast - Cardiomyocyte interaction for atrial dysfunction in HFpEF and hypertensive heart disease.", *Journal of Molecular and Cellular Cardiology*, 2019

Beitrag im Einzelnen: Ich habe die Zellisolation etabliert (Details siehe Publikation 2) und für diese Studie durchgeführt. Ich habe die durchlichtmikroskopischen Experimente (Zellmorphologie: Fig. 2 A,B; Kantendetektion Fig. 2 D-G) durchgeführt, analysiert, statistisch ausgewertet und visualisiert. Ich habe die ratiometrische und konfokale Ca^{2+} sensitive Mikroskopie (Fig. 3-5, Fig. 6 E,F, 7 E-J, 8 A-L) durchgeführt, analysiert, statistisch ausgewertet und visualisiert. Ich habe die molekularbiologische Untersuchung mittels Enzyme-linked Immunosorbent Assay (Fig. 6 A-D, Fig. 8 M-O) durchgeführt, analysiert und visualisiert. Ich habe die Erstfassung des Manuskriptes geschrieben.

Publikation 2: Bode D, Guthof T, Pieske BM, Heinzel FR, Hohendanner, F. "Isolation of Atrial Cardiomyocytes from a Rat Model of Metabolic Syndrome-related Heart Failure with Preserved Ejection Fraction.", *Journal of Visualized Experiments*, 2018

Beitrag im Einzelnen: Ich habe die beschriebene Methode zur Isolation primärer linksatrialer Kardiomyozyten an unserem Standort etabliert (enzymatische Verdauung mittels Langendorff Apparatur) und die Druckmanipulation zur Ergebnisoptimierung entwickelt (siehe Fig. 3). Ich habe das Konzept für die Publikation entworfen. Ich habe die Experimente zur Darstellung repräsentativer Ergebnisse durchgeführt (Fig. 4, 5; Zellisolation, Durchlichtmikroskopie, Ca^{2+} sensitive Mikroskopie, Darstellung mitochondrialer und tubulärer Strukturen) und visuell dargestellt. Ich habe die Anleitungsschemata angefertigt (Fig. 1-3, Tab. 1,2). Ich habe die Erstfassung des Manuskriptes geschrieben. Ich habe die Zellisolation und sukzessive Mikroskopie für die audiovisuelle Aufzeichnung durch die Fachzeitschrift durchgeführt.

Publikation 3: Hohendanner F, Bode D, Primessnig U, Guthof T, Doerr R, Jeuthe S, Reimers S, Zhang K, Bach D, Wakula P, Pieske BM, Heinzel FR, "Cellular mechanisms of metabolic syndrome-related atrial decompensation in a rat model of HFpEF.", *Journal of Molecular and Cellular Cardiology*, 2018

Beitrag im Einzelnen: Ich habe die Zellisolation etabliert (Details siehe Publikation 2) und für diese Studie durchgeführt. Ich habe die die konfokalmikroskopischen Experimente der Ca^{2+} Homöostase (Fig. 2, 4, 5) und des tubulären Netzwerks (Fig. 3) durchgeführt, analysiert und statistisch ausgewertet.

_____

Unterschrift, Datum und Stempel des erstbetreuenden Hochschullehrers

_____

Unterschrift des Doktoranden/der Doktorandin

7. Publications

7.1 Bode D, Lindner D, Schwarzl M, Westermann D, Deissler P, Primessnig U, Hegemann N, Blatter LA, van Linthout S, Tschöpe C, Schoenrath F, Soltani S, Stamm C, Duesterhoeft V, Rolim N, Wisløff U, Knosalla C, Falk V, Pieske BM, Heinzel FR, Hohendanner F. The role of fibroblast - Cardiomyocyte interaction for atrial dysfunction in HFpEF and hypertensive heart disease. Journal of Molecular and Cellular Cardiology. 2019 Jun;131:53-65.

Journal Data Filtered By: **Selected JCR Year: 2018** Selected Editions: SCIE,SSCI Selected Categories: **"CARDIAC and CARDIOVASCULAR SYSTEMS"** Selected Category Scheme: WoS

Gesamtanzahl: 136 Journale

Rank	Full Journal Title	Total Cites	Journal Impact Factor	Eigenfactor Score
1	EUROPEAN HEART JOURNAL	57,358	23.239	0.125920
2	CIRCULATION	166,484	23.054	0.211290
3	JOURNAL OF THE AMERICAN COLLEGE OF CARDIOLOGY	100,986	18.639	0.193290
4	Nature Reviews Cardiology	6,301	17.420	0.018820
5	CIRCULATION RESEARCH	52,988	15.862	0.072290
6	EUROPEAN JOURNAL OF HEART FAILURE	13,107	13.965	0.027620
7	JAMA Cardiology	3,280	11.866	0.019320
8	JACC-Cardiovascular Imaging	8,801	10.975	0.026160
9	JACC-Cardiovascular Interventions	11,555	9.544	0.033640
10	JACC-Heart Failure	3,537	8.910	0.016830
11	JOURNAL OF HEART AND LUNG TRANSPLANTATION	12,436	8.578	0.027310
12	CARDIOVASCULAR RESEARCH	21,828	7.014	0.021500
13	European Heart Journal-Cardiovascular Pharmacotherapy	442	6.723	0.001430
14	Circulation-Heart Failure	6,900	6.526	0.022830
15	BASIC RESEARCH IN CARDIOLOGY	4,137	6.470	0.005590
16	PROGRESS IN CARDIOVASCULAR DISEASES	4,055	6.162	0.008860
17	JOURNAL OF THE AMERICAN SOCIETY OF ECHOCARDIOGRAPHY	10,478	6.111	0.016060
18	EUROPACE	10,908	6.100	0.025320
19	Circulation-Cardiovascular Interventions	5,289	6.060	0.016640

Rank	Full Journal Title	Total Cites	Journal Impact Factor	Eigenfactor Score
20	Cardiovascular Diabetology	5,392	5.948	0.011550
21	Circulation-Cardiovascular Imaging	5,456	5.813	0.018480
22	European Journal of Preventive Cardiology	4,782	5.640	0.013370
23	CANADIAN JOURNAL OF CARDIOLOGY	6,710	5.592	0.018500
24	JOURNAL OF THORACIC AND CARDIOVASCULAR SURGERY	29,599	5.261	0.036950
25	European Heart Journal-Cardiovascular Imaging	5,498	5.260	0.021650
26	HEART RHYTHM	12,344	5.225	0.029030
27	REVISTA ESPANOLA DE CARDIOLOGIA	3,566	5.126	0.004640
28	HEART	18,063	5.082	0.030620
29	JOURNAL OF CARDIOVASCULAR MAGNETIC RESONANCE	5,113	5.070	0.014020
30	JOURNAL OF MOLECULAR AND CELLULAR CARDIOLOGY	14,143	5.055	0.020450
31	Circulation-Arrhythmia and Electrophysiology	6,432	4.968	0.017840
32	Clinical Research in Cardiology	3,022	4.907	0.006760
33	Circulation-Cardiovascular Genetics	3,441	4.864	0.010500
34	Journal of the American Heart Association	13,230	4.660	0.060340
35	TRENDS IN CARDIOVASCULAR MEDICINE	2,667	4.462	0.003930
36	Circulation-Cardiovascular Quality and Outcomes	4,531	4.378	0.014350
37	ATHEROSCLEROSIS	23,442	4.255	0.033500
38	CARDIOVASCULAR DRUGS AND THERAPY	2,109	4.181	0.003140
39	JOURNAL OF NUCLEAR CARDIOLOGY	3,711	4.112	0.004480

Journal of Molecular and Cellular Cardiology 131 (2019) 53–65

Contents lists available at ScienceDirect

Journal of Molecular and Cellular Cardiology

journal homepage: www.elsevier.com/locate/yjmcc

Original article

The role of fibroblast – Cardiomyocyte interaction for atrial dysfunction in HFpEF and hypertensive heart disease

David Bode[a,b,e], Diana Lindner[c,d], Michael Schwarzl[c,d], Dirk Westermann[c,d], Peter Deissler[a,b], Uwe Primessnig[a,b,e], Niklas Hegemann[a,b], Lothar A. Blatter[f], Sophie van Linthout[a,b], Carsten Tschöpe[a,b], Felix Schoenrath[b,g], Sajjad Soltani[b,g], Christof Stamm[b,g], Volker Duesterhoeft[b,g], Natale Rolim[j], Ulrik Wisløff[j], Christoph Knosalla[b,g], Volkmar Falk[b,g,h], Burkert M. Pieske[a,b,e,i], Frank R. Heinzel[a,b], Felix Hohendanner[a,b,e,*]

[a] Department of Internal Medicine and Cardiology, Charité – Universitätsmedizin Berlin, Campus Virchow-Klinikum, Augustenburgerplatz 1, 13353 Berlin, Germany
[b] DZHK (German Centre for Cardiovascular Research), partner site Berlin, Germany
[c] DZHK (German Centre for Cardiovascular Research), partner site Hamburg, Germany
[d] Universitäres Herzzentrum Hamburg, Klinik für Allgemeine und Interventionelle Kardiologie, 20246 Hamburg, Germany
[e] Berlin Institute of Health (BIH), Berlin, Germany
[f] Department of Physiology and Biophysics, Rush University, Chicago, USA
[g] Department of Cardiothoracic Surgery, German Heart Center Berlin, Augustenburgerplatz 1, 13353 Berlin, Germany
[h] Department of Cardiothoracic Surgery, Charité – Universitätsmedizin Berlin, corporate member of Freie Universität Berlin, Humboldt-Universität zu Berlin and Berlin Institute of Health, Germany
[i] Department of Internal Medicine and Cardiology, German Heart Center Berlin, 13353 Berlin, Germany
[j] K.G. Jebsen Center of Exercise in Medicine, Department of Circulation and Medical Imaging, Norwegian University of Science and Technology (NTNU), Trondheim, Norway.

ARTICLE INFO

Keywords:
Atrial remodeling
HFpEF
Cardiac fibroblasts
Atrial cardiomyocyte
Excitation-contraction coupling

ABSTRACT

Aims: Atrial contractile dysfunction is associated with increased mortality in heart failure (HF). We have shown previously that a metabolic syndrome-based model of HFpEF and a model of hypertensive heart disease (HHD) have impaired left atrial (LA) function in vivo (rat). In this study we postulate, that left atrial cardiomyocyte (CM) and cardiac fibroblast (CF) paracrine interaction related to the inositol 1,4,5-trisphosphate signalling cascade is pivotal for the manifestation of atrial mechanical dysfunction in HF and that quantitative atrial remodeling is highly disease-dependent.

Methods and results: Differential remodeling was observed in HHD and HFpEF as indicated by an increase of atrial size in vivo (HFpEF), unchanged fibrosis (HHD and HFpEF) and a decrease of CM size (HHD). Baseline contractile performance of rat CM in vitro was enhanced in HFpEF. Upon treatment with conditioned medium from their respective stretched CF (CM-SF), CM (at 21 weeks) of WT showed increased Ca^{2+} transient (CaT) amplitudes related to the paracrine activity of the inotrope endothelin (ET-1) and inositol 1,4,5-trisphosphate induced Ca^{2+} release. Concentration of ET-1 was increased in CM-SF and atrial tissue from WT as compared to HHD and HFpEF. In HHD, CM-SF had no relevant effect on CaT kinetics. However, in HFpEF, CM-SF increased diastolic Ca^{2+} and slowed Ca^{2+} removal, potentially contributing to an in-vivo decompensation. During disease progression (i.e. at 27 weeks), HFpEF displayed dysfunctional excitation-contraction-coupling (ECC) due to lower sarcoplasmic-reticulum Ca^{2+} content unrelated to CF-CM interaction or ET-1, but associated with enhanced nuclear [Ca^{2+}]. In human patients, tissue ET-1 was not related to the presence of arterial hypertension or obesity.

Conclusions: Atrial remodeling is a complex entity that is highly disease and stage dependent. The activity of fibrosis related to paracrine interaction (e.g. ET-1) might contribute to in vitro and in vivo atrial dysfunction. However, during later stages of disease, ECC is impaired unrelated to CF.

* Corresponding author at: Department of Internal Medicine and Cardiology, Charité University Medicine, CVK, Augustenburger Platz 1, 13353 Berlin, Germany.
E-mail address: felix.hohendanner@charite.de (F. Hohendanner).

https://doi.org/10.1016/j.yjmcc.2019.04.016
Received 17 March 2019; Accepted 17 April 2019
Available online 18 April 2019

List of abbreviations

AF	atrial fibrillation
Bos	Bosentan
CaT	Calcium transient
Ca^{2+}	Calcium
CM	cardiomyocyte
CM-SF	conditioned medium from stretched cardiac fibroblasts
CM-NSF	conditioned medium from non-stretched cardiac fibroblasts
CF	cardiac fibroblast
ECC	excitation-contraction-coupling
ET-1	Endothelin-1
HF	heart failure
HHD	hypertensive heart disease
HFpEF	heart failure with preserved ejection fraction
HFrEF	heart failure with reduced ejection fraction
IL	Interleukin
IP_3	inositol 1,4,5-trisphosphate
LA	left atrium
LA-EF	left atrial ejection fraction
PDGF	Platelet-derived growth factor
RAAS	renin-angiotensin-aldosterone-system
SR	sarcoplasmic reticulum
TGF	Transforming growth factor
TNF	Tumor necrosis factor
WT	Wildtype
2-APB	2-Aminoethoxydiphenyl borate

1. Introduction

Heart failure (HF) with preserved ejection fraction (HFpEF) represents a clinical syndrome with patients suffering from typical symptoms of HF, while showing a normal left-ventricular ejection fraction (LVEF; ≥50%) [1]. HFpEF accounts for 40–71% of HF patients. While pharmacological treatment significantly improved clinical outcomes of patients with systolic heart failure (HFrEF), the prognosis for patients suffering from HFpEF has remained unchanged [2]. Metabolic syndrome has been associated with diastolic dysfunction and identified as an independent predictor of new-onset HFpEF [3].

Left atrial (LA) remodeling is a hallmark feature of HFpEF and other cardiac diseases (e.g. hypertensive heart disease (HHD)) and commonly associated with LA enlargement and dysfunction. LA remodeling is a predictor of new-onset HF [4] and atrial fibrillation (AF), while reduction in LA ejection fraction (LA-EF) is an independent predictor of mortality [5]. Growing insight into the key role of atrial function in cardiac disease has recently given rise to the concept of 'atrial cardiomyopathies' [6]. While highly prevalent, the quantification of different stages of atrial remodeling during HF and preceding conditions as well as the underlying mechanisms remain elusive.

Pathological hypertrophy and interstitial fibrosis are hallmarks of HF. Increased fibrosis per se is an important contributor to mechanical and electrical dysfunction as fibroblasts do not contribute to contractile function and affect electrical propagation. However, fibrosis might influence neighboring CM also directly via paracrine mediators. Recently we have identified neurohumoral activation, involving the renin-angiotensin-aldosterone-system (RAAS) as a potential contributor to contractile dysfunction in HFpEF-related LA remodeling [7]. Beside the RAAS, myocardial inflammation and a pro-fibrotic environment are pivotal triggers of adverse myocardial remodeling and may pose interesting targets for the development of drug therapies [8]. In cardiac tissue, paracrine mediators play an integral part in intercellular communication and have been shown to mediate interstitial myocardial fibrosis [9,10]. In turn, activated cardiac fibroblasts (CF) have been shown to contribute to myocardial inflammation in patients with HFpEF [11]. Experimental studies suggest, that CF-derived mediators are capable of directly altering CM function via regulation of gap junctions and ion channel expression [12].

We postulate, that the interaction between CM and CF via CF-derived mediators is pivotal for atrial in vivo and in vitro dysfunction in HFpEF, as well as in HHD. We also postulate that independent of fibrosis quantity, its "activity" significantly influences atrial function. We further investigated paracrine mediators like ET-1 and their relevance for atrial function in this context. At the same time, we seek to provide evidence that differential cellular and in vivo remodeling can be observed during different stages of HHD and HFpEF. The present data helps to establish a crucial role for direct cellular CM – CF interaction in several clinically highly relevant settings of atrial dysfunction (i.e. hypertensive heart disease and HFpEF). In a translational approach, we also investigated an association of a CF-derived mediator (i.e. atrial tissue ET-1) and the presence of particular co-morbidities (i.e. arterial hypertension, obesity) in humans.

2. Methods

The investigation conforms to the *Guide for the Care and Use of Laboratory Animals* published by the US National Institutes of Health (NIH Publication No. 85–23, revised 1985) and the principles outlined in the *Declaration of Helsinki* (*Br Med J* 1964; **ii:** 177).

2.1. Patient data

All patients gave written informed consent to participate in the study (DZHK Biobank, German Heart Center Berlin). Excess patient tissue was obtained from right atria during routine surgery and clinical data (presence of overt arterial hypertension, i.e. systolic blood pressure > 139 mmHg; obesity, i.e. body mass index > 25 kg/m^2) was gathered from existing in-hospital documentation.

2.2. Animal echocardiography

Echocardiography was performed as previously described [13]. In brief, rats were anesthetized and transthoracic echocardiography performed with a high-resolution micro-imaging system equipped with a 17.5-Mhz linear array transducer (Vevo770TM Imaging System, VisualSonics, USA) using standard 2D imaging. Measurements were performed to assess changes in LA dimensions (LA size) from at least three consecutive cardiac cycles under stable conditions.

2.3. HF model

Animal experiments were approved by local authorities (G0276/16). The well characterized ZFS-1 HF rat model is based on a leptin receptor mutation leading to a lean (heterozygous; arterial hypertension) and obese (homozygous; metabolic syndrome, HFpEF) phenotype [14]. WT, HHD and HFpEF animals were fed a high caloric diet (Formulab Diet 5008). LA CM were isolated from 21-week-old ZSF-1 lean (HHD; $ZSF^{+/-}$), ZFS-1 obese (HFpEF; $ZSF^{+/+}$) and wild type (WT; Wistar Kyoto; Charles River) and after disease progression at 27–28 weeks from HFpEF (still without systolic dysfunction [15]) and WT as previously described [13]. WT animals (CTRL; Wistar; Charles River) for in-vitro experiments with bosentan and 2-APB were fed standard diet for 21 weeks.

2.4. CM isolation

Animals were anesthetized with isoflurane and euthanized by cervical dislocation. The heart was excised, mounted on a Langendorff-apparatus and perfused with nominally Calcium (Ca^{2+})-free Tyrode solution for 3 min, followed by enzyme solution containing 0.035 Wünsch units/ml Liberase TM and 10 μM Ca^{2+}. The LA was separated from the heart, minced, filtered and washed. Isolated cells were stepwise adjusted to Tyrode solution containing 1 mM Ca^{2+} and kept at room temperature until subsequent experimentation.

2.5. ELISA

ELISAs were performed according to the manufacturers' protocol (R &D Systems, Minneapolis, MN: IL-1β, IL-6, IL-10, IL-33, PDGF, TGF-β, TNF-α; Enzo Life Sciences, Lausen, Switzerland: ET-1).

2.6. Histologic analysis

Hearts were excised after euthanasia, washed in phosphate-buffered-saline and the LA separated from the remaining organ. Tissue specimen were fixed and paraffin-embedded. Histologic slides were stained with Picrosirius Red (Morphisto, Frankfurt am Main, Germany) in order to assess cardiac fibrosis.

Interstitial myocardial fibrosis was defined as the percentage fraction of Picrosirius Red-stained collagen fibers from the total image. Endo- and epicardial fibrotic tissue was manually excluded by a blinded expert in veterinary pathology. Interstitial myocardial fibrosis was automatically assessed and calculated using ImageJ (National Institutes of Health, Bethesda, MD; ImageJ Macro attached in Supplement).

2.7. Solution and chemicals

Chemicals were obtained from Sigma-Aldrich (St. Louis, MO, USA) unless noted otherwise. Fluorescent Ca^{2+} indicators Fluo-4 AM and Fura-2 AM were obtained from Thermo Fisher Scientific (Waltham, MA, USA). Tyrode solution contained (in mM): 130 NaCl, 4 KCl, 2 CaCl, 1 $MgCl_2$, 10 Glucose, 10 HEPES; pH adjusted to 7.4 with NaOH. Cells were plated on laminin-coated glass coverslips. For experiments with condition medium derived from CF, the respective medium was diluted 1:1 with Tyrode solution and cells incubated for 1 h at 37 °C. The endothelin receptor blocker Bosentan and the inositol-1,4,5-trisphosphate (IP_3)-receptor blocker 2-Aminoethoxydiphenyl borate (2-APB) were used at a concentration of 100 and 10 μM, respectively.

2.8. Cell culture

The hearts from 21-week-old rats were used to obtain primary CF from LA tissue as described previously [16]. LA tissue was used from a total of 4 animals/group for the subsequent steps. After separation of atria and ventricle, tissue was digested in 0.1 mg/ml Liberase (Roche, Germany) dissolved in Hanks' Balanced Salt Solution while gently shaking at 37 °C for 10 min. The supernatant containing the isolated cells was collected and immediately placed on ice. The remaining tissue was used for an additional digestion cycle. This tissue digestion was repeated six times consecutively. Cells were separated through a cell strainer and enzymatic solution was removed after centrifugation. Cells were collected in complete growth medium (Dulbecco's Modified Eagle Medium (DMEM)) containing 20% fetal calf serum (FCS), 100 U/ml penicillin and 100 μg/ml streptomycin and seeded in cell culture flask. For sub-culturing, cells were detached utilizing trypsin/EDTA solution. To mechanically activate CF, cells were placed on collagen-I coated flexible-bottomed 6-well culture plates (Bioflex plates, Dunn). Mechanical stretch was applied using the Flexercell System FX-4000 Tension Plus (Dunn) to deform the cultured cells using an elongation of 10% at a frequency of 1 Hz. Prior to mechanical stretch, cells were starved overnight in serum reduced medium (DMEM containing 0.5% FCS, 100 U/ml penicillin and 100 μg/ml streptomycin. The mechanical stimulation was performed in the presence of a protease inhibitor cocktail (P1860) for 3 h to investigate gene expression analysis or for 72 h to produce the cell culture supernatant for subsequent cellular experiments.

2.9. Confocal and ratiometric Ca^{2+} measurements

For confocal Ca^{2+} measurements, cells were loaded with Fluo-4 AM as previously described [7]. Transversal or longitudinal confocal line scan images were recorded at 1250 lines per second using a 40× oil-immersion objective lens (NA: 1.49; pixel size 0.12 μm) with a Zeiss LSM 800 system. Ca^{2+} transients (CaT) were elicited by electrical field stimulation (frequency: 1 Hz) of intact LA CM with a pair of platinum electrodes (voltage: ~50% above contractile threshold). Changes in Ca^{2+} are expressed as the amplitude $\Delta F/F_0$, where F represents time-dependent Fluo-4 fluorescence, F_0 represents diastolic fluorescence levels under steady-state conditions during electrical stimulation and $\Delta F = F - F_0$. Tau of a mono-exponential fit of the decay of CaT was obtained as a parameter of Ca^{2+} removal. At 27-weeks, a subset of cells was exposed to Tyrode solution containing caffeine (20 mM) and the subsequent Ca^{2+} release, expressed as $\Delta F/F_0$, taken as a measure of Ca^{2+} content of the sarcoplasmic reticulum (SR).

For ratiometric Ca^{2+} measurements, cells were loaded with Fura-2 AM (1 μM; excitation: 340 nm and 380 nm, emission: 510 ± 10 nm) for 30 min at room temperature. Background signals were subtracted and changes of Ca^{2+} are expressed as the ratio $R = F_{340}/F_{380}$.

2.10. Visualization of global cell shortening

For measurements of contractility cell shortening along the longitudinal axis during 1 Hz electrical stimulation was measured with video edge detection (time resolution: 60 frames/s; PTI FelixGX, HORIBA Scientific, Edison, NJ). Cell shortening is expressed as the change in systolic relative to diastolic cell length. Tau of a mono-exponential fit of the decay of contraction traces was obtained as a parameter of cell relaxation.

2.11. Data analysis and statistics

Data were analyzed as previously described [3]. Results are shown as mean ± standard error. Statistical analysis was performed by using unpaired Student's *t*-test or analysis of variance for multiple comparisons, followed by the Bonferroni post-hoc test. A two-tailed *p* value of < 0.05 was used to indicate statistical significance.

3. Results

3.1. LA remodeling in HFpEF and HHD is not related to the degree of fibrosis

LA fibrosis is a hallmark feature of remodeling and LA in vivo function is impaired in HFpEF [7]. However, LA fibrosis was unchanged in HHD at 21 weeks as compared to WT. In HFpEF at 21 weeks, LA interstitial fibrosis was also unchanged compared to WT and HHD (Fig. 1B and C). In order to evaluate the potential contribution of LA fibrosis in advanced disease progression, interstitial fibrosis of HFpEF was evaluated at a later time-point (27 instead of 21 weeks), where again no difference could be observed compared to WT (Fig. 1F).

Similar results were obtained using a semi-quantitative analysis of localized LA fibrosis. Transmural distribution of fibrosis was unchanged (subendocardial, subepicardial, myocardial; Supp. Fig. 1).

3.2. Differential LA remodeling and enhanced in vitro contractile function can be observed in HHD and HFpEF

In addition to the observed unchanged fibrosis, CM size tended to be reduced in HHD (Fig. 2A and B). At the same time, LA diameter was significantly increased in HFpEF vs. HHD and WT, indicating differential LA remodeling (Fig. 2C).

However, in vitro, this was accompanied by a significantly increased cell shortening of LA CM in comparison to WT (Fig. 2D and E). LA CM in HFpEF showed an acceleration of contractile kinetics: Time-to-peak was shorter compared to WT and relaxation (tau) was faster compared to WT and HHD. However, LA CM from HHD showed a significant acceleration in time-to-peak compared to WT, but no

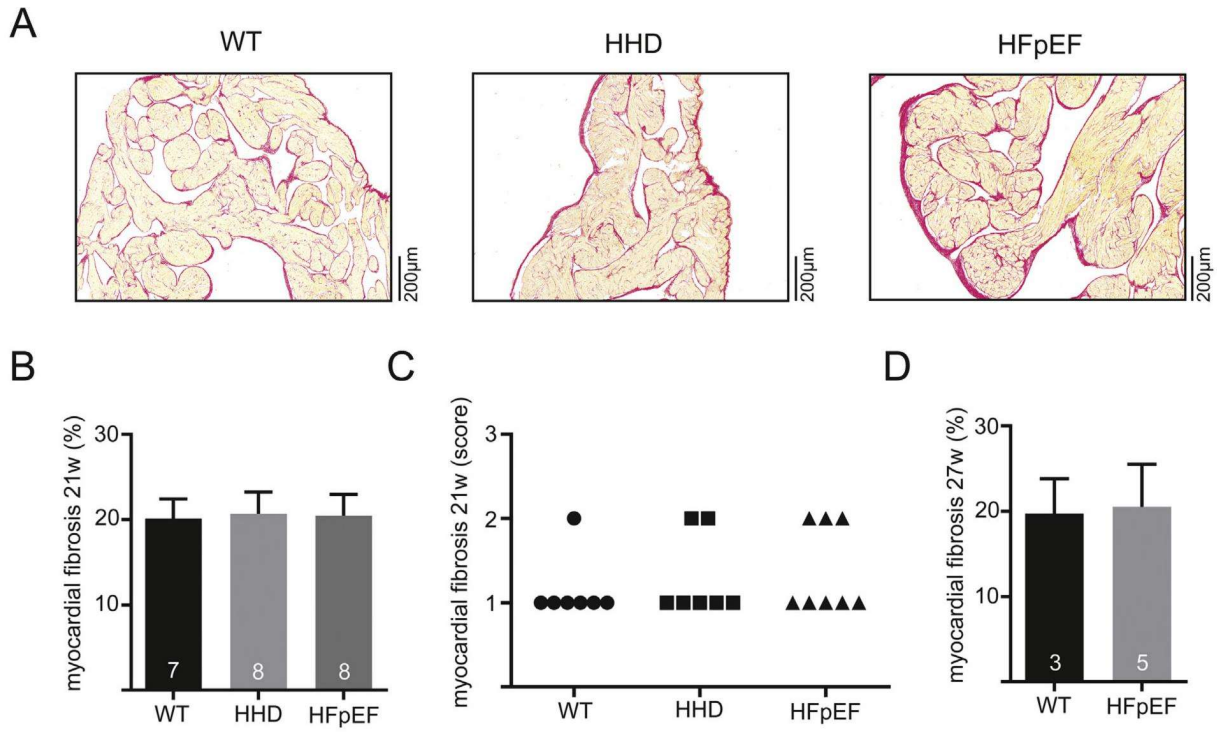

Fig. 1. Example of histologic sections stained with Picro-Sirius Red dye of the left atrium in 21-week-old WT, HHD and HFpEF (A). Fibrotic tissue is indicated by red color. Total myocardial fibrosis quantified by computer-automated analysis (B) and semi-quantitatively assessed by a blinded expert in veterinary pathology at 21 weeks (C). Computer-automated analysis of myocardial fibrosis at 27 weeks (D). (For interpretation of the references to color in this figure legend, the reader is referred to the web version of this article.)

significant change of cell shortening amplitude and cell relaxation (Fig. 2F and G). These results further underscore the differential remodeling observed during HHD and HFpEF at 21 weeks.

3.3. Stretched cardiac fibroblasts enhance Ca^{2+} cycling during excitation-contraction coupling in WT (21w)

LA structure and function showed marked differences on the in vivo and in vitro level in WT, HHD and HFpEF. To resolve the conundrum of an enhanced in vitro function, impaired in vivo function, yet unchanged fibrosis, we next investigated the impact of CF – CM interaction on atrial function in the setting of mechanical stretch in the different models. First, we studied the impact of increased cellular distention as it might occur during conditions of increased preload on WT animals. In order to simulate this condition in vitro, cultured CF from their respective groups were stretched and the conditioned medium collected. Subsequently, isolated LA CM were treated with their respective conditioned medium of unstretched (CM-NSF) or stretched CF (CM-SF) and Ca^{2+} measured ratiometrically. After treatment with CM-NSF, LA CM showed increased diastolic [Ca^{2+}] as compared to control conditions (NT2, Fig. 3B). Interestingly when treated with CM-SF, diastolic [Ca^{2+}] increased even further (Fig. 3B). In addition, CaT amplitudes were significantly increased upon exposure to CM-SF. Similar results were obtained with confocal measurements and a different [Ca^{2+}] sensitive dye (fluo-4, not shown). Confocal measurements were used to differentiate subcellular differences of CaT kinetics: CM-SF led to a faster time-to-peak CaT and faster [Ca^{2+}] removal (i.e. tau was smaller, Fig. 3G and H). The effect was equally strong in subsarcolemmal and central cytosolic compartments of the cells.

3.4. Cardiac fibroblasts alter diastolic Ca^{2+} in HHD (21w)

Next, we repeated these experiments in the HHD animals. Interestingly there was not significant effect on CaT amplitudes or kinetics (Fig. 4C-E), even though diastolic [Ca^{2+}] tended to be increased with CM-NSF as compared to control (NT2, Fig. 4B). In support of this data no difference of amplitude (not shown) or kinetics of CaT were found with confocal [Ca^{2+}] measurements (Fig. 4F-H).

3.5. Stretched cardiac fibroblasts impair LA in vitro function in HFpEF (21w)

LA in HFpEF showed an increased diameter (Fig. 2A), indicating LA remodeling accompanied by increased cellular distention in vivo. Stretch-related changes in the composition of fibroblast medium had significantly different effects on the kinetics of the CaT in CM from HFpEF hearts.

After treatment with CM-SF, LA CM in HFpEF showed significantly increased diastolic Ca^{2+} and a reduced area under the curve for CaT as compared to control. The area under the curve represents a measure of Ca^{2+} exposure of the myofilaments and might therefore correlate with contractility (Fig. 5B and E). As opposed to the previously observed effect in WT, the Ca^{2+} amplitude remained unchanged upon exposure to CM-SF (Fig. 5D). In addition, CM-SF significantly increased tau throughout the cytosol (Fig. 5H), indicating slower cellular relaxation upon exposure to stretched fibroblast media.

3.6. ET-1 and other paracrine mediators are altered in CM-SF and potentially related to the observed functional differences

In order to further explore mechanisms involved in impaired LA function in the animal model, gene expression analysis of cultured CF was performed in search of genomic switches which may contribute to the facilitation of CF-induced ECC dysfunction in LA CM. We found significant changes of IL-6 on the mRNA level upon stretch (Supp. Fig. 2). Additionally, conditioned medium obtained from cultured CF was screened by ELISA for a range of cytokines known to modulate fibrosis and inflammation (Fig. 6). Concentrations of IL-1β, IL-33,

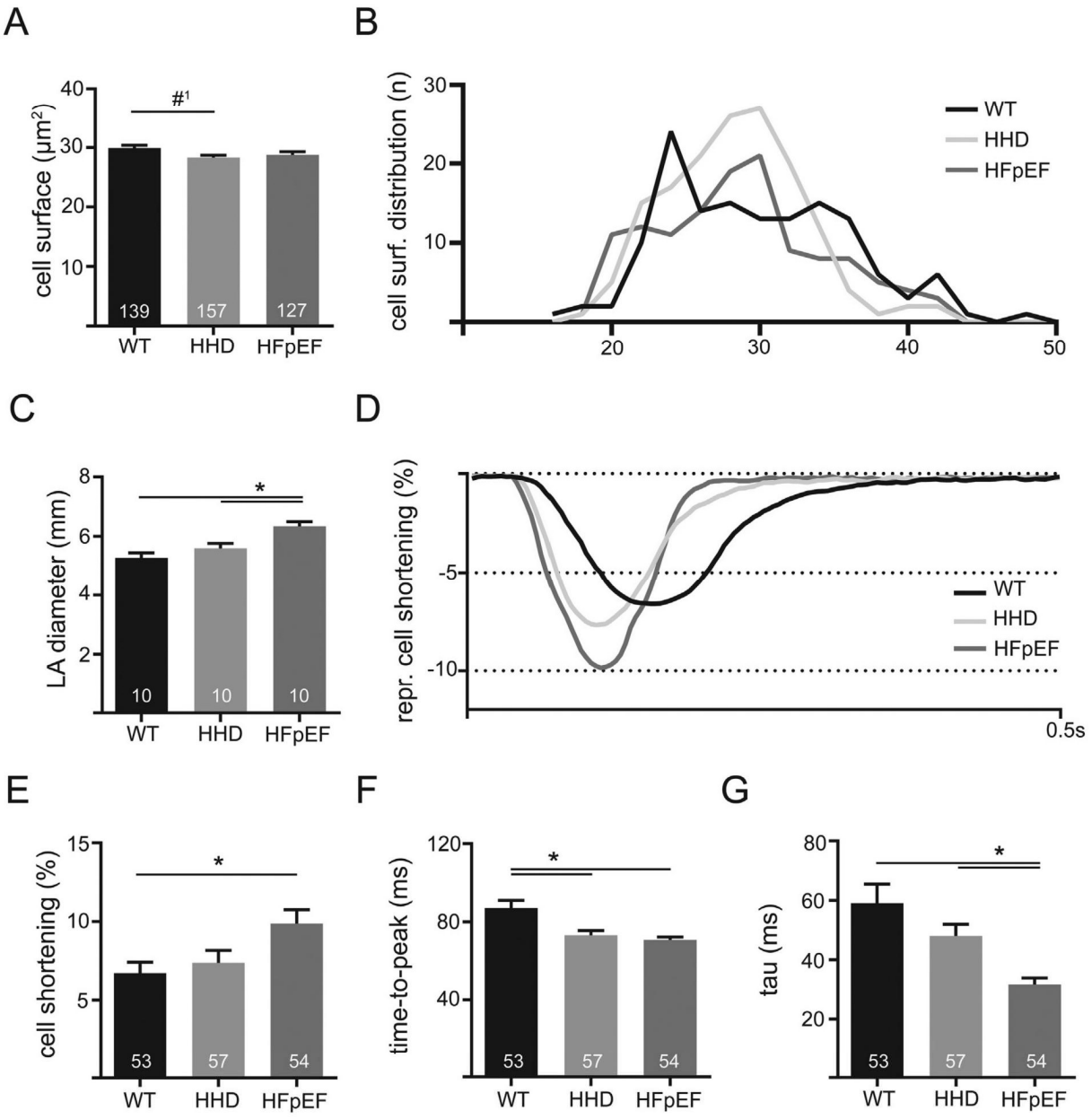

Fig. 2. Cell surface of LA cardiomyocytes of WT, HHD and HFpEF at 21 weeks (A) and the respective distribution frequency (B). LA diameter derived from transthoracic echocardiography in 21-week-old WT, HHD and HFpEF during diastole (C). Example of contractile function recorded with video edge-detection in 21-week-old WT, HHD and HFpEF at baseline conditions and 1 Hz electrical pacing (D). Cell shortening relative to the size of the cell (E), time to reach maximum amplitude (F) and tau of decay (G). *$p < .05$; #¹p = 0.055.

PDGF, TGF-β and TNF-α were below detection threshold (< 31.3 or < 12.5 pg/ml, resp. n.s.). However, as shown in Fig. 6A, ET-1 and IL-6 were especially prevalent in WT CM-SF. While HHD media still contained ET-1 and IL-6 upon stress (Fig. 6B), this response was blunted in HFpEF CM-SF (Fig. 6C). In support of this data, tissue ET-1 concentration was significantly reduced in HFpEF (Fig. 6D). ET-1 is known to be a potent inotrope in a variety of animal models: ET-1 augmented sarcoplasmic reticulum Ca^{2+} release (Suppl. Fig. 3) even in the presence of the ryanodine receptor inhibitor tetracaine. When blocking ET-1 receptors in cells exposed to CM-SF, the inotropic response was mitigated and diastolic and systolic [Ca^{2+}] tended to be even decreased. This indicates that ET-1 is a decisive part of the paracrine "cocktail" mediating positive inotropic effects in WT animals upon stretch (Fig. 6E). In support of this notion, application of the IP_3-receptor blocker 2-APB lowered systolic and diastolic Ca^{2+} to control levels (Fig. 6F). Moreover, the lower concentration of ET-1 in HHD and HFpEF tissue as well as in HHD and HFpEF CM-SF indicates an absent additional production of this inotropic substance upon stretch during atrial remodeling.

3.7. Atrial CM dysfunction is related to impaired excitation-contraction coupling during progression of HFpEF (27w) and paralleled by increased nuclear Ca^{2+}

As shown in Fig. 2, baseline LA CM function was preserved or even improved in HHD and HFpEF, while the interaction between CF and CM led to in vitro decompensation (Figs. 4 and 5). Next, we explored atrial remodeling in the setting of disease progression in HHD and HFpEF. With advanced age, LA diameter was still significantly increased in HHD and HFpEF (Fig. 7B), while LA function was preserved in HHD and

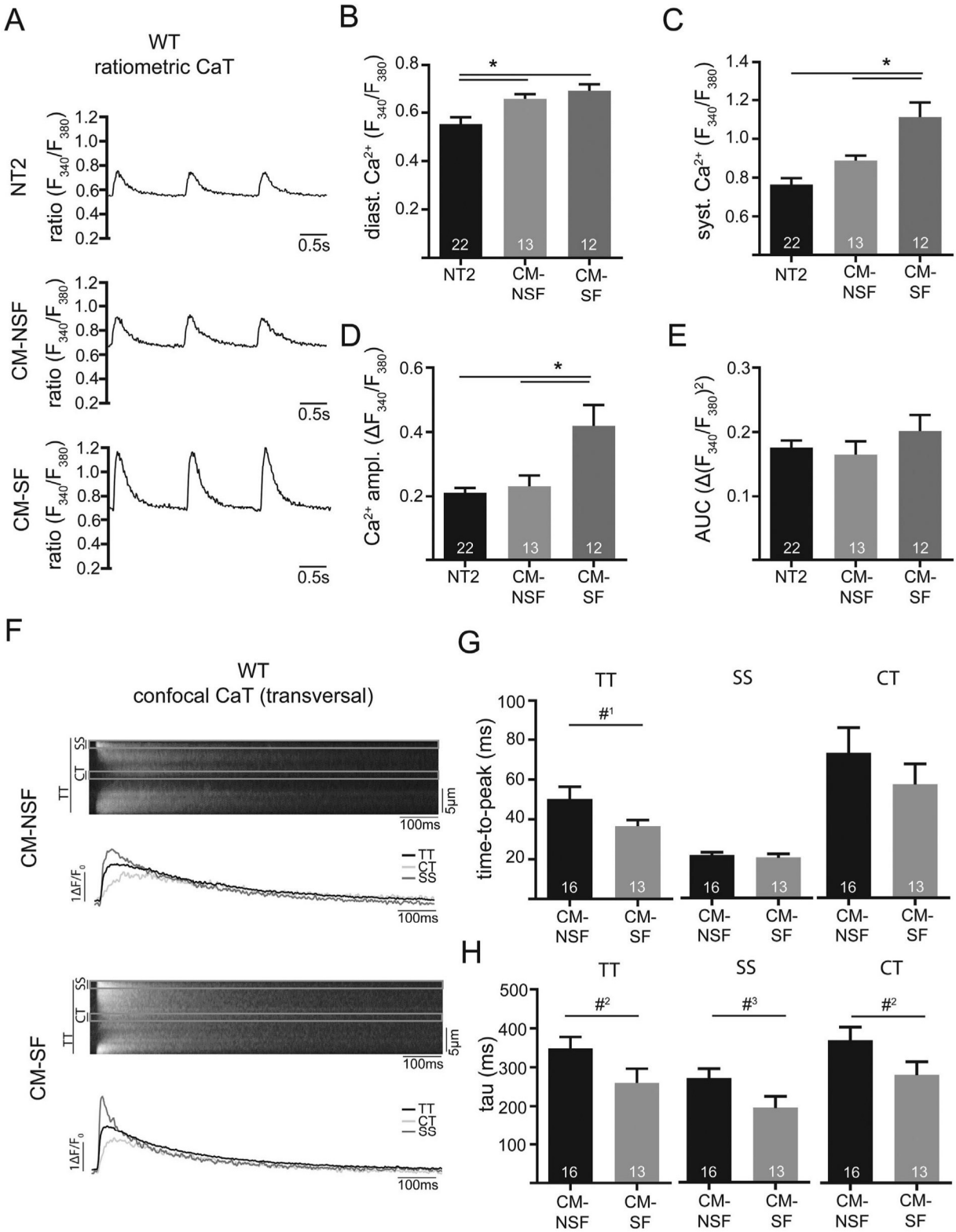

Fig. 3. Example of ratiometrically recorded CaT (Fura-2) after 1 h incubation with either Normal Tyrode (NT2; 2 mM Ca), conditioned-medium from non-stretched CF (CM-NSF; 0% stretch for 72 h; 1.8 mM Ca) and conditioned medium from stretched CF (CM-SF; 10% stretch for 72 h; 1.8 mM Ca) at 1 Hz steady state stimulation in WT at 21 weeks. Quantification of diastolic (B) and systolic Ca (C), as well as Ca amplitude (D) and area under the curve (E). Example of confocal CaT (Fluo-4) after 1 h incubation with CM-NSF and CM-SF at 1 Hz steady state stimulation. Markings indicate the sub-sarcolemmal region (SS; ROI: 1 µm below cell surface), central region (CT; ROI: 1 µm in cell center) and the total transverse line scan (TT). Quantification of cellular (TT) and sub-cellular (CT, SS) CaT time-to-peak (G) and tau of decay (H). *$p < .05$; #$^1p = 0.08$; #$^2p = 0.07$; #$^3p = 0.06$.

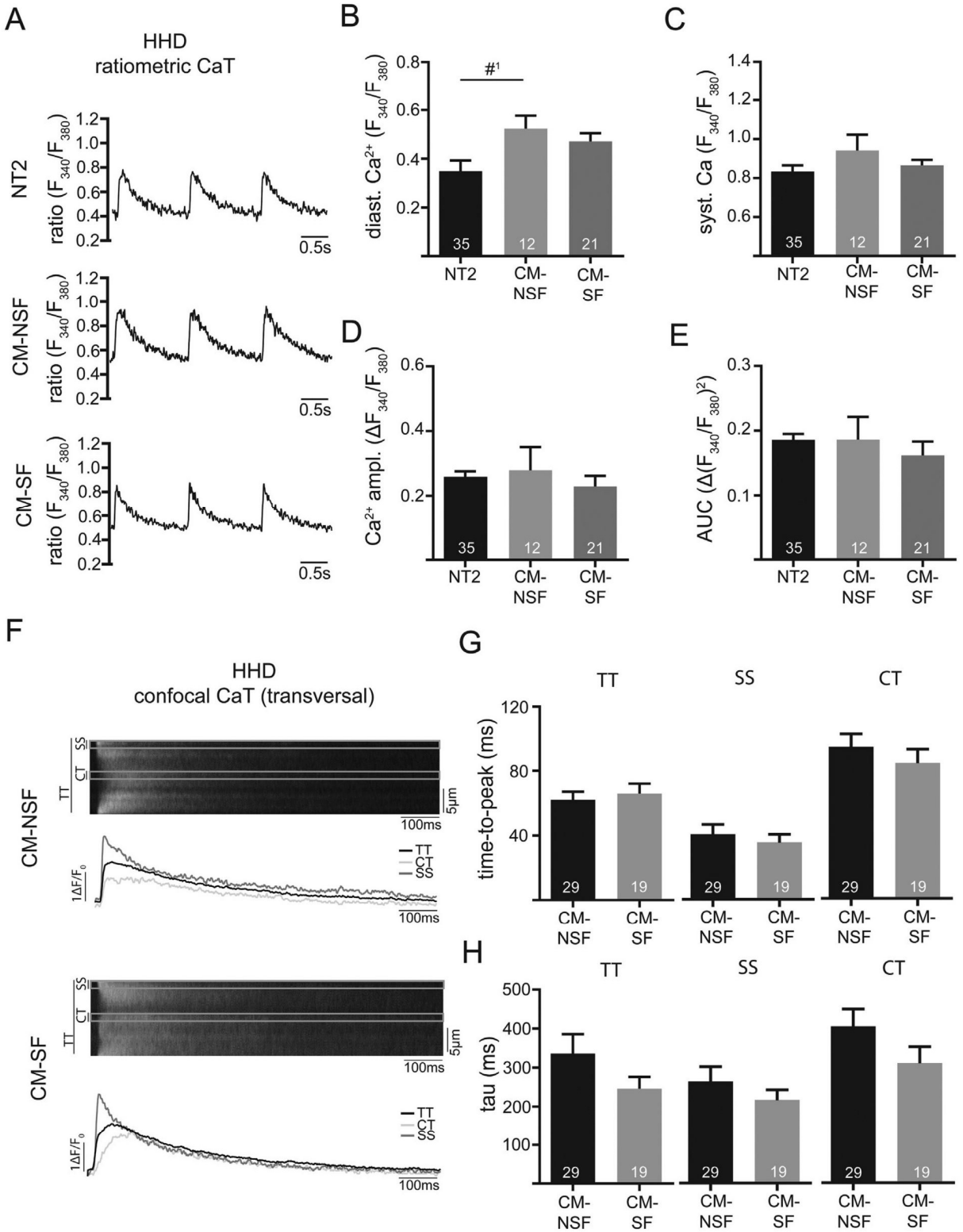

Fig. 4. Example of ratiometrically recorded CaT (Fura-2) after 1 h incubation with either Normal Tyrode (NT2; 2 mM Ca), conditioned-medium from non-stretched CF (CM-NSF; 0% stretch for 72 h; 1.8 mM Ca) and conditioned medium from stretched CF (CM-SF; 10% stretch for 72 h; 1.8 mM Ca) at 1 Hz steady state stimulation in HHD at 21 weeks. Quantification of diastolic (B) and systolic Ca (C), as well as Ca amplitude (D) and area under the curve (E). Example of confocal CaT (Fluo-4) after 1 h incubation with CM-NSF and CM-SF at 1 Hz steady state stimulation. Markings indicate the sub-sarcolemmal region (SS; ROI: 1 µm below cell surface), central region (CT; ROI: 1 µm in cell center) and the total transverse line scan (TT). Quantification of cellular (TT) and sub-cellular (CT, SS) CaT time-to-peak (G) and tau of decay (H). #[1]p = 0.07.

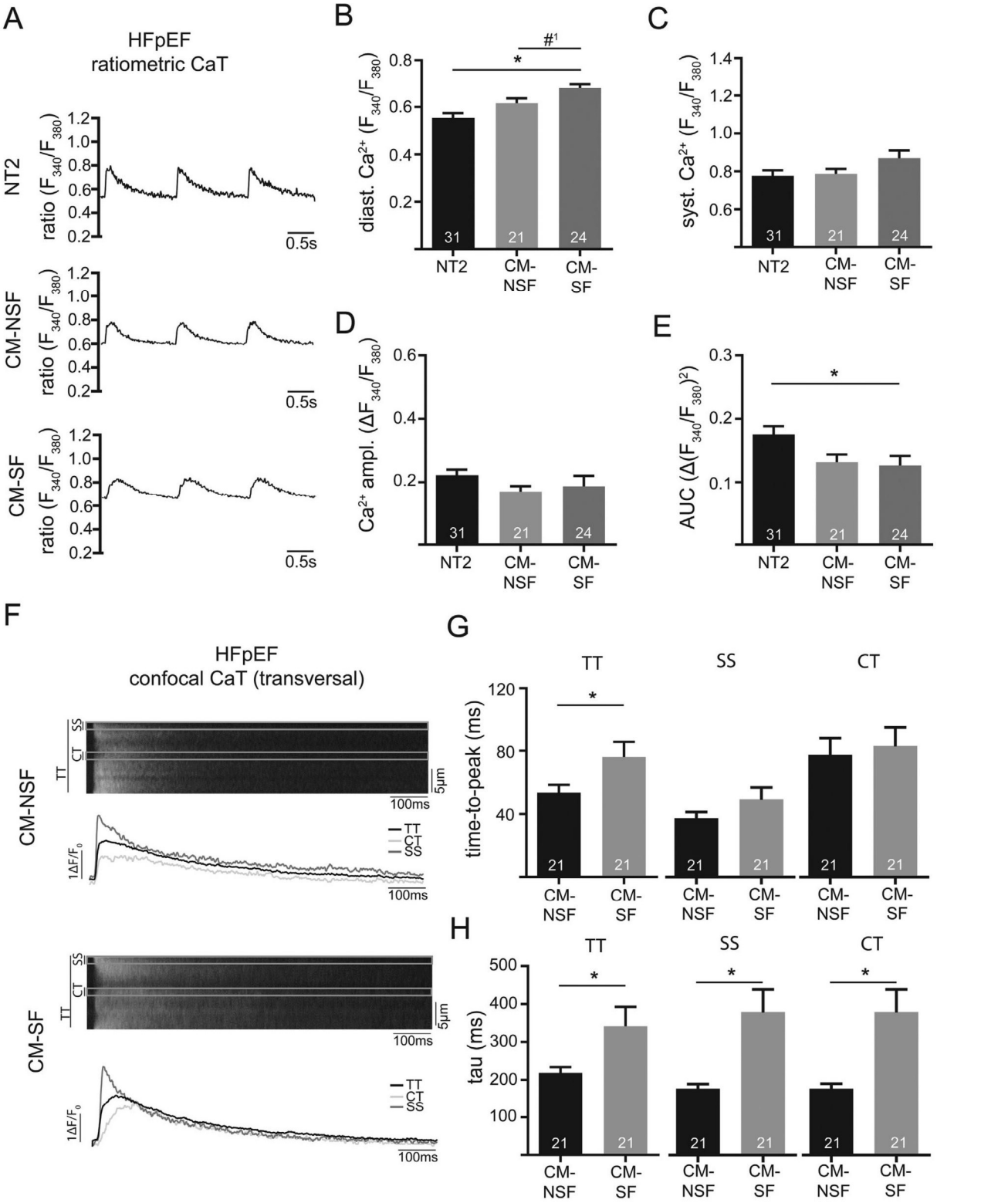

Fig. 5. Example of ratiometrically recorded CaT (Fura-2) after 1 h incubation with either Normal Tyrode (NT2; 2 mM Ca), conditioned-medium from non-stretched CF (CM-NSF; 0% stretch for 72 h; 1.8 mM Ca) and conditioned medium from stretched CF (CM-SF; 10% stretch for 72 h; 1.8 mM Ca) at 1 Hz steady state stimulation in HFpEF at 21 weeks. Quantification of diastolic (B) and systolic Ca (C), as well as Ca amplitude (D) and area under the curve (E). Example of confocal CaT (Fluo-4) after 1 h incubation with CM-NSF and CM-SF at 1 Hz steady state stimulation. Markings indicate the sub-sarcolemmal region (SS; ROI: 1 µm below cell surface), central region (CT; ROI: 1 µm in cell center) and the total transverse line scan (TT). Quantification of cellular (TT) and sub-cellular (CT, SS) CaT time-to-peak (G) and tau of decay (H). *$p < .05$; #[1]p = 0.07.

A

WT

	CM-NSF	CM-SF	
ET-1	51.8	71.3	
IL-1β	<31.3	<31.3	
IL-6	298	232.6	
IL-10	<31.3	89.1	
IL-33	<31.3	<31.3	
PDGF	<31.3	<31.3	
TGF-β	<31.3	<31.3	pg/ml
TNF-α	<12.5	<12.5	

B

HHD

	CM-NSF	CM-SF	
ET-1	9.1	15.2	
IL-1β	<31.3	<31.3	
IL-6	<31.3	142.2	
IL-10	<31.3	148.1	
IL-33	<31.3	<31.3	
PDGF	<31.3	<31.3	
TGF-β	<31.3	<31.3	pg/ml
TNF-α	<12.5	<12.5	

C

HFpEF

	CM-NSF	CM-SF	
ET-1	15	15.7	
IL-1β	<31.3	<31.3	
IL-6	<31.3	<31.3	
IL-10	<31.3	<31.3	
IL-33	<31.3	<31.3	
PDGF	<31.3	<31.3	
TGF-β	<31.3	<31.3	pg/ml
TNF-α	<12.5	<12.5	

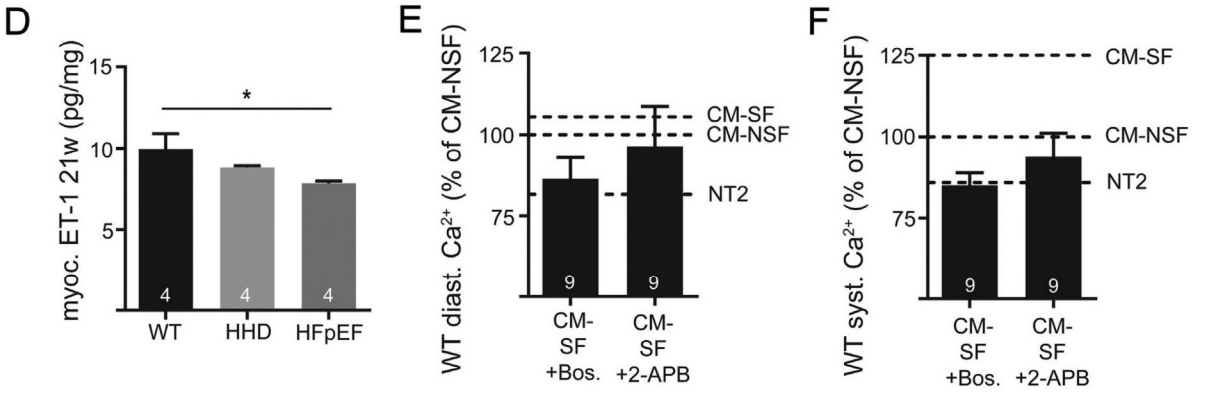

Fig. 6. Quantification of selected cytokines in CM-NSF and CM-SF in WT (A), HHD (B) and HFpEF (C) at 21 weeks. Myocardial tissue levels of ET-1 in the left atrium (D). Diastolic (E) and systolic Ca (F) after 1 h incubation with CM-SF in the presence of ET-1 receptor antagonist Bosentan or IP_3 receptor inhibitor 2-APB. Reference for CM-SF (with or without Bosentan/2-APB) was obtained in two different sets of experiments with $n = 13$ and $n = 11$ CM-NSF cells. Dashed lines indicate respective Ca levels after treatment with NT2, CM-NSF and CM-SF without Bosentan/2-APB. $^*p < .05$.

tended to be reduced in HFpEF (Fig. 7D). Clinically, animals still showed a preserved left ventricular ejection fraction (suppl. Fig. 4D). However, during disease progression (i.e. at 27-weeks) LA CM showed a significant impairment of ECC under baseline conditions. LA CM of HFpEF presented with a lower CaT amplitude, a slower Ca^{2+} removal (almost 2-fold increase of tau) and increased time-to-peak compared to WT (Fig. 7F-H). These observations could be explained by a significant reduction of sarcoplasmic reticulum Ca^{2+} content in HFpEF (Fig. 7I).

An increase of nuclear Ca^{2+} has been associated with cardiac remodeling [17]. Interestingly and in support of this notion, LA CM during later stages of HFpEF had a significantly augmented CaT amplitude during ECC in the nuclear cell compartment (Fig. 7J).

3.8. Stretched cardiac fibroblasts have no adverse effect on Ca^{2+} cycling during excitation-contraction coupling in WT, HHD or HFpEF in disease progression (27w)

We tested if CM-SF had an additional positive or negative effect on CaT amplitudes and kinetics in vitro in WT, HHD and HFpEF, respectively. Upon exposure to CM-SF neither WT cells (Fig. 8A-D), nor HHD (Fig. 8E-H) or HFpEF cells (Fig. 8I-L) showed altered CaT during excitation-contraction coupling. Interestingly at this later disease stage, atrial tissue ET-1 concentration was not significantly different between WT, HHD and HFpEF (Fig. 8M). This supports the notion that atrial enlargement as observed in vivo led to no further increase of fibroblasts ET-1 secretion at 27 weeks. However, ET-1 concentration within the particular groups still positively affected left atrial ejection fraction (Fig. 8N) which is in agreement with the presented results in Figs. 3-5. Last, we tested the hypothesis that tissue ET-1 concentration differed between in humans with arterial hypertension or diastolic dysfunction. Human myocardial ET-1 was quantified by ELISA from a total of 16 patients. However, as compared to control patients, atrial tissue ET-1 was not significantly altered (Fig. 8O).

4. Discussion

Atrial remodeling has been shown to affect morbidity and mortality of patients and recent results from clinical studies like CASTLE-AF suggest that altering the course of atrial cardiomyopathy (with its signature feature atrial fibrillation) positively influences survival [18]. Several disease entities like hypertension or heart failure are associated with atrial remodeling, which is thought to be related to impaired cardiomyocyte function and altered fibrosis [19]. However, even though clinically highly relevant, the exact mechanism of differential atrial cardiomyopathies are not well understood. We therefore investigated the interaction between the most prevalent cell types in atria that contribute to remodeling, cardiomyocytes and fibroblasts, in different disease states and entities. Here, we show for the first time, that an altered "activity of fibrosis", independent of the extent of fibrotic remodeling, affects atrial function in the context of healthy and diseased hearts in a time-dependent manner.

Quantitative differences of fibrosis directly influence atrial contractility in the setting of atrial cardiomyopathy [20,21]. In addition, local differences of fibrosis with potentially pro-arrhythmic and deteriorating effects regarding tissue mechanics have been shown to be especially prevalent in obesity related atrial remodeling [19]. Interestingly however, in our animal model, fibrosis was quantitatively not altered, even though atria were enlarged and atrial function was impaired [7]. This is in line with data presented e.g. by Khan et al. who found no difference in total collagen content in atria of a canine model of heart failure [22]. A setting that allowed us to study the impact of the "activity of fibrosis" on atrial function in HHD and HFpEF in detail.

An interaction between CF and CM and vice-versa leading to altered function has been proposed in the past, yet evidence was lacking [23]. Our data indicates that stretch of CF presents as an important trigger for the activation of fibrosis and changes the paracrine signature of fibroblasts, with differential effects on "neighboring" cardiomyocytes.

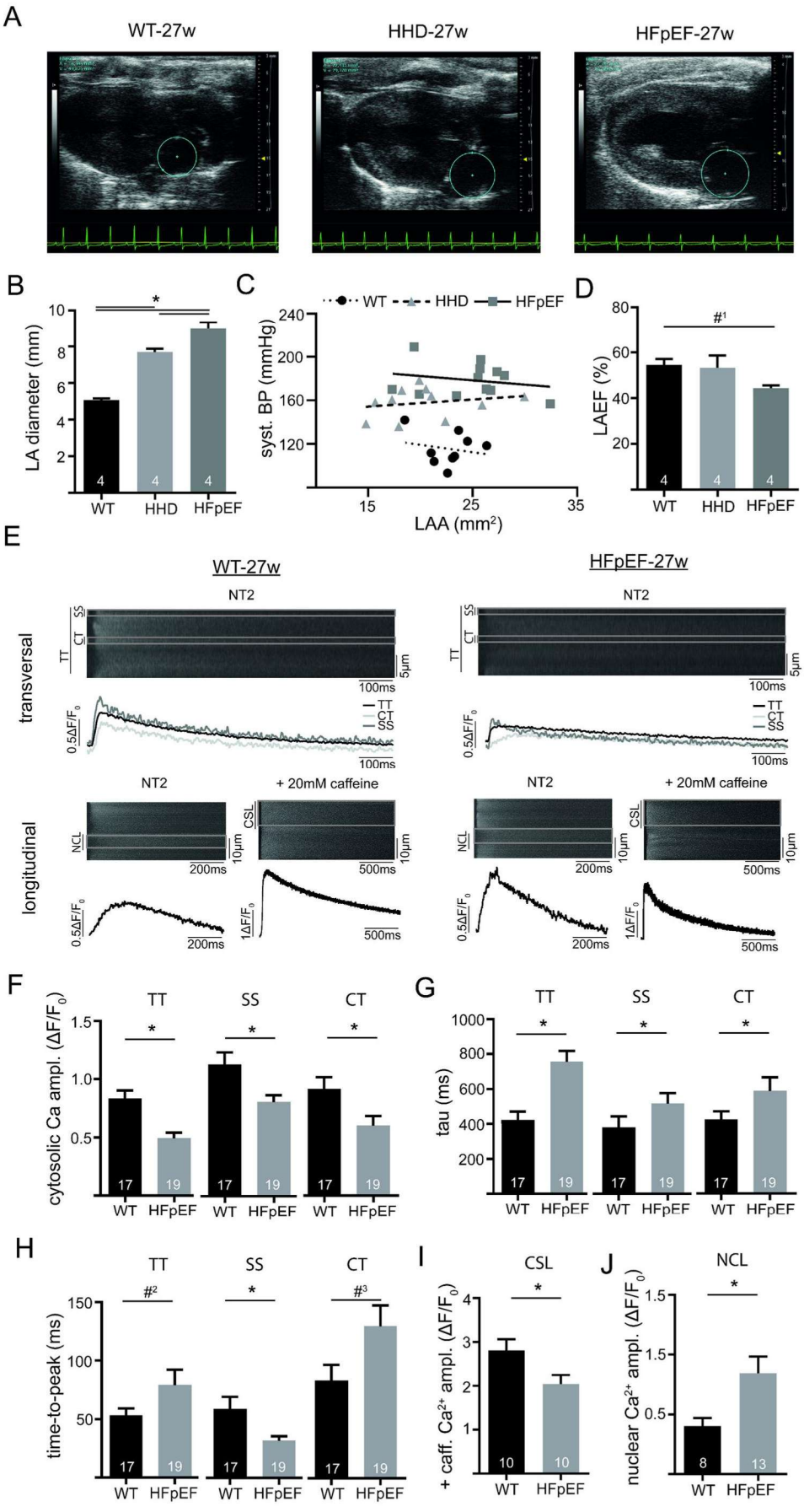

Fig. 7. In vivo atrial function in a model of advanced atrial remodeling. Example of parasternal longitudinal axis images obtained with echocardiography in WT, HHD and HFpEF at 27 weeks (A). Marked area depicts the left atrium. LA diameter during diastole (B) and LA ejection fraction (D). Correlation of systolic blood pressure (invasive catheterization) with LA area (C). Example of confocally recorded transversal and longitudinal CaT (E; Fluo4) at baseline conditions in 27-week-old WT and HFpEF at 1 Hz steady state stimulation (transversal and longitudinal) and application of caffeine (longitudinal; 20 mM; without electric stimulation). Markings in the transversal line scans indicate the sub-sarcolemmal region (SS; ROI: 1 µm below cell surface), central region (CT; ROI: 1 µm in cell center) and the total line scan (TT), while markings in the longitudinal line scans indicate the cytosolic region between the sarcolemma and nucleus (CSL) and the nucleus (NCL). Cytosolic (TT) and subcellular (SS, CT) Ca amplitude (F), tau of decay (G) and time-to-peak (H) at 1 Hz steady state stimulation in NT2. Caffeine-triggered (20 mM) cytosolic Ca release without electrical stimulation (I). Nuclear Ca amplitude at 1 Hz steady state stimulation (J). *$p < .05$; #$^1p = 0.21$; #$^2 = 0.09$; #$^3p = 0.051$.

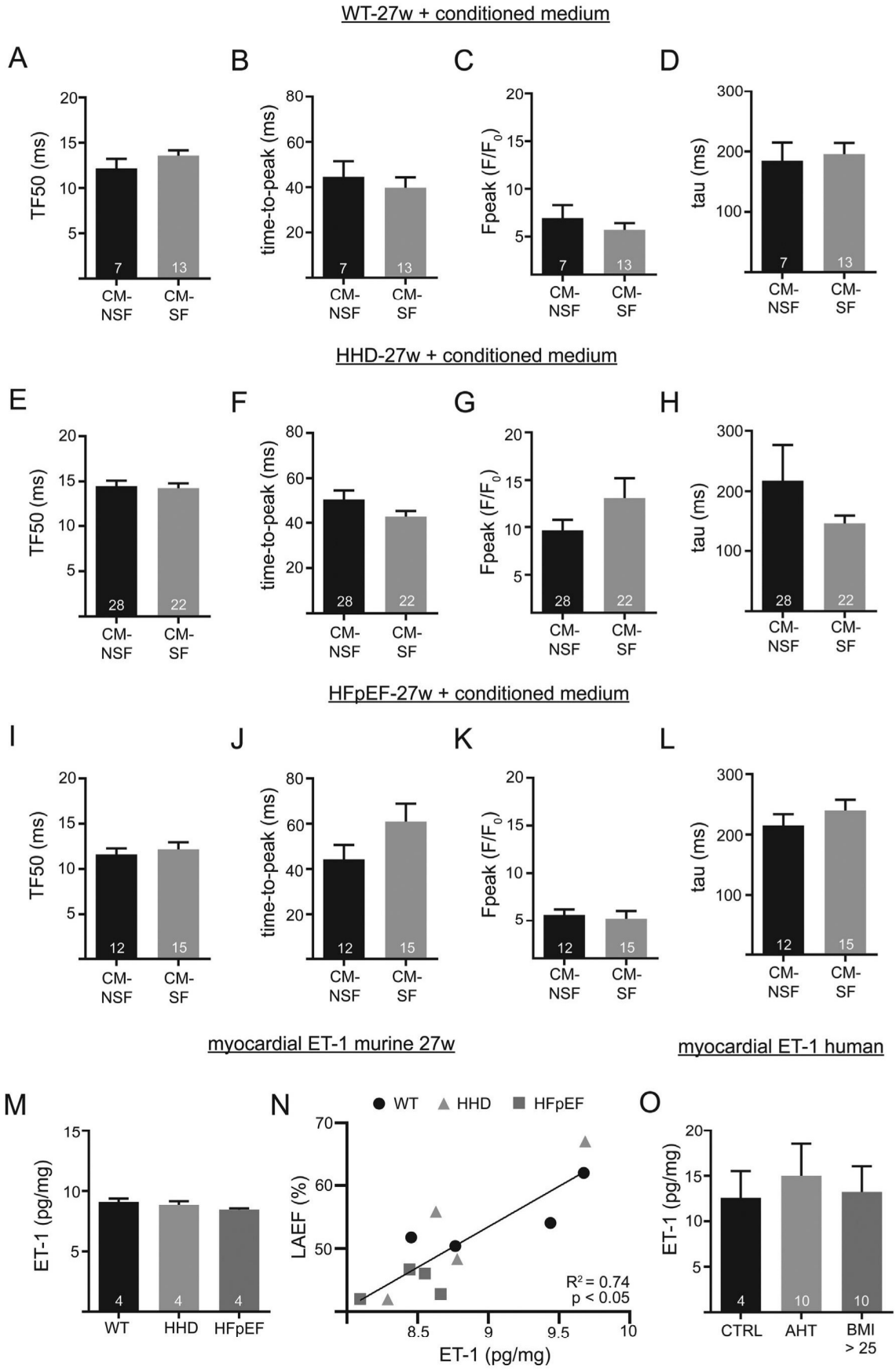

Fig. 8. Confocal Ca imaging in 27-week-old animals after 1 h incubation with CM-NSF and CM-SF from 21-week-old animals. Transversal line scans at 1 Hz steady state stimulation. TF50, time-to-peak, Ca peak, and tau of decay of WT (A-D), HHD (*E*-H) and HFpEF (I-L). Myocardial tissue levels of ET-1 in the left atrium at 27 weeks (M). Correlation of LA ejection fraction and myocardial ET-1 (N). Myocardial tissue levels of ET-1 in a cohort of patients (O). The control group is represented by patients with a BMI ≤ 25 and no history of AHT.

Indeed, stretch has been shown to activate a plethora of different cell types to augment or alter their function [11]. Our data shows an increase in IL-6 expression mirroring this cellular activation through stretch.

ET-1 is a potent inotrope [24] that allows to even overcome impaired Ca^{2+} release through ryanodine receptors most likely via its activation of inositol-1,4,5-phosphate receptors [25]. ET-1 release has been linked to mechanical stress [26]. It can also foster remodeling processes like enhanced fibrosis and hypertrophy with prolonged exposure [27]. In the studied healthy WT rats, stretched fibroblasts secreted high concentrations of ET-1 which led to an IP_3-receptor dependent augmentation of CM function. IP_3R mediated Ca^{2+} release has been shown to be highly important in atrial cells and to allow compensatory augmentation of contractility [28]. Indeed, tissue ET-1 concentrations positively correlated with left atrial function in our animal model. In vivo, fibroblast ET-1 release upon stretch and its impact on CM function might therefore very well represent a compensatory mechanism to account for increased hemodynamic demands.

Stretch however has been shown to also have opposite effects, especially in the context of cardiac disease. Chronic overload as occurring during HF has been associated with impaired ECC in CM [29]. In addition, pro-fibrotic signalling cascades and cytokines, known to modulate CF activity and enhance remodeling, are activated through stretch in this setting [30]. CF activity itself is altered through stretch [31]. In support of this notion, Ca^{2+} cycling during ECC was impaired in early stage HFpEF due to an altered composition of CF secretions, potentially contributing to the observed in vivo phenotype of an impaired atrial contractility [7]. Various cytokines and paracrine mediators that are excreted by CF have been associated with a potential impairment of contractile function [32]. Even though we found no detectable change in IL-1β, IL-6, IL-10, IL-33, PDGF, TGF-β or TNF-α in the supernatant in the animal model, it is likely that a cytokine "cocktail" has potentiating possibly adverse effects on tissue mechanics [33].

During disease progression in our animal model and in human patients, we found no association between tissue ET-1 concentrations and arterial hypertension or obesity, further challenging the relevance of ET-1 as the sole mediator for the observed effects of mechanically stressed atrial fibroblasts on atrial function during particular states of remodeling. Even though plasma levels of ET-1 have been shown to be elevated in HFrEF patients [34], previous studies have failed to correlate myocardial ET-1 with LA remodeling in the absence of AF [35] in humans, corroborating our results.

Interestingly, in early stage and progressive hypertensive heart disease the CF – CM interaction was of less importance regarding cellular function. LA diameter was unchanged as compared to WT and significantly smaller than in HFpEF. In addition, CM size tended to be decreased. At the same time, the extent of fibrosis was unchanged. These morphological findings indicate an earlier but also differential state of remodeling. Others described similar findings in early stage heart failure, where total collagen was unchanged and gelatinase and metalloprotease activity influencing "dynamic collagen turnover" was increased [22]. In HHD, CM-SF, showing smaller yet relevant concentrations of ET-1 and IL-6 as compared to WT, significantly increased diastolic Ca^{2+}, indicating a less pronounced activation of CF upon stress and a less pronounced susceptibility of CM towards CM-SF. In progressive HHD (27w), LA were significantly enlarged, yet left atrial function was unimpaired. As opposed to the great impact of CM-SF on HFpEF (21w), in progressive HHD (27w) CM-SF had no effect on ECC, again underscoring differences in cellular remodeling. Others have shown that atrial enlargement occurs in rats with a comparable genetic background at older ages of up to 25 months and that LA myocytes eventually show impaired baseline ECC during further disease progression [36]. Moreover, in progressive HHD, left ventricular function was preserved indicating that atrial macroscopic remodeling can be observed even before ventricular changes become apparent. Similar findings have been reported in larger animal models by others [37].

In advanced HFpEF, contractile function was even impaired without exposure to CF derived factors. This could be related to decreased sarcoplasmic reticulum Ca^{2+} content and therefore altered ECC per se [38], possibly due to a maximal *baseline* activation of IP_3Rs. The fact that CM-SF had no additional effect on ECC in advanced HFpEF is in agreement with earlier results from HF rabbits, where increased *baseline* activation of the IP_3R signalling cascade itself could be shown to contribute to the Ca^{2+} related atrial contractile dysfunction [28].

The variety of mechanisms leading to atrial mechanical dysfunction at different stages and with different underlying causes of disease is underscored by findings from Yeh et al.: The group has even found enhanced Ca^{2+} release in combination with impaired cellular contractility in atrial remodeling caused by congestive heart failure. They reported that this was related to altered phosphorylation states of myosin-binding protein C rather than Ca^{2+} release itself. Others have associated progressive remodeling processes with altered nuclear $[Ca^{2+}]$ [17]. Interestingly and in support of this concept, in our older animals, nuclear Ca^{2+} release was enhanced.

In summary, we show an interaction between stressed CF and CM, potentially representing a compensatory mechanism in healthy atria, that might contribute to in vivo atrial dysfunction in the setting of HFpEF. We identified ET-1 as a contributor to enhanced left atrial ejection fraction and cellular contractility under normal conditions, but with adverse effects in HFpEF. However, we also found CF - CM interactions to be highly stage and underlying-disease dependent, as Ca^{2+} release was impaired independently of CF during progression of HFpEF. In support of this, CF had no effect on atria in hypertensive remodeling and ET-1 tissue concentrations were unaltered in human arterial hypertension or obesity. Our findings underscore the complex mechanisms underlying atrial remodeling and establish the "activity of fibrosis" related to paracrine interaction with CM (e.g. via ET-1) as an important stage-dependent contributor to in vitro and in vivo atrial dysfunction.

Acknowledgements

The authors thank Mareile Schröder for technical assistance.

Funding

This work was supported by the German Society of Cardiology, the Else-Kröner-Fresenius Stiftung, the DZHK (German Centre for Cardiovascular Research) and by the BMBF (German Ministry of Education and Research) (F.H.). D.B. is an MD stipend of the Berlin Institute of Health. Dr. Hohendanner is participant in the BIH-Charité Clinical Scientist Program funded by the Charité –Universitätsmedizin Berlin and the Berlin Institute of Health. L.A.B. was supported by National Institute of Health grants HL057832, HL132871 and HL134781.

Conflicts of interest

Conflicts of Interest: none declared.

Appendix A. Supplementary data

Supplementary data to this article can be found online at https://doi.org/10.1016/j.yjmcc.2019.04.016.

References

[1] P. Ponikowski, et al., ESC guidelines for the diagnosis and treatment of acute and chronic heart failure: the task force for the diagnosis and treatment of acute and chronic heart failure of the European Society of Cardiology (ESC). Developed with the special contribution of the heart failure association (HFA) of the ESC, Eur. J. Heart Fail. 18 (8) (2016) 891–975.

[2] T.E. Owan, et al., Trends in prevalence and outcome of heart failure with preserved

ejection fraction, N. Engl. J. Med. 355 (3) (2006) 251–259.
[3] F. Hohendanner, et al., Intracellular dyssynchrony of diastolic cytosolic [ca(2)(+)] decay in ventricular cardiomyocytes in cardiac remodeling and human heart failure, Circ. Res. 113 (5) (2013) 527–538.
[4] M. Habibi, et al., Association of CMR-measured LA function with heart failure development: results from the MESA study, JACC Cardiovasc. Imaging 7 (6) (2014) 570–579.
[5] S. Gupta, et al., Left atrial structure and function and clinical outcomes in the general population, Eur. Heart J. 34 (4) (2013) 278–285.
[6] A. Goette, et al., EHRA/HRS/APHRS/SOLAECE expert consensus on atrial cardiomyopathies: definition, characterisation, and clinical implication, J Arrhythm 32 (4) (2016) 247–278.
[7] F. Hohendanner, et al., Cellular mechanisms of metabolic syndrome-related atrial decompensation in a rat model of HFpEF, J. Mol. Cell. Cardiol. 115 (2018) 10–19.
[8] S. Heymans, et al., Inflammation as a therapeutic target in heart failure? A scientific statement from the translational research Committee of the Heart Failure Association of the European Society of Cardiology, Eur. J. Heart Fail. 11 (2) (2009) 119–129.
[9] G. Esposito, et al., Sitagliptin reduces inflammation, fibrosis and preserves diastolic function in a rat model of heart failure with preserved ejection fraction, Br. J. Pharmacol. 174 (22) (2017) 4070–4086.
[10] N. Takeda, et al., Cardiac fibroblasts are essential for the adaptive response of the murine heart to pressure overload, J. Clin. Invest. 120 (1) (2010) 254–265.
[11] D. Lindner, et al., Cardiac fibroblasts support cardiac inflammation in heart failure, Basic Res. Cardiol. 109 (5) (2014) 428.
[12] C. Vasquez, et al., Enhanced fibroblast-myocyte interactions in response to cardiac injury, Circ. Res. 107 (8) (2010) 1011–1020.
[13] D. Bode, et al., Isolation of atrial cardiomyocytes from a rat model of metabolic syndrome-related heart failure with preserved ejection fraction, J. Vis. Exp. (137) (2018).
[14] N. Hamdani, et al., Myocardial titin hypophosphorylation importantly contributes to heart failure with preserved ejection fraction in a rat metabolic risk model, Circ. Heart Fail. 6 (6) (2013) 1239–1249.
[15] T.S. Bowen, et al., Exercise training reveals inflexibility of the diaphragm in an animal model of patients with obesity-driven heart failure with a preserved ejection fraction, J. Am. Heart Assoc. 6 (10) (2017).
[16] S. Hinrichs, et al., Precursor proadrenomedullin influences cardiomyocyte survival and local inflammation related to myocardial infarction, Proc. Natl. Acad. Sci. U. S. A. 115 (37) (2018) E8727–E8736.
[17] S. Ljubojevic, et al., Early remodeling of perinuclear Ca2+ stores and nucleoplasmic Ca2+ signaling during the development of hypertrophy and heart failure, Circulation 130 (3) (2014) 244–255.
[18] N.F. Marrouche, et al., Catheter ablation for atrial fibrillation with heart failure, N. Engl. J. Med. 378 (5) (2018) 417–427.
[19] R. Mahajan, et al., Electrophysiological, Electroanatomical, and structural remodeling of the atria as consequences of sustained obesity, J. Am. Coll. Cardiol. 66 (1) (2015) 1–11.
[20] F. Hohendanner, et al., Extent and magnitude of low-voltage areas assessed by ultra-high-density electroanatomical mapping correlate with left atrial function, Int. J. Cardiol. 272 (2018) 108–112.
[21] H. Gasparovic, et al., Atrial apoptosis and fibrosis adversely affect atrial conduit, reservoir and contractile functions, Interact. Cardiovasc. Thorac. Surg. 19 (2) (2014) 223–230 (discussion 230).
[22] A. Khan, et al., The cardiac atria are chambers of active remodeling and dynamic collagen turnover during evolving heart failure, J. Am. Coll. Cardiol. 43 (1) (2004) 68–76.
[23] A. Tao, et al., Cardiomyocyte-fibroblast interaction contributes to diabetic cardiomyopathy in mice: role of HMGB1/TLR4/IL-33 axis, Biochim. Biophys. Acta 1852 (10 Pt A) (2015) 2075–2085.
[24] M. Kang, J.W. Walker, Endothelin-1 and PKC induce positive inotropy without affecting pHi in ventricular myocytes, Exp Biol Med (Maywood) 231 (6) (2006) 865–870.
[25] X. Li, et al., Endothelin-1-induced arrhythmogenic Ca2+ signaling is abolished in atrial myocytes of inositol-1,4,5-trisphosphate(IP3)-receptor type 2-deficient mice, Circ. Res. 96 (12) (2005) 1274–1281.
[26] T. Gustafsson, et al., Elevations of local intravascular pressures release vasoactive substances in humans, Clin. Physiol. Funct. Imaging 33 (1) (2013) 38–44.
[27] P.J. Wermuth, et al., Stimulation of transforming growth factor-beta1-induced endothelial-to-mesenchymal transition and tissue fibrosis by Endothelin-1 (ET-1): a novel Profibrotic effect of ET-1, PLoS One 11 (9) (2016) e0161988.
[28] F. Hohendanner, et al., Inositol-1,4,5-trisphosphate induced Ca2+ release and excitation-contraction coupling in atrial myocytes from normal and failing hearts, J. Physiol. 593 (6) (2015) 1459–1477.
[29] M. Ibrahim, et al., Cardiomyocyte Ca2+ handling and structure is regulated by degree and duration of mechanical load variation, J. Cell. Mol. Med. 16 (12) (2012) 2910–2918.
[30] K.M. Herum, et al., Mechanical regulation of cardiac fibroblast profibrotic phenotypes, Mol. Biol. Cell 28 (14) (2017) 1871–1882.
[31] J. Wang, et al., Mechanical force regulation of myofibroblast differentiation in cardiac fibroblasts, Am. J. Physiol. Heart Circ. Physiol. 285 (5) (2003) H1871–H1881.
[32] X. Yu, R.H. Kennedy, S.J. Liu, JAK2/STAT3, not ERK1/2, mediates interleukin-6-induced activation of inducible nitric-oxide synthase and decrease in contractility of adult ventricular myocytes, J. Biol. Chem. 278 (18) (2003) 16304–16309.
[33] D. MacKenna, S.R. Summerour, F.J. Villarreal, Role of mechanical factors in modulating cardiac fibroblast function and extracellular matrix synthesis, Cardiovasc. Res. 46 (2) (2000) 257–263.
[34] J.J. McMurray, et al., Plasma endothelin in chronic heart failure, Circulation 85 (4) (1992) 1374–1379.
[35] F. Mayyas, et al., Association of left atrial endothelin-1 with atrial rhythm, size, and fibrosis in patients with structural heart disease, Circ. Arrhythm. Electrophysiol. 3 (4) (2010) 369–379.
[36] F. Pluteanu, et al., Progressive impairment of atrial myocyte function during left ventricular hypertrophy and heart failure, J. Mol. Cell. Cardiol. 114 (2018) 253–263.
[37] D.H. Lau, et al., Characterization of cardiac remodeling in a large animal "one-kidney, one-clip" hypertensive model, Blood Press. 19 (2) (2010) 119–125.
[38] D.A. Eisner, et al., Physiological and pathological modulation of ryanodine receptor function in cardiac muscle, Cell Calcium 35 (6) (2004) 583–589.

7.2 Bode D, Guthof T, Pieske BM, Heinzel FR, Hohendanner F. Isolation of Atrial Cardiomyocytes from a Rat Model of Metabolic Syndrome-related Heart Failure with Preserved Ejection Fraction. Journal of Visualized Experiments. 2018 Jul 26(137).

Journal Data Filtered By: **Selected JCR Year: 2018** Selected Editions: SCIE,SSCI Selected Categories: **"MULTIDISCIPLINARY SCIENCES"** Selected Category Scheme: WoS

Gesamtanzahl: 69 Journale

Rank	Full Journal Title	Total Cites	Journal Impact Factor	Eigenfactor Score
1	NATURE	745,692	43.070	1.285010
2	SCIENCE	680,994	41.037	1.070190
3	National Science Review	1,842	13.222	0.006500
4	Science Advances	21,901	12.804	0.110010
5	Nature Communications	243,793	11.878	1.103290
6	Nature Human Behaviour	1,230	10.575	0.006550
7	PROCEEDINGS OF THE NATIONAL ACADEMY OF SCIENCES OF THE UNITED STATES OF AMERICA	661,118	9.580	1.022190
8	Science Bulletin	3,569	6.277	0.009840
9	Scientific Data	3,240	5.929	0.015610
10	Frontiers in Bioengineering and Biotechnology	1,994	5.122	0.006540
11	Journal of Advanced Research	2,691	5.045	0.004780
12	Research Synthesis Methods	1,932	5.043	0.005420
13	GigaScience	2,674	4.688	0.012510
14	Annals of the New York Academy of Sciences	46,385	4.295	0.025840
15	Scientific Reports	302,086	4.011	1.061540
16	Journal of the Royal Society Interface	12,933	3.224	0.029190
17	NPJ Microgravity	203	3.111	0.000670
18	PHILOSOPHICAL TRANSACTIONS OF THE ROYAL SOCIETY A-MATHEMATICAL PHYSICAL AND ENGINEERING SCIENCES	19,227	3.093	0.028200

Rank	Full Journal Title	Total Cites	Journal Impact Factor	Eigenfactor Score
19	FRACTALS-COMPLEX GEOMETRY PATTERNS AND SCALING IN NATURE AND SOCIETY	1,429	2.971	0.001120
20	Journal of Radiation Research and Applied Sciences	860	2.963	0.001860
21	MIT Technology Review	929	2.893	0.001910
22	JOURNAL OF KING SAUD UNIVERSITY SCIENCE	1,120	2.835	0.001670
23	PROCEEDINGS OF THE ROYAL SOCIETY A-MATHEMATICAL PHYSICAL AND ENGINEERING SCIENCES	18,683	2.818	0.018940
24	PLoS One	650,727	2.776	1.706770
25	COMPLEXITY	2,753	2.591	0.003890
26	Royal Society Open Science	4,118	2.515	0.017150
27	PeerJ	11,911	2.353	0.045900
28	SCIENCE AND ENGINEERING ETHICS	1,719	2.275	0.003450
29	INTERNATIONAL JOURNAL OF BIFURCATION AND CHAOS	7,008	2.145	0.007390
30	Symmetry-Basel	2,097	2.143	0.002590
31	SCIENTIFIC AMERICAN	6,609	1.946	0.003540
32	Science of Nature	508	1.839	0.002000
33	PROCEEDINGS OF THE JAPAN ACADEMY SERIES B-PHYSICAL AND BIOLOGICAL SCIENCES	1,532	1.833	0.001960
34	Journal of Taibah University for Science	779	1.640	0.001240
35	Frontiers in Life Science	241	1.622	0.000500
36	ARABIAN JOURNAL FOR SCIENCE AND ENGINEERING	3,838	1.518	0.005840
37	SCIENCE PROGRESS	521	1.500	0.000400

Selected JCR Year: 2018; Selected Categories: “MULTIDISCIPLINARY SCIENCES”

Rank	Full Journal Title	Total Cites	Journal Impact Factor	Eigenfactor Score
38	Proceedings of the Romanian Academy Series A-Mathematics Physics Technical Sciences Information Science	497	1.402	0.000900
39	SOUTH AFRICAN JOURNAL OF SCIENCE	2,604	1.351	0.002010
40	ISSUES IN SCIENCE AND TECHNOLOGY	428	1.214	0.000990
41	Jove-Journal of Visualized Experiments	13,650	1.108	0.035180
42	RENDICONTI LINCEI-SCIENZE FISICHE E NATURALI	750	1.087	0.001080
43	ENDEAVOUR	540	1.068	0.000440
44	DISCRETE DYNAMICS IN NATURE AND SOCIETY	1,962	0.973	0.003690
45	Mathematical Modelling of Natural Phenomena	679	0.949	0.001930
46	ANAIS DA ACADEMIA BRASILEIRA DE CIENCIAS	2,841	0.938	0.003410
47	Kuwait Journal of Science	225	0.891	0.000340
48	ADVANCES IN COMPLEX SYSTEMS	618	0.867	0.000340
49	JOURNAL OF THE ROYAL SOCIETY OF NEW ZEALAND	648	0.774	0.000400
50	CURRENT SCIENCE	10,540	0.756	0.006420
51	JOURNAL OF THE INDIAN INSTITUTE OF SCIENCE	391	0.742	0.000530
52	Iranian Journal of Science and Technology Transaction A-Science	499	0.692	0.000460
53	PROCEEDINGS OF THE NATIONAL ACADEMY OF SCIENCES INDIA SECTION A-PHYSICAL SCIENCES	309	0.681	0.000400
54	TRANSACTIONS OF THE ROYAL SOCIETY OF SOUTH AUSTRALIA	444	0.667	0.000200
55	DEFENCE SCIENCE JOURNAL	928	0.589	0.000560
56	Sains Malaysiana	1,337	0.540	0.001320
57	Proceedings of the Estonian Academy of Sciences	523	0.510	0.000490
58	AMERICAN SCIENTIST	2,425	0.507	0.001110

Video Article

Isolation of Atrial Cardiomyocytes from a Rat Model of Metabolic Syndrome-related Heart Failure with Preserved Ejection Fraction

David Bode[1,2], Tim Guthof[1], Burkert M. Pieske[1,2], Frank R. Heinzel[1,2], Felix Hohendanner[1,2]

[1]Department of Internal Medicine and Cardiology, Charité University Medicine

[2]German Center for Cardiovascular Research (DZHK)

Correspondence to: Felix Hohendanner at felix.hohendanner@charite.de

URL: https://www.jove.com/video/57953
DOI: doi:10.3791/57953

Keywords: Medicine, Issue 137, Atrial remodeling, HFpEF, metabolic syndrome, atrial myocyte isolation, atrial dysfunction, rat model

Date Published: 7/26/2018

Citation: Bode, D., Guthof, T., Pieske, B.M., Heinzel, F.R., Hohendanner, F. Isolation of Atrial Cardiomyocytes from a Rat Model of Metabolic Syndrome-related Heart Failure with Preserved Ejection Fraction. *J. Vis. Exp.* (137), e57953, doi:10.3791/57953 (2018).

Abstract

In this article, we describe an optimized, Langendorff-based procedure for the isolation of single-cell atrial cardiomyocytes (ACMs) from a rat model of metabolic syndrome (MetS)-related heart failure with preserved ejection fraction (HFpEF). The prevalence of MetS-related HFpEF is rising, and atrial cardiomyopathies associated with atrial remodeling and atrial fibrillation are clinically highly relevant as atrial remodeling is an independent predictor of mortality. Studies with isolated single-cell cardiomyocytes are frequently used to corroborate and complement *in vivo* findings. Circulatory vessel rarefication and interstitial tissue fibrosis pose a potentially limiting factor for the successful single-cell isolation of ACMs from animal models of this disease.

We have addressed this issue by employing a device capable of manually regulating the intraluminal pressure of cardiac cavities during the isolation procedure, substantially increasing the yield of morphologically and functionally intact ACMs. The acquired cells can be used in a variety of different experiments, such as cell culture and functional Calcium imaging (*i.e.*, excitation-contraction-coupling).

We provide the researcher with a step-by-step protocol, a list of optimized solutions, thorough instructions to prepare the necessary equipment, and a comprehensive troubleshooting guide. While the initial implementation of the procedure might be rather difficult, a successful adaptation will allow the reader to perform state-of-the-art ACM isolations in a rat model of MetS-related HFpEF for a broad spectrum of experiments.

Video Link

The video component of this article can be found at https://www.jove.com/video/57953/

Introduction

MetS describes a cluster of risk factors for diabetes mellitus type-2 and cardiovascular disease and includes an increased arterial blood pressure, dyslipidemia (raised triglycerides and lowered high-density lipoprotein cholesterol), increased fasting glucose, and central obesity[1]. The worldwide prevalence of MetS is estimated to be 25–30% and constantly rising[2]. HFpEF is a heterogenous clinical syndrome often associated with MetS. The cardiac remodeling during HFpEF and its preceding phases (*i.e.*, hypertensive heart disease) is also accompanied by a remodeling of the atria[3]. Reduced contractile function and structural changes of the left atrium have been associated with increased mortality, atrial fibrillation, and new-onset heart failure[4]. Atrial remodeling is characterized by changes in the ion channel function, Ca^{2+} homeostasis, atrial structure, fibroblast activation, and tissue fibrosis[5]. Left atrial remodeling in MetS-related HFpEF and its underlying pathological mechanisms are still poorly understood and require a further in-depth investigation. Animal models have proven to be a valuable tool and lead to many advances in the field of atrial cardiomyopathies[6,7,8,9].

Studies with isolated single-cell cardiomyocytes are frequently used to corroborate and complement *in vivo* findings. An isolation, and the potential subsequent cell culture, allow for the investigation of signaling pathways, ionic channel currents, and excitation-contraction-coupling. Under physiologic conditions, cardiomyocytes do not proliferate. The fusion between the transcriptional regulatory sequences of an atrial natriuretic factor and a simian virus 40 large T antigen in transgenic mice led to the creation of the first immortalized ACMs, named AT-1[10]. The further development of AT-1 cells gave rise to HL-1 cells, which cannot only be serially passaged but also contract spontaneously[11]. They do, however, show structural and functional differences compared to freshly isolated cells, such as a less organized ultrastructure, a high occurrence of developing myofibrils[11], and a hyperpolarization-activated inward current[12]. The isolation of ventricular cardiomyocytes (VCM) in rats and mice from a variety of models is well established[13,14,15,16,17,18,19]. Generally, the excised heart is mounted to a Langendorff apparatus and retrogradely perfused with a Ca^{2+}-free buffer containing digestive enzymes, such as collagenases and proteases. Calcium is then reintroduced in a stepwise manner to the physiological conditions. However, even though protocols dedicated to the isolation of ACMs are available[20,21], due to increased fibrosis and pressure-related differences, their usefulness in disease models with atrial remodeling is limited.

In this article, we have implemented a protocol for the isolation of atrial single-cell cardiomyocytes from animals that show atrial remodeling (*i.e.*, in particular for the ZFS1 rat model for MetS-related HFpEF)[22]. Existing isolation protocols were optimized and complemented by a simple,

custom-made device to control and modify the intraluminal pressure of the cardiac cavities, leading to higher yields of morphologically and functionally intact cardiomyocytes. The following protocol provides the researcher with a step-by-step guide, a detailed description of the custom-made equipment, a list of solutions, as well as a comprehensive troubleshooting guide.

Protocol

All experiments were approved by the local Ethics Committee (TVA T0060/15 and T0003-15) and performed in agreement with the Guidelines for the Care and Use of Laboratory Animals (National Institute of Health, U.S.A.).

NOTE: A simplified flowchart of the procedure is shown in **Figure 1**.

1. Prearrangements

1. **Prepare the buffers according to Table 1.**

	Solution	PB	CB	DB	SB	S1	S2	S3	NT
Reagent (mM)									
NaCl		135	135	135	135	135	135	135	135
KCl		4.7	4.7	4.7	4.7	4.7	4.7	4.7	4
KH_2PO_4		0.6	0.6	0.6	0.6	0.6	0.6	0.6	
Na_2HPO_4		0.6	0.6	0.6	0.6	0.6	0.6	0.6	
$MgSO_4$		1.2	1.2	1.2	1.2	1.2	1.2	1.2	
MgCl									1
HEPES		10	10	10	10	10	10	10	10
Taurine		30	30	30	30	30	30	30	
Glucose		10	10	10	10	10	10	10	
BDM		10	10	10	10	10	10	10	
$CaCl_2$			1	0.01		0.125	0.25	0.5	1
BSA					150	70	70	70	
Purified enzyme blend (medium Thermolysin)				0.195 Wünsch units/mL					
pH adjusted to		7.4	7.4	7.4	7.4	7.4	7.4	7.4	7.4
pH adjusted at		37 °C	4 °C	37 °C	37 °C	37 °C	37 °C	37 °C	37 °C
pH adjusted with		NaOH	NaOH	NaOH	NaOH	NaOH	NaOH	NaOH	NaOH

Table 1: List of Buffers. PB: perfusion buffer, which can be stored for 3 days at 4 °C (300 mL per animal). CB: cannulation buffer, which can be stored for 3 days at 4 °C (200 mL per animal). DB: digestion buffer, which has to be used within the day (40 mL per animal). SB: stopping buffer, which has to be used within the day (2 mL per animal). S1: Step 1 buffer, which has to be used within the day (2 mL per animal). S2: Step 2 buffer, which has to be used within the day (2 mL per animal). S3: Step 3 buffer, which has to be used within the day (2 mL per animal). NT: normal Tyrode, which has to be used within the day (50 mL per animal).

2. **Prepare the Langendorff apparatus (Figure 2A).**
    1. Flush the system with 100 mL of 70% ethanol, followed by 2 flushes of 100 mL distilled water. Fill the system with 200 mL of perfusion buffer (PB).
    2. Set the flow rate of the peristaltic pump to 3 mL/min.
    3. Calibrate the temperature of the PB leaving the Langendorff apparatus to 39 °C.
        1. Place the custom-made cannula [16 G, 25 mm long, sharp tip removed (**Figure 3A**)] on top of the Langendorff apparatus and start the flow. Turn on the heating module and adjust the value of the heating module to reach the desired temperature of the PB at the tip of the cannula. Once the temperature calibration is completed, move the custom-made cannula to the syringe used for the cannulation (**Figure 2B**).
    4. Prepare the pressure control device (**Figure 3C**) next to the Langendorff system. Mount the butterfly needle onto the tripod clamp and prepare 3 blocking knots.

NOTE: Collagenase enzyme activity varies with temperature. A temperature monitoring of the left atrium, as well as a dynamic adjustment thereof, is required later in the procedure.

3. Set up the equipment for the organ excision and the cannulation according to **Figure 2B**. Fill up the beaker, syringe, and Petri dish with an ice-cold cannulation buffer (CB) and prepare the cannulation knots.
4. **Heparinize the rat with 500 I.U. of heparin per 100 g of the rat's body weight as follows.**
    1. Put 2 mL of 100% isoflurane in an anesthesia induction chamber suitable for rodents. Transfer the 21 week-old ZFS-1 obese rat from the cage to the induction chamber. Allow the rat to enter deep anesthesia, indicated by a deceleration of the breathing to half of its initial frequency.
    2. Remove the rat from the induction chamber. Inject 500 I.U. of heparin per 100 g of the rat's body weight into the peritoneum using a heparin syringe.
    3. Return the rat into its cage and allow for it to wake up.
    NOTE: It is not necessary to maintain sterility during step 1.4. Wait 20 min before proceeding to the next step. An incomplete anticoagulation can cause blood clotting, leading to micro-infarctions, which can substantially impact the quality and yield of isolated cardiomyocytes.

2. Heart Preparation

1. Put 2 mL of 100% isoflurane in an anesthesia induction chamber suitable for rodents. Transfer the 21 week-old ZFS-1 obese rat from the cage to the induction chamber. Allow the rat to enter deep anesthesia, indicated by a deceleration of the breathing to half of its initial frequency.
2. Euthanize the animal by decapitation using a guillotine suitable for rodents. Fixate the limbs of the rat on a polystyrene foam surface. Lift and remove the skin covering the xiphoid process with surgical scissors. Open the peritoneum below the rib cages on both sides and expose the diaphragm.
3. Open the diaphragm by making an incision along the anterior arc using fine scissors. Cut through the ribs on both sides along the *linea mediaclavicularis* to the clavicular bone, using surgical scissors, to expose the mediastinum *in situ*.
4. Remove the lungs at the distal ends of the hila with fine scissors. Cut out the thymus to expose the aortic arch.
5. Pinch the base of the heart using forceps and gently pull down towards the tail of the animal. Cut across the aorta while maintaining a pull on the heart, leaving a 5 mm long segment of the aorta attached to the heart. Quickly transfer the heart into the 50 mL ice-cold CB in the 50 ml beaker (**Figure 2B**).
NOTE: During steps 2.5–3.3, the heart is effectively in ischemic conditions. Avoid exceeding a total of 3 min for these steps in order not to damage the cardiomyocytes.

3. Cannulation

1. Wait approximately 10 s for the heart to cool down and seize contractions. Transfer the heart into a Petri dish containing 50 mL of fresh, ice-cold CB. Carefully remove the fatty tissue surrounding the aorta using forceps and scissors.
2. Insert the custom-made cannula (the same as used in step 1.2.3), which is attached to the 10 mL syringe filled with ice-cold CB, 3 mm into the aorta. Fixate the aorta onto the cannula by tying one of the two cannulation knots (**Figure 3B**) in the indentation proximal to the tip of the cannula.
NOTE: Be careful not to damage the aortic valve by a penetration with the cannula.
3. Gently flush the aorta with 5 mL of ice-cold CB using the syringe attached to the cannula until no more blood is visible in the coronary arteries. Gently massage the left atrium using forceps and inject the remaining 5 mL of CB, allowing for any excess blood to be removed from the cavity into the Petri dish.
4. Tie the second cannulation knot (suture: USP 3/0, silk) in the indentation distal to the tip of the cannula. Unmount the cannula with the attached heart from the syringe. Mount the cannula with the attached heart to the Langendorff using an appropriate adapter.
NOTE: This protocol employs elevated pressure in the ventricular cavity during the perfusion at the Langendorff apparatus. The additional cannulation knot is required to maintain this pressure by avoiding any anterograde buffer leakage through the aorta.

4. Pressure Manipulation and Digestion

1. Start the peristaltic pump of the Langendorff apparatus to initiate the perfusion of the cardiac tissue with PB. Tie a double overhand knot (suture: USP 3/0, silk) around the base of the heart, excluding the aorta. Repeat this step until an inflation of the right and left atrium, as well as the coronary sinus, is noticed.
2. Puncture the atrium with the butterfly needle of the pressure control device (**Figure 3D**) and allow the atrium to deflate. Manipulate the intraluminal pressure of the atrium by adjusting the elevation of the butterfly hose. Keep the atrium slightly inflated throughout the rest of the procedure; monitor and adjust accordingly.
NOTE: This step needs to be performed swiftly, as a prolonged inflation of the left atrium will result in cardiomyocyte death.
3. Measure the approximate temperature of the left atrium by positioning a temperature probe between the left atrium and the left ventricle. Adjust the temperature of the Langendorff heating module accordingly, targeting an approximate temperature of 37 °C of the left atrium.
4. Perfuse the heart with PB for a total of 3 min.
5. Switch the perfusion to a digestion buffer (DB) for approximately 14–18 min.
NOTE: The digestion is complete when the left atrial structure collapses and the tissue acquires a milky texture.
6. Pinch the atrium using forceps and enact a slight pull. Remove the left atrium using fine scissors and transfer the atrium into a large weighing boat containing 2 mL of stopping buffer (SB), fully submerging the tissue.
7. Dispose of the remaining cardiac tissue following the guidelines of the laboratory where the procedure is performed.

5. Cell Processing and Calcium Re-adaptation

1. Mince the atrial tissue into small pieces of roughly 2 mm x 2 mm using fine scissors.
2. Disperse the tissue by a gentle suction and ejection of the tissue chunks using a transfer pipette. Continue this procedure for approximately 5 min until a macroscopic dissociation of the tissue can be observed.
   NOTE: Avoid any air bubbles during this step, as exposing the cells to air will result in cardiomyocyte death.
3. Transfer the cells to a 15 mL conical tube. Allow the tissue chunks to settle for 30 s. Transfer the supernatant into another 15 mL conical tube. Allow the cells to settle for 15 min.
4. Remove and discard the supernatant. Add 2 mL of Step 1 buffer (see **Table 1**). Allow the cardiomyocytes to settle for 10 min.
   NOTE: The discarded supernatant also includes fibroblasts and endothelial cells. Please refer to other protocols if it is desired to use these cells for experiments[14,23]. The pellet will contain mostly atrial cardiomyocytes, which can be confirmed by light microscopy. The microscopic characteristics of atrial cardiomyocytes are discussed in step 6.1.
5. Remove and discard the supernatant. Add 2 mL of Step 2 buffer. Allow the cardiomyocytes to settle for 10 min.
6. Remove and discard the supernatant. Add 2 mL of Step 3 buffer. Allow the cardiomyocytes to settle for 10 min.
7. Remove and discard the supernatant. Add 250 µL of normal Tyrode (NT) containing 1 mM Ca^{2+}.
8. Transfer 50 µL of the normal Tyrode containing atrial cardiomyocytes onto a glass-bottom dish, which has been coated with 25% laminin (and allowed to dry beforehand). Allow the cardiomyocytes to settle for 10 min.
9. Fill a glass-bottom dish with 500 µL of NT containing 1 mM $CaCl_2$.

6. Functional Evaluation of Excitation-contraction-coupling

1. Evaluate the cell morphology and viability under a light microscope using a 20X magnification (**Figure 4A** and **4B**). Randomly select approximately 100 cells and classify them as either viable or unviable in order to estimate the viability of the cell isolation procedure.
   NOTE: Viable cells are characterized by symmetric sarcomere structure, the absence of membrane blebs, and a rod shape.
2. **Load the cells with the Ca^{2+}-sensitive fluorescent dye within 20 min of completing step 5.9.**
   1. Add 10 µM Fluo4-AM to 500 µL of NT. Remove the supernatant from the glass-bottom dish (from step 5.9). Add the NT containing Fluo4-AM to the glass-bottom dish. Incubate the mixture for 20 min at room temperature. Remove and discard the supernatant. Wash the sample 2x using 500 µL of NT.
3. **Visualize the Ca^{2+}-excitation with a confocal microscope as follows.**
   1. Transfer the glass-bottom dish to a confocal microscope and visualize the Ca^{2+}-excitation with a confocal microscope (laser intensity at 5.8%, excitation at 488 nm, emission at 515 nm) using a 40X magnification.
   2. Perfuse the cells with NT heated to 37 °C using an appropriate superfusion device. Alternatively, keep the cells warm using a microscope-mounted heat incubator.
   3. Stimulate the cardiomyocytes in an electrical field with commercially available, microscope-mounted stimulator electrodes at a frequency of 1 Hz and an electrical current of 24 A. Wait for 1 min to allow the cells to reach a steady-state of Ca^{2+} handling.
   4. Place the scan line parallel to the transversal axis, half-way between the nucleus and the edge of a randomly selected, macroscopically contracting cell. Acquire line scan images by repetitive scanning.
   5. Use freely available imaging software to estimate the signal intensity immediately before an electric stimulation (F_0) across the entire cell. Plot the signal intensity across the entire cell over the course of 1 stimulation cycle (F). Divide (F) by (F_0) to obtain the respective Ca^{2+} transient.

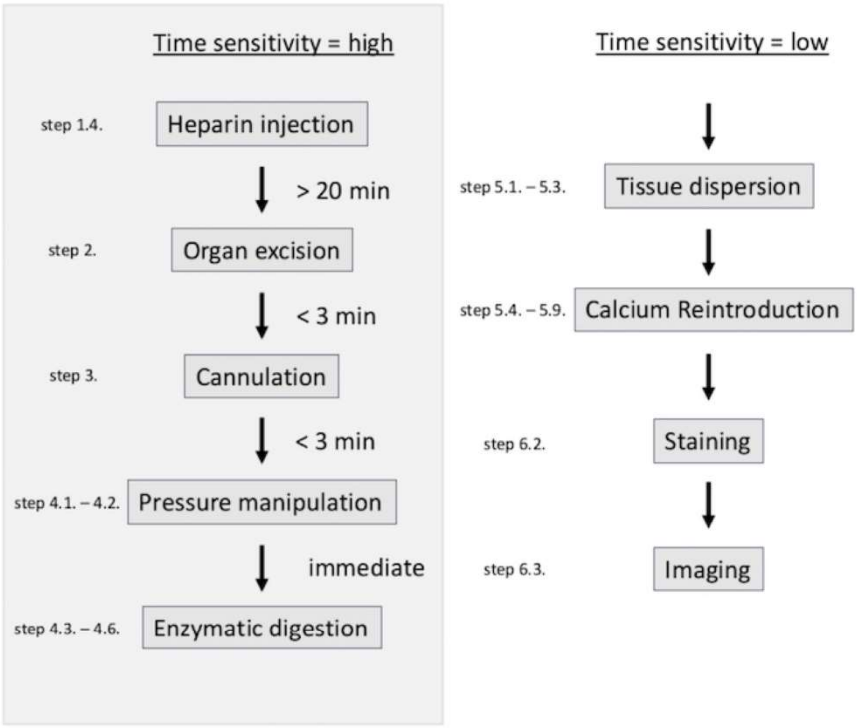

Figure 1: Simplified flowchart of the isolation procedure. The procedure is highly time-sensitive until the enzymatic digestion of the myocytes is completed. Please click here to view a larger version of this figure.

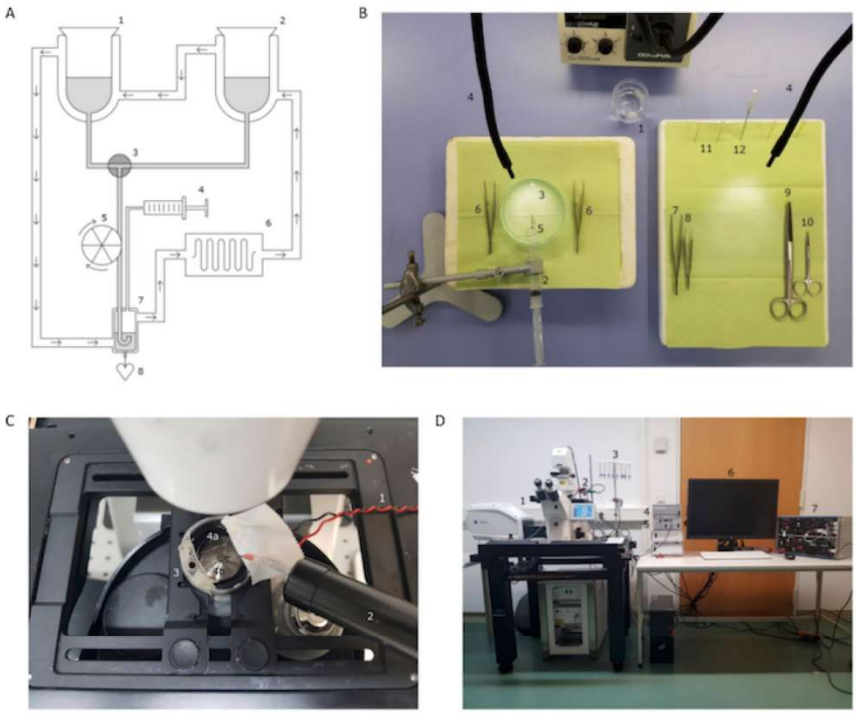

Figure 2: Preparation of equipment prior to the isolation. (**A**) This panel shows a self-made Langendorff apparatus: (1) a jacketed reaction vessel with PB; (2) a jacketed reaction vessel with CB; (3) a 3-way stopcock; (4) a syringe; (5) a peristaltic pump; (6) a heating immersion; (7) a jacketed bubble trap; and (8) the cannula and heart. (**B**) This panel shows the set-up for the cannulation and organ excision for an optimized work flow: (1) a 100 mL beaker with 50 mL of ice-cold CB; (2) a 10 mL syringe with ice-cold CB; (3) a Petri dish with ice-cold CB; (4) a light source; (5) the custom-made cannula with a cannulation knot (see also **Figure 3A** and **3B**); (6) fine, curved forceps; (7) tissue forceps; (8) fine forceps, angled 45°; (9) abdominal surgical scissors; (10) fine surgical scissors; (11) 4 x 30 G needles; and (12) a 15 G needle. (**C**) This panel shows the microscope-mounted equipment for the confocal imaging: (1) electric stimulator electrodes; (2) a superfusion pen; (3) a glass-bottom dish with the ACMs; and (4) immersed platinum electric stimulator electrodes. **(D**) This panel shows the microscope set-up for the confocal imaging: (1) the confocal microscope; (2) a superfusion pen; (3) a superfusion buffer reservoir; (4) a superfusion flow regulator; (5) a superfusion heating module; (6) a computer workstation; and (7) an electric stimulator. Please click here to view a larger version of this figure.

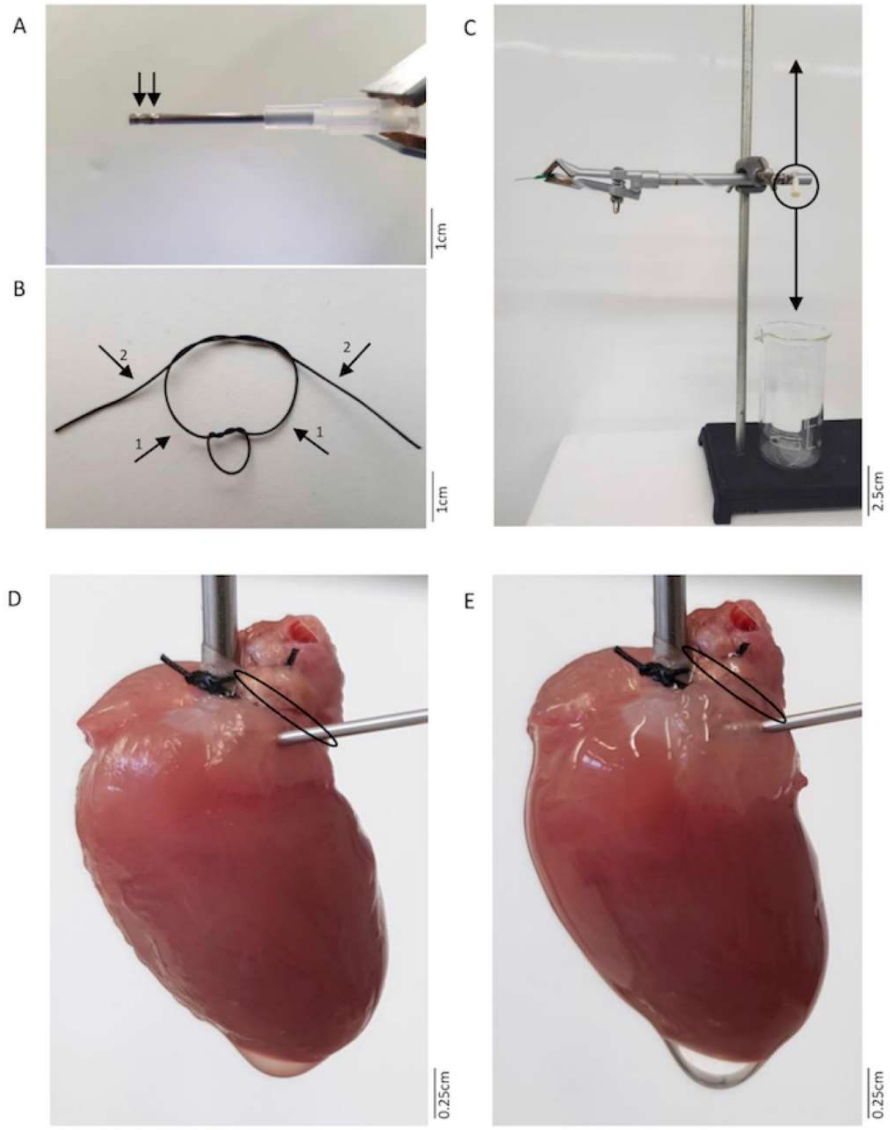

Figure 3: Custom-made equipment. (**A**) This panel shows the manipulated 15 G cannula with a Luer lock. The arrows indicate two indentations for the cannulation knots. (**B**) These are the cannulation knots, two double overhand knots placed on top of each other for rapid tightening. The arrows indicate where and in which order the knot needs to be tightened. (**C**) This panel shows the assembled pressure control device. A 21 G butterfly needle is hooked into a tripod clamp. The hose is kept at the same height as the needle. The screw top is opened. The elevation of the butterfly hose can be altered as indicated by the arrows in order to change the intraluminal pressure of the left atrium. (**D**) The left atrium is punctured with the pressure control device. This picture shows an ideally inflated left atrium. The ellipse marks the placement of the overhand knot. (**E**) The left atrium is punctured with the pressure control device. This picture shows an over-inflated left atrium, which will result in a lower yield of viable ACMs. The ellipse marks the placement of the overhand knot. Please click here to view a larger version of this figure.

Representative Results

At 21 weeks of age, 60–90% of viable ACMs (estimated as described in step 6.1), after the calcium re-adaptation (step 5.4–5.7), can be isolated from ZSF-1 obese rats by this method (**Figure 4A**). In rats, ACMs are characterized by a different and more heterogenous phenotype compared to VCMs[24,25]. **Figure 4B** shows an individual ACM with preserved membranes and sarcomere structure, both strong indicators of a functionally integral cell.

The acquired ACMs can be processed in a variety of ways. As exemplified in **Figure 5**, the cells might be loaded with fluorescent dyes used to study morphology and/or function. For instance, di-8-ANEPPS was used to delineate the tubular system in an atrial rat cell (**Figure 5A**). In another set of experiments, mitochondria-staining far red-fluorescence dye (*e.g.*, mitotracker-Red-FM) is employed to detect cytosolic mitochondria (**Figure 5B**) in atrial remodeling. As shown in **Figure 5C**, ACMs isolated with this protocol are also suitable for live-cell Ca^{2+} imaging and show intact excitation-contraction coupling with a 1 Hz field-stimulation. All images can be used for further analysis using a variety of algorithms available to the researcher[6,7] (**Figure 5D**).

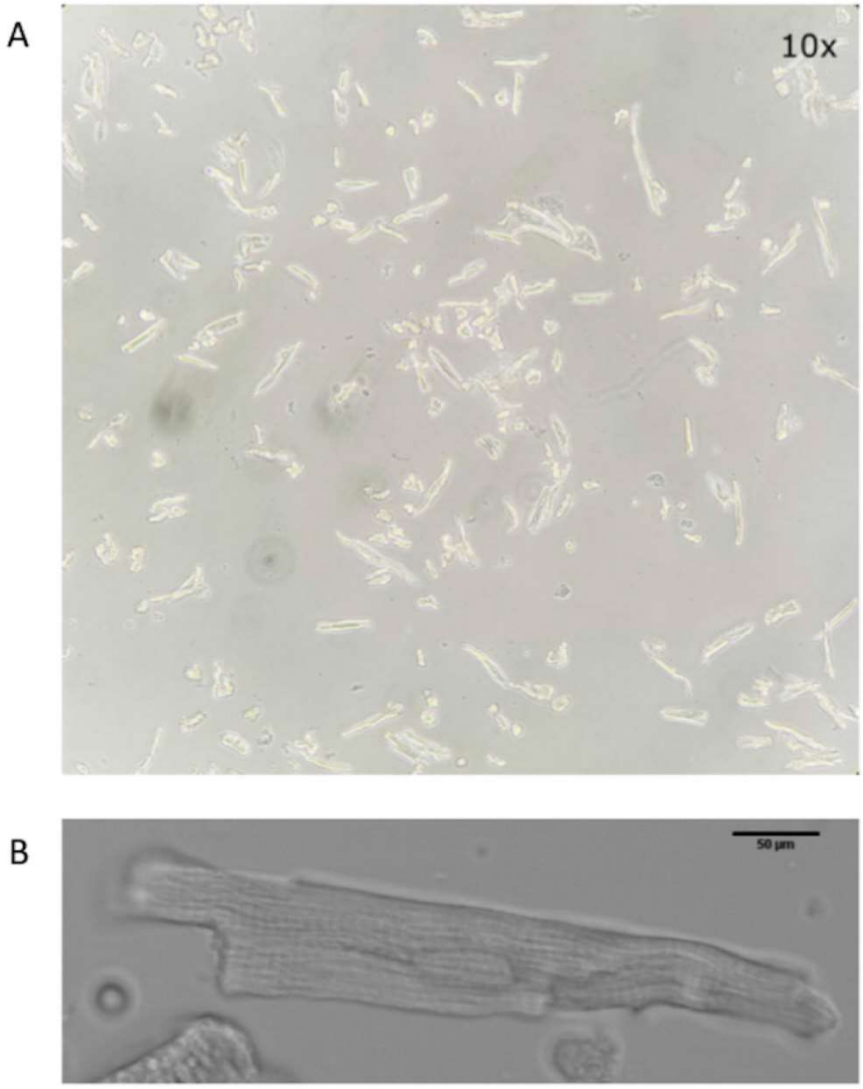

Figure 4: Respective yield of viable, single-cell AM. (**A**) This panel shows the yield of an isolation after the re-adaptation of ACMs to 1 mM Ca^{2+} in NT. (**B**) This panel shows an isolated, single-cell atrial cardiomyocyte. The sarcomere structure, cell membrane, and nucleus are clearly visible. Please click here to view a larger version of this figure.

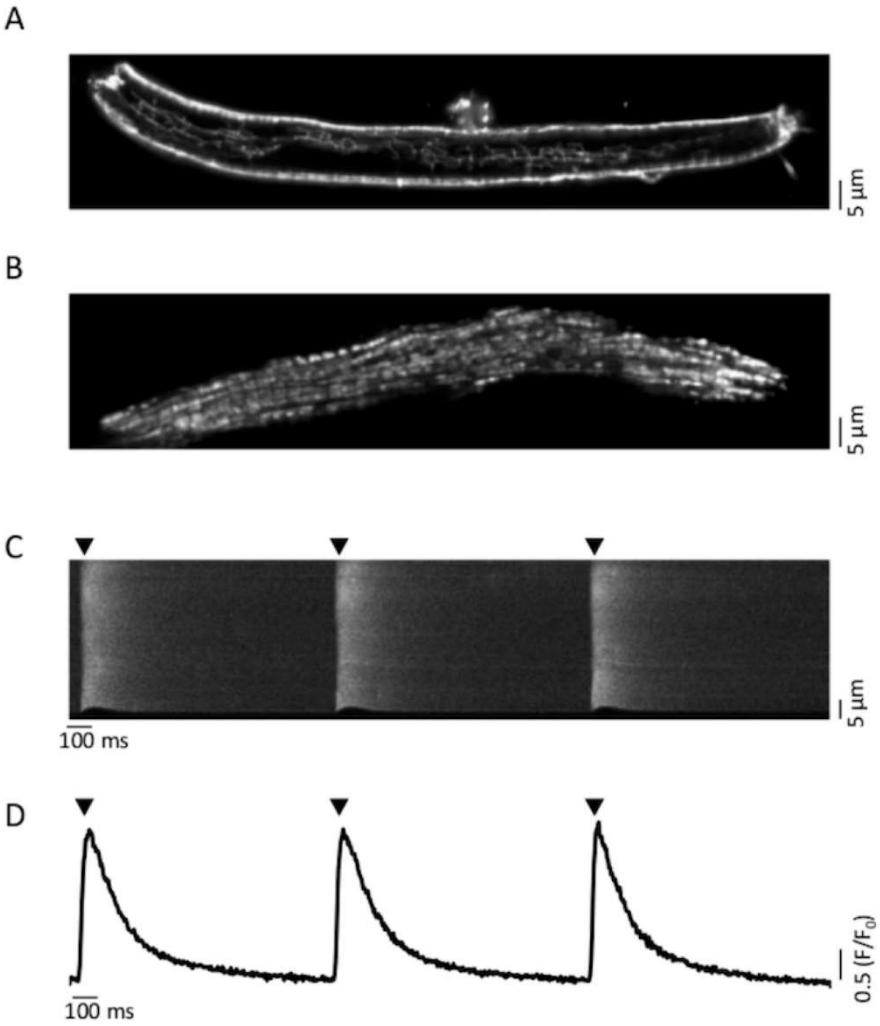

Figure 5: Staining of rat ACMs with fluorescent dyes. (**A**) This panel shows the staining of a cell membrane and tubular network with the fluorescent dye Di8ANNEPS. (**B**) This panel shows the staining of mitochondria with the fluorescent dye mitotracker-Red-FM. (**C**) This panel shows the transversal line scan of a Ca^{2+}-excitation with the fluorescent dye Fluo4-AM over a single cell. The arrows indicate the electrical stimulation, conducted at 1 Hz. (**D**) This panel shows the longitudenal Ca^{2+} transients derived from panel **C**. Please click here to view a larger version of this figure.

Discussion

Here, we first described a protocol for the isolation of single-cell ACMs from a rat model of MetS-related HFpEF that shows marked atrial remodeling[22]. The procedure is uniquely challenging as excessive fatty tissue can make the surgical preparation, as well as the cannulation of the aorta, increasingly difficult. The troubleshooting guide provided in **Table 2** addresses the most common issues of the isolation procedure.

Problem	Possible Cause	Solution
No flow through butterfly hose	Improper closure of the aorta with the cannulation knots	Remove fatty tissue before tightening
		Add 3rd cannulation knot with respective indentation
		Pull knot with hand for increased force
	Blocked needle	Readjust position into the lumen
		Unblock by gentle pull with syringe
Right atrium / coronary sinus not inflated	Improper closure of the heart base	Block flow with additional knots
	Right atrium damaged during preparation	Close leakage with clips/knots
Poor digestion / atrium does not soften	Reduced enzyme activity through wrong temperature	Adjust temperature to 37 °C
	Inactive/degraded enzyme	Replace
	Old/overly fibrotic atrium	Increase digestion time (in steps of +50%)
	Damaged aortic valve	Shallow penetration during cannulation
Poor cell yield	Atrium over-digested	Decrease digestion time (in steps of +25%)
		Reduce intraluminal pressure by lowering the butterfly hose
	Atrium under-digested	Increase digestion time (in steps of 25%)
		Increase intraluminal pressure by raising the butterfly hose
	Cell dispersion too aggressive	Be more gentle

Table 2: Troubleshooting guide. This table displays common issues of the isolation procedure and their respective solutions.

In a recent study, we have shown that the ZFS-1 obese rat model exhibits extensive atrial remodeling with an increased atrial size[22]. An increase in the left atrial size has been recognized as an important prognostic marker for diastolic dysfunction[26] and causes a rarefication of the microvascular vessels relative to the tissue. This leads to a decreased distribution of the digestive buffer through the retrograde perfusion of the aorta during the isolation procedure, rendering the single-cell isolation in this model especially challenging. Other hallmark features of atrial remodeling, atrial fibrosis, and increased fibrosis have been shown for ZDF rats—a rat model for metabolic diabetes and one parent strain of the ZFS1 rats[27]. Collagen deposits impair the efficacy of the digestive enzymes to liberate the cardiomyocytes from the extracellular matrix and, therefore, require further adjustments of the cell isolation procedure[28].

The mechanism by which the pressure device facilitates the improved isolation results in this model of atrial remodeling is most likely related to a localized attenuation of the coronary blood flow of the left atrium. One major component of the coronary blood flow is coronary perfusion pressure, which is defined as the gradient between the coronary artery pressure and the end-diastolic pressure of the respective cavity[29]. During the described procedure, a blockage of the heart base leads to a global increase in coronary artery pressure and intraluminal pressure throughout the heart. The subsequent puncture of the left atrium facilitates a local, selective drop of intraluminal pressure in the left atrial cavity. Thus, not only a large coronary perfusion pressure gradient is established, but the perfusion volume is also increased by the diverted digestion solution from the congested left ventricle to the left atrium.

In addition, the choice of digestion enzymes is crucial for the ACM isolation: purified enzyme blends of collagenase I and II have been shown to be superior to less targeted and less pure enzymes like collagenases[30]. This enzyme does not only allow for a higher yield of morphologically and functionally intact cardiomyocytes but also minimizes any clumping of single cells after their isolation[31]. Purified enzyme blends of collagenases with an additional high dispase or medium thermolysin content are most commonly used for rat cardiomyocyte isolations. While VCMs are best isolated at higher concentrations, the best results of atrial myocytes were acquired with a concentration of 0.195 Wünsch Units/mL using this protocol[32].

As the prevalence of MetS-related HFpEF is rising[2] and atrial cardiomyopathies leading to atrial remodeling and atrial fibrillation are clinically highly relevant, research in this field is of pivotal interest. Many new animal models for HFpEF are emerging[33,34] and atrial remodeling in line with an increased incidence of atrial rhythm disorders are hallmark features of the disease. The described method allows researchers to isolate viable single cardiomyocytes from rat models with atrial remodeling for a further study with an exceptionally high yield and preserved mechanical and electrical function.

Disclosures

The authors have nothing to disclose.

Acknowledgements

This research was supported by the DZHK (German Centre for Cardiovascular Research, D.B.), the EKFS (Else-Kröner-Fresenius Stiftung, F.H.), and by the BMBF (German Ministry of Education and Research), as well as the BIH-Charité clinical scientist program funded by the Charité - Universitätsmedizin Berlin and the Berlin Institute of Health (F.H.).

References

1. Alberti, K. G. *et al.* Harmonizing the metabolic syndrome: a joint interim statement of the International Diabetes Federation Task Force on Epidemiology and Prevention; National Heart, Lung, and Blood Institute; American Heart Association; World Heart Federation; International Atherosclerosis Society; and International Association for the Study of Obesity. *Circulation.* **120** (16), 1640-1645 (2009).
2. International Diabetes Federation Task Force on Epidemiology and Prevention. *IDF Consensus Worldwide Definition of the Metabolic Syndrome.* www.idf.org/e-library/consensus-statements/60-idfconsensus-worldwide-definitionof-the-metabolic-syndrome.html (2006).
3. Melenovsky, V. *et al.* Left atrial remodeling and function in advanced heart failure with preserved or reduced ejection fraction. *Circulation: Heart Failure.* **8** (2), 295-303 (2015).
4. Goette, A. *et al.* EHRA/H/APHRS/SOLAECE expert consensus on atrial cardiomyopathies: definition, characterization, and clinical implication. *EP Europace.* **18** (10), 1455-1490 (2016).
5. Schotten, U., Verheule, S., Kirchhof, P., Goette, A. Pathophysiological mechanisms of atrial fibrillation: a translational appraisal. *Physiological Reviews.* **91** (1), 265-325 (2011).
6. Hohendanner, F., DeSantiago, J., Heinzel, F. R., Blatter, L. A. Dyssynchronous calcium removal in heart failure-induced atrial remodeling. *American Journal of Physiology-Heart and Circulatory Physiology.* **311** (6), H1352-H1359 (2016).
7. Hohendanner, F. *et al.* Inositol-1,4,5-trisphosphate induced Ca2+ release and excitation-contraction coupling in atrial myocytes from normal and failing hearts. *The Journal of Physiology.* **593** (6), 1459-1477 (2015).
8. Tada, Y. *et al.* Role of mineralocorticoid receptor on experimental cerebral aneurysms in rats. *Hypertension.* **54** (3), 552-557 (2009).
9. Iwasaki, Y. K. *et al.* Atrial fibrillation promotion with long-term repetitive obstructive sleep apnea in a rat model. *Journal of the American College of Cardiology.* **64** (19), 2013-2023 (2014).
10. Field, L. J. Atrial natriuretic factor-SV40 T antigen transgenes produce tumors and cardiac arrhythmias in mice. *Science.* **239** (4843), 1029-1033 (1988).
11. Claycomb, W. C. *et al.* HL-1 cells: a cardiac muscle cell line that contracts and retains phenotypic characteristics of the adult cardiomyocyte. *Proceedings of the National Academy of Sciences of the United States of America.* **95** (6), 2979-2984 (1998).
12. Sartiani, L., Bochet, P., Cerbai, E., Mugelli, A., Fischmeister, R. Functional expression of the hyperpolarization-activated, non-selective cation current I(f) in immortalized HL-1 cardiomyocytes. *The Journal of Physiology.* **545** (Pt 1), 81-92 (2002).
13. Louch, W. E., Sheehan, K. A., Wolska, B. M. Methods in cardiomyocyte isolation, culture, and gene transfer. *Journal of Molecular and Cellular Cardiology.* **51** (3), 288-298 (2011).
14. Gunduz, D., Hamm, C. W., Aslam, M. Simultaneous Isolation of High Quality Cardiomyocytes, Endothelial Cells, and Fibroblasts from an Adult Rat Heart. *Journal of Visualized Experiments.* (123), e55601 (2017).
15. Li, D., Wu, J., Bai, Y., Zhao, X., Liu, L. Isolation and culture of adult mouse cardiomyocytes for cell signaling and *in vitro* cardiac hypertrophy. *Journal of Visualized Experiments.* (87), e51357 (2014).
16. Graham, E. L. *et al.* Isolation, culture, and functional characterization of adult mouse cardiomyoctyes. *Journal of Visualized Experiments.* (79), e50289 (2013).
17. Roth, G. M., Bader, D. M., Pfaltzgraff, E. R. Isolation and physiological analysis of mouse cardiomyocytes. *Journal of Visualized Experiments.* (91), e51109 (2014).
18. Thum, T., Borlak, J. Isolation and cultivation of Ca2+ tolerant cardiomyocytes from the adult rat: improvements and applications. *Xenobiotica.* **30** (11), 1063-1077 (2000).
19. Egorova, M. V., Afanas'ev, S. A., Popov, S. V. A simple method for isolation of cardiomyocytes from adult rat heart. *Bulletin of Experimental Biology and Medicine.* **140** (3), 370-373 (2005).
20. Kohncke, C. *et al.* Isolation and Kv channel recordings in murine atrial and ventricular cardiomyocytes. *Journal of Visualized Experiments.* (73), e50145 (2013).
21. Wagner, E., Brandenburg, S., Kohl, T., Lehnart, S. E. Analysis of tubular membrane networks in cardiac myocytes from atria and ventricles. *Journal of Visualized Experiments.* (92), e51823 (2014).
22. Hohendanner, F. *et al.* Cellular mechanisms of metabolic syndrome-related atrial decompensation in a rat model of HFpEF. *Journal of Molecular and Cellular Cardiology.* **115**, 10-19 (2017).
23. Seluanov, A., Vaidya, A., Gorbunova, V. Establishing primary adult fibroblast cultures from rodents. *Journal of Visualized Experiments.* (44), e2033 (2010).
24. Bootman, M. D., Higazi, D. R., Coombes, S., Roderick, H. L. Calcium signalling during excitation-contraction coupling in mammalian atrial myocytes. *Journal of Cell Science.* **119** (Pt 19), 3915-3925 (2006).
25. Smyrnias, I. *et al.* Comparison of the T-tubule system in adult rat ventricular and atrial myocytes, and its role in excitation-contraction coupling and inotropic stimulation. *Cell Calcium.* **47** (3), 210-223 (2010).
26. Pritchett, A. M. *et al.* Diastolic dysfunction and left atrial volume: a population-based study. *Journal of the American College of Cardiology.* **45** (1), 87-92 (2005).
27. Linz, D. *et al.* Cathepsin A mediates susceptibility to atrial tachyarrhythmia and impairment of atrial emptying function in Zucker diabetic fatty rats. *Cardiovascular Research.* **110** (3), 371-380 (2016).
28. Ackers-Johnson, M. *et al.* A Simplified, Langendorff-Free Method for Concomitant Isolation of Viable Cardiac Myocytes and Nonmyocytes From the Adult Mouse Heart. *Circulation Research.* **119** (8), 909-920 (2016).
29. Ramanathan, T., Skinner, H. Coronary blood flow. *Continuing Education in Anaesthesia Critical Care & Pain.* **5** (2), 61-64 (2005).
30. Bond, M. D., Van Wart, H. E. Characterization of the individual collagenases from Clostridium histolyticum. *Biochemistry.* **23** (13), 3085-3091 (1984).

31. Deel, E. D. *et al*. In vitro model to study the effects of matrix stiffening on Ca(2+) handling and myofilament function in isolated adult rat cardiomyocytes. *The Journal of Physiology.* **595** (14), 4597-4610 (2017).
32. Wuensch, E., Heidrich, H. G. [On the Quantitative Determination of Collagenase]. *Hoppe-Seyler's Zeitschrift für physiologische Chemie.* **333**, 149-151 (1963).
33. Conceicao, G., Heinonen, I., Lourenco, A. P., Duncker, D. J., Falcao-Pires, I. Animal models of heart failure with preserved ejection fraction. *Netherlands Heart Journal.* **24** (4), 275-286 (2016).
34. Horgan, S., Watson, C., Glezeva, N., Baugh, J. Murine models of diastolic dysfunction and heart failure with preserved ejection fraction. *Journal of Cardiac Failure.* **20** (12), 984-995 (2014).

7.3 Hohendanner F, Bode D, Primessnig U, Guthof T, Doerr R, Jeuthe S, Reimers S, Zhang K, Bach D, Wakula P, Pieske BM, Heinzel FR. Cellular mechanisms of metabolic syndrome-related atrial decompensation in a rat model of HFpEF. Journal of Molecular and Cellular Cardiology. 2018 Feb;115:10-19.

Journal Data Filtered By: **Selected JCR Year: 2018** Selected Editions: SCIE,SSCI Selected Categories: **"CARDIAC and CARDIOVASCULAR SYSTEMS"** Selected Category Scheme: WoS

Gesamtanzahl: 136 Journale

Rank	Full Journal Title	Total Cites	Journal Impact Factor	Eigenfactor Score
1	EUROPEAN HEART JOURNAL	57,358	23.239	0.125920
2	CIRCULATION	166,484	23.054	0.211290
3	JOURNAL OF THE AMERICAN COLLEGE OF CARDIOLOGY	100,986	18.639	0.193290
4	Nature Reviews Cardiology	6,301	17.420	0.018820
5	CIRCULATION RESEARCH	52,988	15.862	0.072290
6	EUROPEAN JOURNAL OF HEART FAILURE	13,107	13.965	0.027620
7	JAMA Cardiology	3,280	11.866	0.019320
8	JACC-Cardiovascular Imaging	8,801	10.975	0.026160
9	JACC-Cardiovascular Interventions	11,555	9.544	0.033640
10	JACC-Heart Failure	3,537	8.910	0.016830
11	JOURNAL OF HEART AND LUNG TRANSPLANTATION	12,436	8.578	0.027310
12	CARDIOVASCULAR RESEARCH	21,828	7.014	0.021500
13	European Heart Journal-Cardiovascular Pharmacotherapy	442	6.723	0.001430
14	Circulation-Heart Failure	6,900	6.526	0.022830
15	BASIC RESEARCH IN CARDIOLOGY	4,137	6.470	0.005590
16	PROGRESS IN CARDIOVASCULAR DISEASES	4,055	6.162	0.008860
17	JOURNAL OF THE AMERICAN SOCIETY OF ECHOCARDIOGRAPHY	10,478	6.111	0.016060
18	EUROPACE	10,908	6.100	0.025320
19	Circulation-Cardiovascular Interventions	5,289	6.060	0.016640

Rank	Full Journal Title	Total Cites	Journal Impact Factor	Eigenfactor Score
20	Cardiovascular Diabetology	5,392	5.948	0.011550
21	Circulation-Cardiovascular Imaging	5,456	5.813	0.018480
22	European Journal of Preventive Cardiology	4,782	5.640	0.013370
23	CANADIAN JOURNAL OF CARDIOLOGY	6,710	5.592	0.018500
24	JOURNAL OF THORACIC AND CARDIOVASCULAR SURGERY	29,599	5.261	0.036950
25	European Heart Journal-Cardiovascular Imaging	5,498	5.260	0.021650
26	HEART RHYTHM	12,344	5.225	0.029030
27	REVISTA ESPANOLA DE CARDIOLOGIA	3,566	5.126	0.004640
28	HEART	18,063	5.082	0.030620
29	JOURNAL OF CARDIOVASCULAR MAGNETIC RESONANCE	5,113	5.070	0.014020
30	JOURNAL OF MOLECULAR AND CELLULAR CARDIOLOGY	14,143	5.055	0.020450
31	Circulation-Arrhythmia and Electrophysiology	6,432	4.968	0.017840
32	Clinical Research in Cardiology	3,022	4.907	0.006760
33	Circulation-Cardiovascular Genetics	3,441	4.864	0.010500
34	Journal of the American Heart Association	13,230	4.660	0.060340
35	TRENDS IN CARDIOVASCULAR MEDICINE	2,667	4.462	0.003930
36	Circulation-Cardiovascular Quality and Outcomes	4,531	4.378	0.014350
37	ATHEROSCLEROSIS	23,442	4.255	0.033500
38	CARDIOVASCULAR DRUGS AND THERAPY	2,109	4.181	0.003140
39	JOURNAL OF NUCLEAR CARDIOLOGY	3,711	4.112	0.004480

Print

Aus Gründen des Urheberrechts aus der Online-Version der Dissertation entfernt.

https://doi.org/10.1016/j.yjmcc.2017.12.012

Aus Gründen des Urheberrechts aus der Online-Version der Dissertation entfernt.

https://doi.org/10.1016/j.yjmcc.2017.12.012

Aus Gründen des Urheberrechts aus der Online-Version der Dissertation entfernt.

https://doi.org/10.1016/j.yjmcc.2017.12.012

Aus Gründen des Urheberrechts aus der Online-Version der Dissertation entfernt.

https://doi.org/10.1016/j.yjmcc.2017.12.012

Aus Gründen des Urheberrechts aus der Online-Version der Dissertation entfernt.

https://doi.org/10.1016/j.yjmcc.2017.12.012

Aus Gründen des Urheberrechts aus der Online-Version der Dissertation entfernt.

https://doi.org/10.1016/j.yjmcc.2017.12.012

Aus Gründen des Urheberrechts aus der Online-Version der Dissertation entfernt.

https://doi.org/10.1016/j.yjmcc.2017.12.012

Aus Gründen des Urheberrechts aus der Online-Version der Dissertation entfernt.

https://doi.org/10.1016/j.yjmcc.2017.12.012

Aus Gründen des Urheberrechts aus der Online-Version der Dissertation entfernt.

https://doi.org/10.1016/j.yjmcc.2017.12.012

Aus Gründen des Urheberrechts aus der Online-Version der Dissertation entfernt.

https://doi.org/10.1016/j.yjmcc.2017.12.012

8. Curriculum Vitae

Mein Lebenslauf wird aus datenschutzrechtlichen Gründen in der elektronischen Version meiner Arbeit nicht veröffentlicht.

9. List of Publications

Parwani AS, Hohendanner F, **Bode D**, Kuhlmann S, Blaschke F, Lacour P, Heinzel FR, Pieske B, Boldt LH. The force stability of tissue contact and lesion size index during radiofrequency ablation: An ex-vivo study. Pacing and clinical electrophysiology : PACE. 2020;43:327-331. Impact factor: 1.340 (2018).

Hohendanner F, **Bode D**. Mitochondrial Calcium in heart failure with preserved ejection fraction-friend or foe? Acta physiologica. 2019:e13415. Impact factor: 5.868 (2018).

Bode D, Lindner D, Schwarzl M, Westermann D, Deissler P, Primessnig U, Hegemann N, Blatter LA, van Linthout S, Tschöpe C, Schoenrath F, Soltani S, Stamm C, Duesterhoeft V, Rolim N, Wisløff U, Knosalla C, Falk V, Pieske BM, Heinzel FR, Hohendanner F. The role of fibroblast - Cardiomyocyte interaction for atrial dysfunction in HFpEF and hypertensive heart disease. Journal of Molecular and Cellular Cardiology. 2019 Jun;131:53-65. Impact factor: 5.055 (2018).

Bode D, Guthof T, Pieske BM, Heinzel FR, Hohendanner F. Isolation of Atrial Cardiomyocytes from a Rat Model of Metabolic Syndrome-related Heart Failure with Preserved Ejection Fraction. Journal of Visualized Experiments. 2018 Jul 26(137). Impact factor: 1.108.

Hohendanner F, Messroghli D, **Bode D**, Blaschke F, Parwani A, Boldt, LH. Atrial remodelling in heart failure: recent developments and relevance for heart failure with preserved ejection fraction. ESC Heart Failure. 2018 Feb 19. Impact factor: 3.407.

Hohendanner F, **Bode D**, Primessnig U, Guthof T, Doerr R, Jeuthe S, Reimers S, Zhang K, Bach D, Wakula P, Pieske BM, Heinzel FR. Cellular mechanisms of metabolic syndrome-related atrial decompensation in a rat model of HFpEF. Journal of Molecular and Cellular Cardiology. 2018 Feb;115:10-19. Impact factor: 5.055.

10. Acknowledgements

I thank Prof. Dr. Heinzel and Priv. Doz. Dr. Hohendanner for their mentorship.

I thank my family for their continuous support and guidance.

I thank Lisa for always having my back.